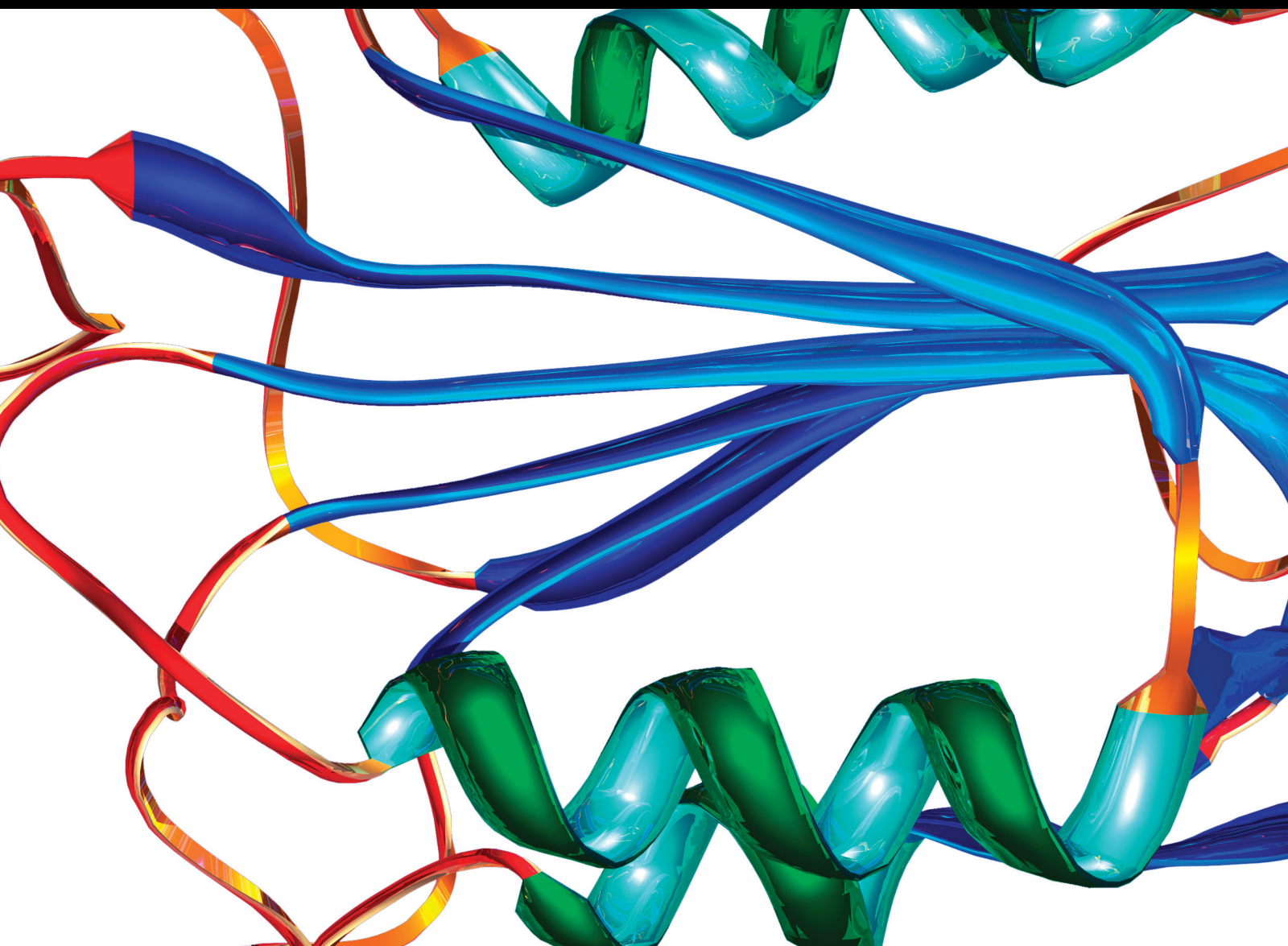# Molecular Biomarkers and Imaging Markers in the Prediction, Diagnosis, and Prognosis of Heart Diseases

Lead Guest Editor: Agata Bielecka-Dabrowa
Guest Editors: Ibadete Bytyçi, Maciej Banach, and Agata Sakowicz

Molecular Biomarkers and Imaging Markers in the Prediction, Diagnosis, and Prognosis of Heart Diseases

Molecular Biomarkers and Imaging Markers in the Prediction, Diagnosis, and Prognosis of Heart Diseases

Lead Guest Editor: Agata Bielecka-Dabrowa
Guest Editors: Ibadete Bytyçi, Maciej Banach, and Agata Sakowicz

Alexander G. Mathioudakis, United Kingdom

Andrea Maugeri, Italy

Prasenjit Mitra, India

Ekansh Mittal, USA

Hiroshi Miyamoto, USA

Naoshad Muhammad, USA

Chiara Nicolazzo, Italy

Xing Niu, China

Dong Pan, USA

Dr.Krupakar Parthasarathy, India

Robert Pichler, Austria

Dimitri Poddighe, Kazakhstan

Roberta Rizzo, Italy

Maddalena Ruggieri, Italy

Tamal Sadhukhan, USA

Pier P. Sainaghi, Italy

Cristian Scheau, Romania

Jens-Christian Schewe, Germany

Alexandra Scholze, Denmark

Shabana, Pakistan

Anja Hviid Simonsen, Denmark

Eric A. Singer, USA

Daniele Sola, Italy

Timo Sorsa, Finland

Yaying Sun, China

Mohammad Tarique, USA

Jayaraman Tharmalingam, USA

Sowjanya Thatikonda, USA

Stamatios E. Theocharis, Greece

Tilman Todenhöfer, Germany

Anil Tomar, India

Alok Tripathi, India

Drenka Trivanović, Germany

Natacha Turck, Switzerland

Azizah Ugusman, Malaysia

Shailendra K. Verma, USA

Aristidis S. Veskoukis, Greece

Arianna Vignini, Italy

Jincheng Wang, Japan

Zhongqiu Xie, USA

Yuzhen Xu, China

Zhijie Xu, China

Guan-Jun Yang, China

Yan Yang, USA

Chengwu Zeng, China

Jun Zhang Zhang, USA

Qun Zhang, China

Changli Zhou, USA

Heng Zhou, China

Jian-Guo Zhou, China

Contents

Research Article

Identification of Featured Metabolism-Related Genes in Patients with Acute Myocardial Infarction

Hang Xie, Enfa Zha [ID], and Yushun Zhang [ID]

Department of Structural Heart Disease, The First Affiliated Hospital of Xi'an Jiaotong University, Xi'an 710061, China

Correspondence should be addressed to Yushun Zhang; zys2889@sina.com

Objective. A growing body of emerging evidence indicates that metabolic processes play a pivotal role in the biological processes underlying acute myocardial infarction (AMI). The aim of the current study was to identify featured metabolism-related genes in patients with AMI using a support vector machine (SVM) and to further explore the value of these genes in the diagnosis of AMI. *Methods*. Gene microarray expression data related to AMI were downloaded from the GSE66360 dataset in the Gene Expression Omnibus (GEO) database. This data set consisted of 50 AMI samples and 49 normal controls that were randomly classified into a discovery cohort (21 AMI samples and 22 normal controls) and a validation cohort (28 AMI and 28 normal controls). We applied a machine learning method that combined SVM with recursive feature elimination (RFE) to discriminate AMI patients from normal controls. Based on this, an SVM classifier was constructed. Receiver operating characteristic (ROC) analysis was used to investigate the predictive value for the early diagnosis of AMI in the two cohorts and was then further verified in an independent external cohort. *Results*. Three metabolism-related genes were identified based on SVM-RFE (*AKR1C3*, *GLUL*, and *PDE4B*). The SVM classifier based on the three genes allowed for excellent discrimination between AMI and healthy samples in both the discovery cohort (AUC = 0.989) and the validation cohort (AUC = 0.964), and this was further confirmed in the GSE68060 dataset (AUC = 0.839). Additionally, the SVM classifier allowed for perfect discrimination between recurrent AMI events and nonrecurrent events in the GSE68060 cohort (AUC = 0.992). GO and KEGG pathway enrichment analysis of the identified featured genes revealed significant enrichment of specific metabolic pathways. *Conclusion*. The identified metabolism-related genes may play important roles in the development of AMI and may represent diagnostic and therapeutic biomarkers of AMI.

1. Introduction

AMI results from interrupted blood flow to a certain area of the heart and is considered one of the primary causes of disability and death from cardiovascular disease worldwide, thus posing a serious threat to human health [1]. Over the last decade, the primary therapeutic strategies, including percutaneous coronary intervention, coronary artery bypass surgery, and medications, have improved the prognosis of AMI. However, approximately one-third of eligible patients failed to receive early reperfusion therapy due to late detection [2]. Early diagnosis and interventional therapy are beneficial in that they significantly reduce mortality and improve prognosis [3]. Therefore, an early diagnosis may markedly contribute to overall survival.

The diagnosis of AMI is typically based upon the observation of changes in a surface electrocardiogram (ECG) and blood levels of sensitive and specific biomarkers such as cTnI/T and CKMB. However, the sensitivity and specificity of these biomarkers remain unsatisfactory, often resulting in a lack of diagnosis or misdiagnosis [3, 4]. Based on this, potential biomarkers possessing high sensitivity and specificity for early diagnosis of AMI are urgently required and could ultimately contribute to improved clinical survival. Gene expression profiles related to AMI have been previously studied. The differentially expressed genes related to cardiovascular events exhibit similar variation components to those of AMI-related genes. Regardless of if they are upregulated or downregulated, they change in the same direction [5]. This study suggests that differentially expressed genes may provide a new biomarker

for predicting AMI. Recently, metabolic pathways in cardiovascular disease have been demonstrated to represent potential new valuable targets for drug therapy [6, 7]. A recent study revealed that exercise improves cardiac function and glucose metabolism in mice with experimental myocardial infarction by inhibiting phosphorylated histone deacetylase 4 (*HDAC4*) and upregulating glucose transporter 1 (*GLUT1*) expression. These results demonstrated that metabolic processes play a pivotal role in the biological processes underlying AMI. Metabolism-related genes have been studied in the context of cardiac ischemia. By inhibiting miR-92a-3p, LNA-92a can increase endothelial cell autophagy and regulate the expression of metabolism-related genes, thereby increasing myocardial fatty acid uptake and mitochondrial function. These prosurvival mechanisms may reduce tissue damage after myocardial infarction [8]. However, the role of metabolism-related genes in AMI remains to be fully elucidated.

In this study, differentially expressed metabolism-related genes were identified in normal and AMI samples. Next, an SVM classifier consisting of three risk genes was established. This classifier allowed patient samples to be distinguished from normal controls.

2. Materials and Methods

2.1. Microarray Data. To investigate metabolism-related genes, the microarray data for AMI were collected from the GEO (http://www.ncbi.nlm.nih.gov/geo/) database under the accession number GSE66360, where 50 AMI samples and 49 normal controls were included. The dataset was divided into a discovery cohort (21 AMI samples and 22 normal controls) and a validation cohort (28 AMI samples and 28 normal controls). Furthermore, the GSE48060 dataset consisting of 31 AMI patients and 21 healthy controls was obtained to confirm the performance of the SVM classifier. Additionally, 5 recurrence and 26 no-recurrence samples over a 1.5-year follow-up period were included in the GSE48060 dataset. All datasets were produced using the Affymetrix Human Genome U133 Plus 2.0 Array. Background correction and normalization were performed using linear models for the microarray data (LIMMA) software package. Normalization between arrays was performed using the quantile algorithm in LIMMA.

2.2. Metabolism-Related Genes. Metabolism-related genes were obtained from the Molecular Signatures Database v7.1 (MSigDB) (http://software.broadinstitute.org/gsea/msigdb) by searching using the term "metabolism." The C2 (c2.cp.kegg.v7.1.symbols.gmt) subcollection was selected as the reference gene set (Supplementary Table 1). A total of 948 unique metabolism-related genes were obtained. Next, we extracted the metabolism-related gene expression matrix from the GSE66360 dataset using the R language merge package. Finally, a gene expression matrix consisting of 862 gene expression values was obtained in the discovery cohort.

2.3. Screening of Differentially Expressed Metabolism-Related Genes. The analysis of differentially expressed metabolism-related genes between AMI and normal samples was con-

ducted using the LIMMA package implemented in the R statistical package (http://www.r-project.org). The threshold for the identification of differentially expressed genes was set at a P value of <0.05 and a |log 2fold change (FC) | ≥1.

2.4. Featured Gene Selection and the SVM Classifier Construction. The featured selection technique is an efficient tool for identifying meaningful information from a given gene dataset [9]. SVM is a supervised learning model that is aimed at classifying data points by maximizing the distance of a hyperplane for classification and regression analysis with high accuracy [10]. SVM-RFE is a popular feature selection technique and has exhibited promising and expanding applications for the analysis of high-dimensional data. It is much more robust with regard to data overfitting and classification accuracy than many other feature selection methods, and this technique has demonstrated its power in many fields, including metabolomics [11–13]. Therefore, we applied a machine learning method that combined SVM with RFE to select the best parameters for gene selection among all differentially expressed metabolism-related genes. Using this algorithm, optional feature genes were identified as risk genes in the context of AMI. Next, the identified feature genes were added into an SVM classifier with a radial basis function (RBF) kernel and 5-fold cross-validation to achieve predictions. To test the value of the identified featured genes, a heat map was clustered using the pheatmap package in R for all samples in the two cohorts (clustering method = "ward"). The Euclidean distance was used to cluster samples. Furthermore, the discriminatory power of the SVM classifier was measured according to the AUC (defined as the area under the receiver operating curve) in both cohorts, and this was further validated in the independent external cohort. Additionally, the performance of the SVM classifier was further explored in terms of AMI recurrence and nonrecurrence.

2.5. Functional Enrichment Analysis of Identified Feature Genes. To explore the functions and pathways of the identified feature genes, gene ontology (GO) and Kyoto Encyclopedia of Genes and Genomes (KEGG) pathway enrichment analyses were performed to identify potential functional components and pathways underlying numerous genes using the clusterProfiler package [14]. $P < 0.05$ was considered to be statistically significant.

2.6. Statistical Analysis. The differentially expressed metabolism-related genes were identified using the Limma package with $P < 0.05$ and |log 2fold change (FC) | ≥1 as the cut-off criteria. Featured gene selection was performed using the RFE function in the caret package with 5-fold cross-validation. The SVM classifier was constructed using R package e1071 with 5-fold cross-validation. Hierarchical clustering analysis was used for the identified featured genes using the pheatmap package in R. ROC analysis was performed, and the area under the curve (AUC) was calculated to evaluate the predictive performance of the classifier. $P < 0.05$ was considered to indicate a statistically significant difference. All statistical analyses were performed using R software (version 3.6.3, http://www.r-project.org).
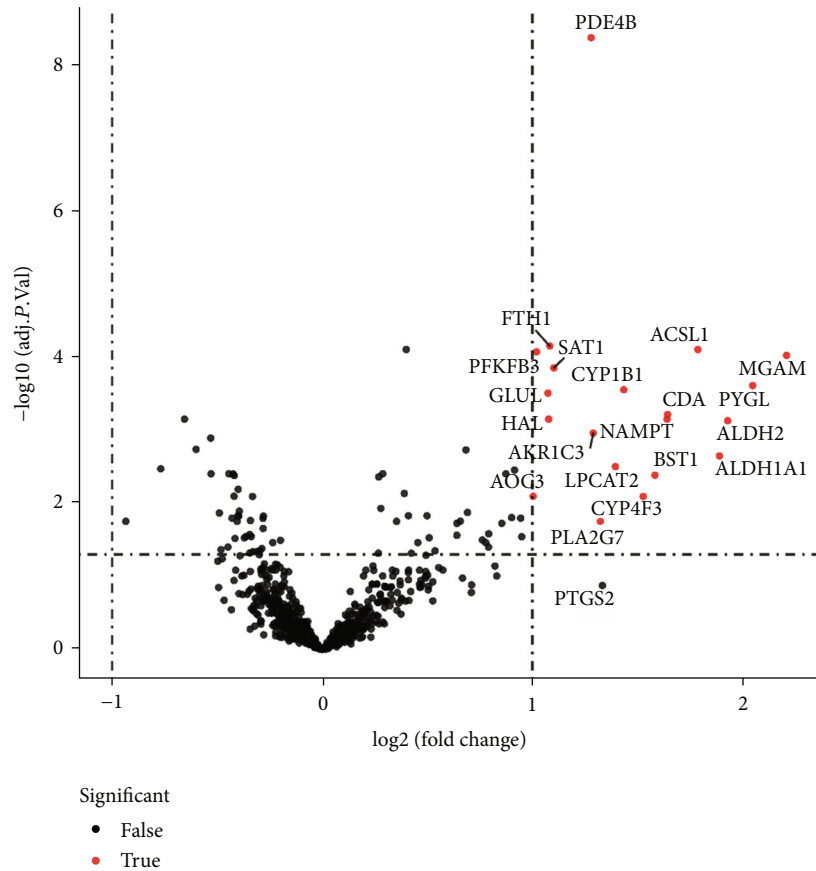
FIGURE 1: Differential expression of metabolic-related genes in AMI tissue and normal samples.

3. Results

3.1. Identification of Differentially Expressed Metabolism-Related Genes and Feature Genes. A total of 17 differentially expressed upregulated genes were identified between AMI tissues and normal tissues (Figure 1.). Based on the SVM-RFE algorithm, three genes (*AKR1C3*, *GLUL*, and *PDE4B*) with minimum root mean square error were fit into the SVM classifier (Figure 2). Hierarchical clustering analysis in the discovery cohort (Figure 3(a)) and the validation cohort (Figure 3(b)) revealed that patients could be clearly separated into two clusters based on the expression levels of the three identified feature genes. To validate the expression levels of three featured genes, the identified featured genes were confirmed in the validation cohort. As shown in Figure 4, the expression levels of two featured genes (*GLUL* and *PDE4B*) in AMI tissues were significantly higher than those in the control group (*P* < 0.05).

3.2. Diagnostic Value of Three Feature Genes in AMI. As presented in Figure 5(a), the results of the 5-fold cross-validation illustrated that the SVM classifier allowed for good classification in the discovery cohort between AMI and normal controls with an AUC of 0.989 (95% CI = 0.966-1.00), a sensitivity of 95.24%, and a specificity of 100.00%. The SVM classifier demonstrated excellent discriminatory ability in the validation cohort with an AUC of 0.964 (95% CI = 0.925
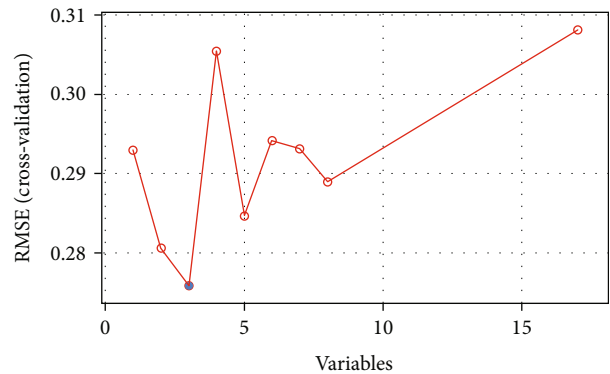
FIGURE 2: A plot of feature metabolic-related gene selection by recursive feature elimination.

-1.000), a sensitivity of 85.71%, and a specificity of 92.86% (Figure 5(b)). The discrimination power was confirmed in the independent GSE48060 cohort with an AUC of 0.839 (95% CI = 0.715-0.962), a sensitivity of 83.87%, and a specificity of 90.95% (Figure 5(c)). Furthermore, we investigated the discrimination ability of the classifier in the context of recurrent AMI. The classifier exhibited outstanding discrimination ability of recurrent AMI with an AUC of 0.992 (95% CI = 0.971-1.00), a sensitivity of 100%, and a specificity of 96.15% (Figure 5(d)).
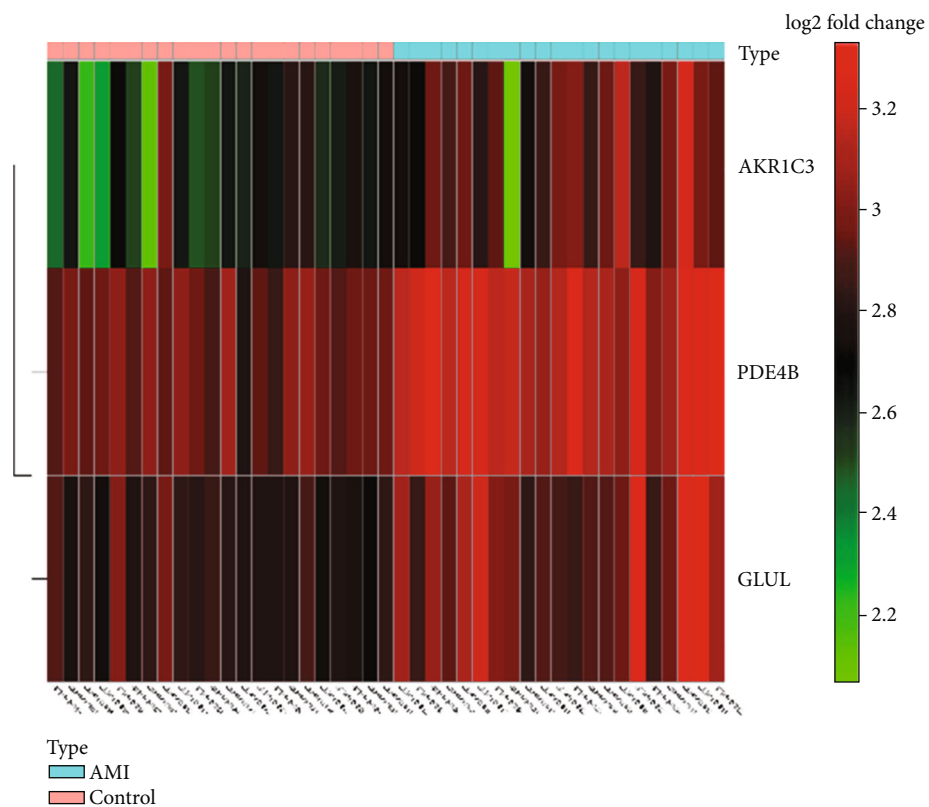
(a)
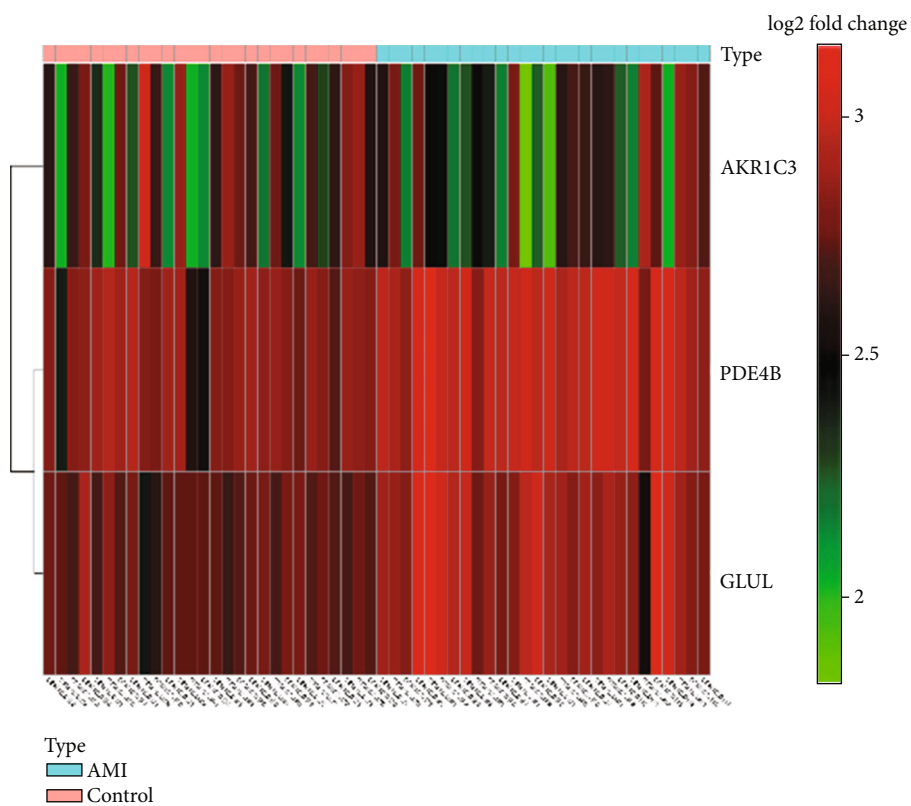
(b)

FIGURE 3: Hierarchical clustering analysis demonstrates identified metabolic-related gene expression patterns between AMI and normal tissues in the discovery cohort (a) and validation cohort (b).
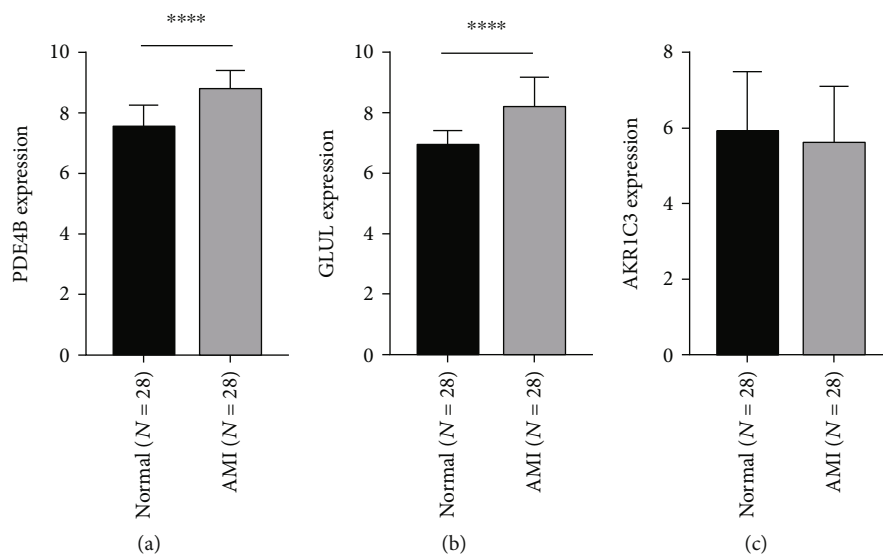
FIGURE 4: Validation of expression level of identified feature genes in patients with AMI and normal tissues in the validation cohort. (a) PDE4B, (b) GLUL, and (c) AKR1C3.

3.3. *Functional Analysis of Feature Genes.* Based on our results, cellular response to starvation, cellular response to nutrient levels, cellular response to extracellular stimulus, diterpenoid biosynthetic process, small molecule catabolic process, cyclooxygenase pathway, and negative regulation of hormone metabolic processes were the most significantly enriched biological processes (Figure 6(a)). Additionally, nitrogen metabolism, arginine biosynthesis, and folate biosynthesis were considered to be the most remarkably enriched pathways (Figure 6(b)).

4. Discussion

AMI remains a primary cause of death and disability worldwide despite significant improvements in diagnosis. The in-hospital mortality for AMI remains high [15]. Recently, metabolism-related processes have been reported to be involved in the pathogenesis of AMI [7, 16]. *PRODH* overexpression increases the number of gene transcripts related to metabolism, and this gene is related to the maintenance of normal mitochondrial function, ATP level, and redox homeostasis of human cardiomyocytes in a hypoxic environment [17]. However, the potential role of metabolism-related genes in AMI remains poorly understood. Single-nucleotide polymorphisms (SNPs) in some lipid metabolism-related genes are closely related to blood lipids and can cause coronary artery disease [18]. A study from Pakistan revealed that SNPs in lipid metabolism genes are significantly associated with MI susceptibility [19]. Circadian rhythm disorders can cause worsening of atherosclerosis [20]. A large number of metabolism-related genes exhibit a circadian rhythm [21]. Zhu et al. found that abnormal light can aggravate the circadian rhythm of lipid metabolism genes [22]. The above studies indicate that metabolic genes may increase the risk of AMI by affecting lipid metabolism.

To identify the metabolism-related genes that are involved in AMI, GSE66360 datasets were used to screen differentially expressed genes in patient tissues and control tissues. By comparing the expression levels of metabolism-related genes between AMI patients and healthy samples, we found that 17 genes were differentially expressed in AMI compared to healthy samples, indicating that metabolism-related genes may play critical roles in the occurrence of AMI. Next, three featured genes in AMI samples were identified using the SVM-RFE algorithm that allows AMI samples to be distinguished from normal samples. The SVM classifier based on the identified featured genes allowed for good classification with an AUC of 0.989 for the patient samples. The discrimination power values of the classifiers for the validation cohort and the independent validation cohort were 0.964 and 0.839, respectively. Furthermore, the SVM classifier can successfully distinguish patients with recurrent and nonrecurrent AMI with an AUC of 0.992. Therefore, the present study suggested that the featured genes could provide useful markers for identifying patients with AMI.

The present study demonstrated the potential value of metabolic-related genes in the context of AMI in the clinical setting. *GLUL*, *PDE4B*, and *AKR1C3* were identified as potential metabolism-related genes that were associated with AMI and the recurrence of AMI. Glutamate-ammonia ligase (*GLUL*) belongs to the glutamine synthetase family and functions to catalyze the synthesis of glutamine from glutamate and ammonia in an ATP-dependent reaction [23]. Genetic studies have revealed a *GLUL* rs10911021 polymorphism that is associated with cardiovascular disease morbidity and mortality among people with type 2 diabetes [24]. Genome-wide association analyses suggested that the *GLUL* may regulate the risk of coronary heart disease by affecting glutamate/glutamine metabolism and the activity of the γ-glutamine cycle [25]. Coronary heart disease is the primary cause of death in patients with diabetes, and genetic factors can also act as risk factors for increased mortality. Clinical studies from European populations indicate that SNP rs10911021 is an independent risk factor for all-cause mortality in patients with
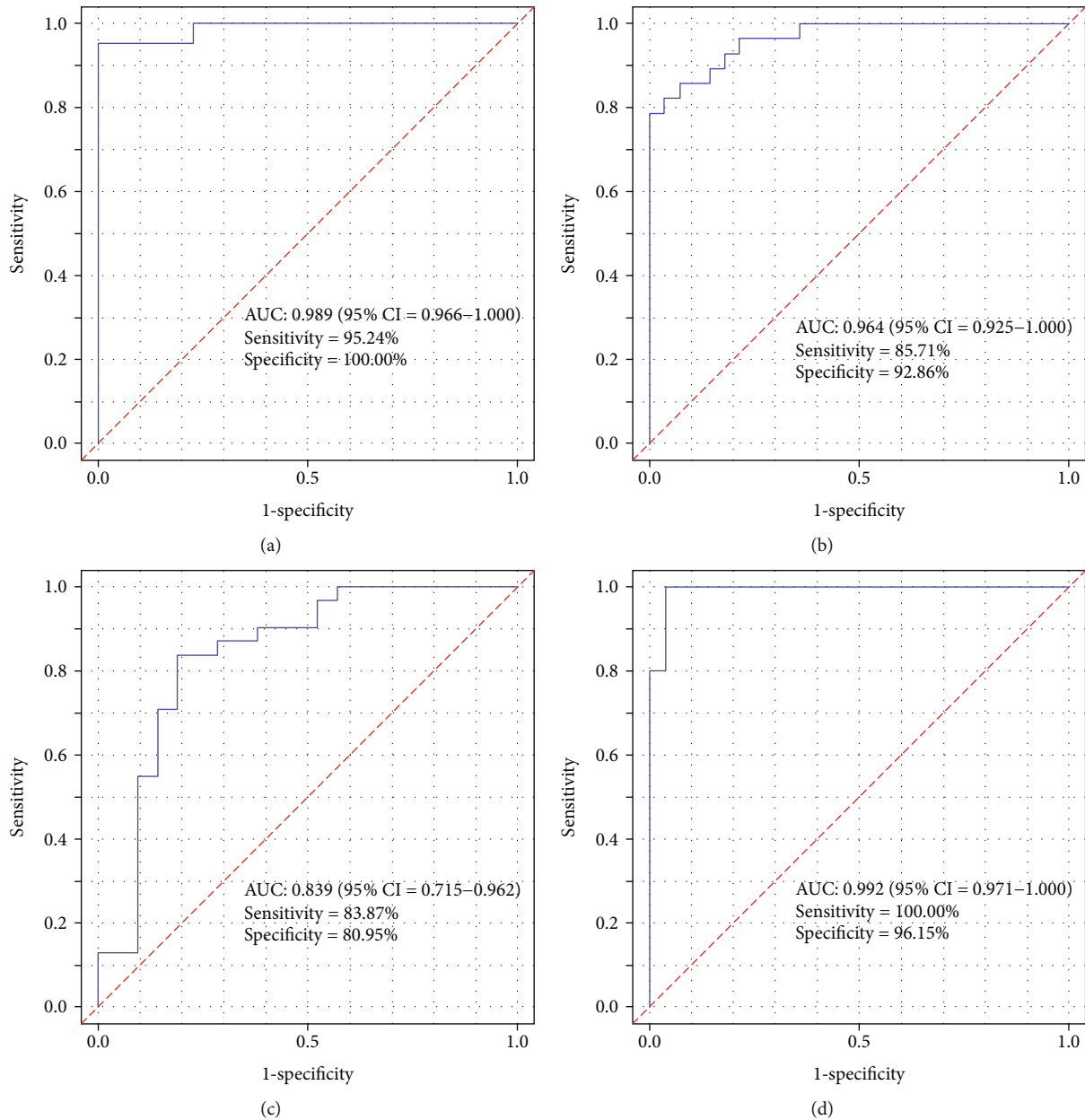
FIGURE 5: Receiver operating characteristic curves of support vector machine classifier for the discovery cohort (a), the validation cohort (b), the independent external cohort (c), and ROC analysis of the SVM classifier for AMI recurrent prediction in the independent external cohort (d).

type 2 diabetes, and the risk may be due to cardiovascular disease [26]. *GLUL* has also been reported to be involved in endothelial cell motility, a process that affects endothelial cell junctional integrity [27]. These studies provide possible explanations for the role of *GULU* in AMI.

The phosphodiesterase 4B (*PDE4B*) gene is a member of the type IV cAMP-specific, cyclic nucleotide phosphodiesterase (PDE) family that regulates the cellular concentrations of cyclic nucleotides and thereby plays a role in signal transduction. In the myocardium, the PDE3 and PDE4 families are primarily used to degrade cAMP and regulate excitation-contraction coupling (ECC). PDE4 is responsible for 40% of cAMP-hydrolysis activity in human heart tissue [28]. Animal experiments have demonstrated that the primary

function of PDE4 is the control of the cAMP signal, and PDE4 is responsible for the majority of the cAMP degradation activity in rat ventricular cells [29, 30]. In the heart, cAMP regulates contraction, relaxation, and autonomy. When the regulation of this molecule is imbalanced, it significantly promotes the development of heart disease. Wang et al. demonstrated that a moderate increase in cAMP levels prevents the Ca^{2+}-induced mitochondrial permeability transition pore (MPTP) from opening through Epac1, thus affecting the death of cardiomyocytes [31]. A number of studies have also confirmed that PDE4 is related to arrhythmia and heart failure [32–34]. These studies may reveal the molecular mechanism of *PDE4B* in AMI; however, more detailed mechanisms require further exploration.

(a)

(b)
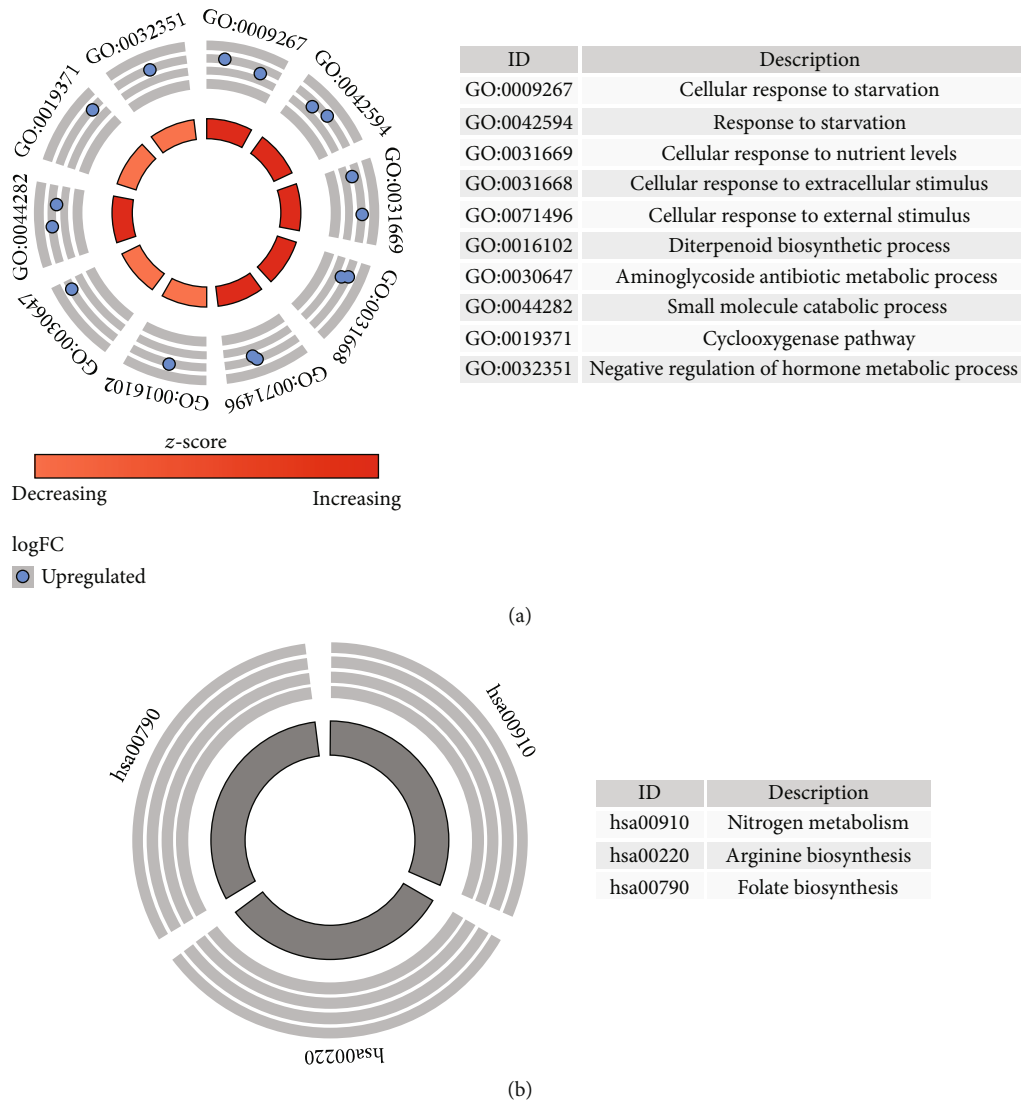
FIGURE 6: GO and KEGG pathway analysis of identified feature genes.

The aldo-keto reductase family 1 member C3 (*AKR1C3*) gene is the only 17β-HSD that is not a short-chain dehydrogenase/reductase, and this gene encodes a member of the aldose/-ketoreductase superfamily. *AKR1C3* has been confirmed to play a regulatory role in a variety of endocrine diseases [35]. Su et al. confirmed that *AKR1C3* modulates vasodilation and vasoconstriction by regulating the biosynthesis of prostaglandins [36]. Prostacyclin is a vasodilator that can inhibit platelet activation. Imbalances in prostacyclin production can result in an increased risk for coronary events [37]. *AKR1C3* did not show a significant difference in expression in AMI and control in the validation dataset GSE48060. Based on this, *AKR1C3* may influence AMI; however, given the small number of research studies examining this process, more research is required to provide a fuller understanding of the relationship between *AKR1C3* and AMI.

As revealed in the GO and KEGG pathway analyses, these featured genes were primarily enriched in metabolism-related processes, thus indicating that metabolism-related

genes play an important role in AMI. As an important process of lipid metabolism, autophagy is activated by starvation [38, 39]. Autophagy is also a regulated pathway of cellular deprivation [40]. Prostaglandins have been reported to be related to AMI [41, 42]. Thyroid hormone exerts an important therapeutic effect by reducing the infarct size and improving myocardial function after acute myocardial infarction [43]. Clinical studies have shown that in adults with hypertension, both low folate and high folate levels are associated with an increased risk for death from cardiovascular disease [44]. Arginine has also been confirmed to be associated with AMI [45, 46].

Our study does possess certain limitations. First, we failed to validate the discriminatory ability of the SVM classifier in the independent cohort with respect to the recurrent event. Second, although the ROC analysis of the support vector machine classifier for AMI recurrence prediction yields good results, the sample size for recurrent AMI was small, and its accuracy requires further verification using larger sample

sizes. Finally, it should be noted that this research was based on bioinformatics analyses. Therefore, further validations *in vivo* and *in vitro* are required.

5. Conclusion

The present study identified three metabolic-related genes (*GLUL*, *PDE4B*, and *AKR1C3*) in patients with AMI, and these genes may be useful as potential biomarkers in the diagnosis of AMI. Knowledge of these genes will improve our understanding of the molecular mechanism underlying the occurrence of AMI.

Data Availability

The raw data of this study are derived from the GEO data portal (https://www.ncbi.nlm.nih.gov/geo/; accession numbers: GSE66360 and GSE68060), which is a publicly available database.

Conflicts of Interest

The authors declare that they have no conflicts of interest.

Authors' Contributions

Hang Xie and Enfa Zhao contributed equally to this work and should be considered co-first authors.

Supplementary Materials

Supplementary table 1: reference gene set. *(Supplementary Materials)*

References

[1] J. Guo, H.-B. Liu, C. Sun et al., "MicroRNA-155 promotes myocardial infarction-induced apoptosis by targeting RNA-binding protein QKI," *Oxidative Medicine and Cellular Longevity*, vol. 2019, Article ID 4579806, 14 pages, 2019.

[2] M. Cohen, G. F. Gensini, F. Maritz et al., "Prospective evaluation of clinical outcomes after acute ST-elevation myocardial infarction in patients who are ineligible for reperfusion therapy: preliminary results from the TETAMI registry and randomized trial," *Circulation*, vol. 108, no. 90161, pp. 14-III--14II21, 2003.

[3] E. Braunwald, "Unstable angina and non-ST elevation myocardial infarction," *American Journal of Respiratory and Critical Care Medicine*, vol. 185, no. 9, pp. 924–932, 2012.

[4] J. P. Park, M. K. Park, and J. W. Yun, "Proteomic biomarkers for diagnosis in acute myocardial infarction," *Biomarkers*, vol. 16, no. 1, pp. 1–11, 2010.

[5] J. Kim, N. Ghasemzadeh, D. J. Eapen et al., "Gene expression profiles associated with acute myocardial infarction and risk of cardiovascular death," *Genome Medicine*, vol. 6, no. 5, p. 40, 2014.

[6] D. M. Lloyd-Jones, "Cardiovascular risk prediction: basic concepts, current status, and future directions," *Circulation*, vol. 121, no. 15, pp. 1768–1777, 2010.

[7] G. D. Lewis, A. Asnani, and R. E. Gerszten, "Application of metabolomics to cardiovascular biomarker and pathway discovery," *Journal of the American College of Cardiology*, vol. 52, no. 2, pp. 117–123, 2008.

[8] E. M. Rogg, W. T. Abplanalp, C. Bischof et al., "Analysis of cell type-specific effects of microRNA-92a provides novel insights into target regulation and mechanism of action," *Circulation*, vol. 138, no. 22, pp. 2545–2558, 2018.

[9] X. Lin, F. Yang, L. Zhou et al., "A support vector machine-recursive feature elimination feature selection method based on artificial contrast variables and mutual information," *Journal of Chromatography. B, Analytical Technologies in the Biomedical and Life Sciences*, vol. 910, pp. 149–155, 2012.

[10] V. Cherkassky, "The nature of statistical learning theory~," *IEEE Transactions on Neural Networks*, vol. 8, no. 6, p. 1564, 1997.

[11] I. Guyon, "Erratum: gene selection for cancer classification using support vector machines," *Machine Learning*, vol. 46, no. 1-3, pp. 389–422, 2001.

[12] M. Pirooznia, J. Y. Yang, M. Q. Yang, and Y. Deng, "A comparative study of different machine learning methods on microarray gene expression data," *BMC Genomics*, vol. 9, Supplement 1, p. S13, 2008.

[13] S. Mahadevan, S. L. Shah, T. J. Marrie, and C. M. Slupsky, "Analysis of metabolomic data using support vector machines," *Analytical Chemistry*, vol. 80, no. 19, pp. 7562–7570, 2008.

[14] G. Yu, L. G. Wang, Y. Han, and Q. Y. He, "clusterProfiler: an R package for comparing biological themes among gene clusters," *OMICS*, vol. 16, no. 5, pp. 284–287, 2012.

[15] S. Boateng and T. Sanborn, "Acute myocardial infarction," *Disease-a-Month*, vol. 59, no. 3, pp. 83–96, 2013.

[16] H. Jiang, D. Jia, B. Zhang et al., "Exercise improves cardiac function and glucose metabolism in mice with experimental myocardial infarction through inhibiting HDAC4 and upregulating GLUT1 expression," *Basic Research in Cardiology*, vol. 115, no. 3, p. 28, 2020.

[17] J. B. N. Moreira, M. Wohlwend, S. Fenk et al., "Exercise reveals proline dehydrogenase as a potential target in heart failure," *Progress in Cardiovascular Diseases*, vol. 62, no. 2, pp. 193–202, 2019.

[18] C. J. Willer, S. Sanna, A. U. Jackson et al., "Newly identified loci that influence lipid concentrations and risk of coronary artery disease," *Nature Genetics*, vol. 40, no. 2, pp. 161–169, 2008.

[19] R. Iqbal, N. Jahan, Y. Sun, and H. Xue, "Genetic association of lipid metabolism related SNPs with myocardial infarction in the Pakistani population," *Molecular Biology Reports*, vol. 41, no. 3, pp. 1545–1552, 2014.

[20] C. B. Anea, M. Zhang, D. W. Stepp et al., "Vascular disease in mice with a dysfunctional circadian clock," *Circulation*, vol. 119, no. 11, pp. 1510–1517, 2009.

[21] K. F. Storch, O. Lipan, I. Leykin et al., "Extensive and divergent circadian gene expression in liver and heart," *Nature*, vol. 417, no. 6884, pp. 78–83, 2002.

[22] Z. Zhu, B. Hua, Z. Shang et al., "Altered clock and lipid metabolism-related genes in atherosclerotic mice kept with abnormal lighting condition," *BioMed Research International*, vol. 2016, Article ID 5438589, 14 pages, 2016.

[23] Y. Wang, S. Fan, J. Lu et al., "GLUL promotes cell proliferation in breast cancer," *Journal of Cellular Biochemistry*, vol. 118, no. 8, pp. 2018–2025, 2017.

[24] H. Tang and C. Gao, "Comment on The Look AHEAD Research Group. Prospective association ofGLULrs10911021 with cardiovascular morbidity and mortality among individuals with type 2 diabetes: the Look AHEAD Study. Diabetes 2016;65:297-302," *Diabetes*, vol. 65, no. 9, p. e29, 2016.

[25] L. Qi, Q. Qi, S. Prudente et al., "Association between a genetic variant related to glutamic acid metabolism and coronary heart disease in individuals with type 2 diabetes," *JAMA*, vol. 310, no. 8, pp. 821–828, 2013.

[26] S. Prudente, H. Shah, D. Bailetti et al., "Genetic variant at the GLUL locus predicts all-cause mortality in patients with type 2 diabetes," *Diabetes*, vol. 64, no. 7, pp. 2658–2663, 2015.

[27] G. Eelen, C. Dubois, A. R. Cantelmo et al., "Role of glutamine synthetase in angiogenesis beyond glutamine synthesis," *Nature*, vol. 561, no. 7721, pp. 63–69, 2018.

[28] D. Mika, P. Bobin, M. Lindner et al., "Synergic PDE3 and PDE4 control intracellular cAMP and cardiac excitation-contraction coupling in a porcine model," *Journal of Molecular and Cellular Cardiology*, vol. 133, pp. 57–66, 2019.

[29] J. Leroy, A. Abi-Gerges, V. O. Nikolaev et al., "Spatiotemporal dynamics of β-Adrenergic cAMP signals and L-type Ca2+Channel regulation in adult rat ventricular Myocytes," *Circulation Research*, vol. 102, no. 9, pp. 1091–1100, 2008.

[30] M. Mongillo, T. McSorley, S. Evellin et al., "Fluorescence resonance energy transfer-based analysis of cAMP dynamics in live neonatal rat cardiac myocytes reveals distinct functions of compartmentalized phosphodiesterases," *Circulation Research*, vol. 95, no. 1, pp. 67–75, 2004.

[31] Z. Wang, D. Liu, A. Varin et al., "A cardiac mitochondrial cAMP signaling pathway regulates calcium accumulation, permeability transition and cell death," *Cell Death & Disease*, vol. 7, no. 4, p. e2198, 2016.

[32] C. E. Molina, J. Leroy, W. Richter et al., "Cyclic adenosine monophosphate phosphodiesterase type 4 protects against atrial arrhythmias," *Journal of the American College of Cardiology*, vol. 59, no. 24, pp. 2182–2190, 2012.

[33] P. Bobin, A. Varin, F. Lefebvre, R. Fischmeister, G. Vandecasteele, and J. Leroy, "Calmodulin kinase II inhibition limits the pro-arrhythmic Ca2+ waves induced by cAMP-phosphodiesterase inhibitors," *Cardiovascular Research*, vol. 110, no. 1, pp. 151–161, 2016.

[34] S. Karam, J. P. Margaria, A. Bourcier et al., "Cardiac overexpression of PDE4B blunts β-adrenergic response and maladaptive remodeling in heart failure," *Circulation*, vol. 142, no. 2, pp. 161–174, 2020.

[35] T. M. Penning, "AKR1C3 (type 5 17β-hydroxysteroid dehydrogenase/prostaglandin F synthase): roles in malignancy and endocrine disorders," *Molecular and Cellular Endocrinology*, vol. 489, pp. 82–91, 2019.

[36] E. J. Su, L. Ernst, N. Abdallah et al., "Estrogen receptor-β and fetoplacental endothelial prostanoid biosynthesis: a link to clinically demonstrated fetal growth restriction," *The Journal of Clinical Endocrinology and Metabolism*, vol. 96, no. 10, pp. E1558–E1567, 2011.

[37] P. M. Kearney, C. Baigent, J. Godwin, H. Halls, J. R. Emberson, and C. Patrono, "Do selective cyclo-oxygenase-2 inhibitors and traditional non-steroidal anti-inflammatory drugs increase the risk of atherothrombosis? Meta-analysis of randomised trials," *BMJ*, vol. 332, no. 7553, pp. 1302–1308, 2006.

[38] R. Singh, S. Kaushik, Y. Wang et al., "Autophagy regulates lipid metabolism," *Nature*, vol. 458, no. 7242, pp. 1131–1135, 2009.

[39] N. Mizushima, "Autophagy: process and function," *Genes & Development*, vol. 21, no. 22, pp. 2861–2873, 2007.

[40] D. J. Klionsky and S. D. Emr, "Autophagy as a regulated pathway of cellular degradation," *Science*, vol. 290, no. 5497, pp. 1717–1721, 2000.

[41] C. W. Sung, J. H. Jung, S. H. Lee et al., "Acute myocardial infarction due to vasospasm induced by prostaglandin," *The Canadian Journal of Cardiology*, vol. 25, no. 10, pp. e359–e360, 2009.

[42] A. A. Elesber, P. J. Best, R. J. Lennon et al., "Plasma 8-iso-prostaglandin F2alpha, a marker of oxidative stress, is increased in patients with acute myocardial infarction," *Free Radical Research*, vol. 40, no. 4, pp. 385–391, 2009.

[43] A. Jabbar, A. Pingitore, S. H. S. Pearce, A. Zaman, G. Iervasi, and S. Razvi, "Thyroid hormones and cardiovascular disease," *Nature Reviews. Cardiology*, vol. 14, no. 1, pp. 39–55, 2017.

[44] S. Nkemjika, E. Ifebi, L. T. Cowan et al., "Association between serum folate and cardiovascular deaths among adults with hypertension," *European Journal of Clinical Nutrition*, vol. 74, no. 6, pp. 970–978, 2020.

[45] P. Tripathi, M. K. Misra, and S. Pandey, "Role of l-arginine on dyslipidemic conditions of acute myocardial infarction patients," *Indian Journal of Clinical Biochemistry*, vol. 27, no. 3, pp. 296–299, 2012.

[46] M. Du, W. Yang, S. Schmull, J. Gu, and S. Xue, "Inhibition of peptidyl arginine deiminase-4 protects against myocardial infarction induced cardiac dysfunction," *International Immunopharmacology*, vol. 78, p. 106055, 2020.

Research Article

Reversed Septal Curvature Is Associated with Elevated Troponin Level in Hypertrophic Cardiomyopathy

Renata Rajtar-Salwa,[1] **Tomasz Tokarek** [ID],[1] **and Paweł Petkow Dimitrow** [ID][2]

[1]*Department of Cardiology and Cardiovascular Interventions, University Hospital, Jakubowskiego 2 St., 30-688 Krakow, Poland*
[2]*2nd Department of Cardiology, Institute of Cardiology, Jagiellonian University Medical College, 31-501 Krakow, Poland*

Correspondence should be addressed to Paweł Petkow Dimitrow; dimitrow@mp.pl

The aim of study was to compare patients with hypertrophic cardiomyopathy divided according to septal configuration assessed in a 4-chamber apical window. The study group consisted of 56 consecutive patients. Reversed septal curvature (RSC) and non-RSC were diagnosed in 17 (30.4%) and 39 (69.6%) patients, respectively. Both RSC and non-RSC groups were compared in terms of the level of high-sensitivity troponin I (hs-TnI), NT-proBNP (absolute value), NT-proBNP/ULN (value normalized for sex and age), and echocardiographic parameters, including left ventricular outflow tract gradient (LVOTG). A higher level of hs-TnI was observed in RSC patients as compared to the non-RSC group (102 (29.2-214.7) vs. 8.7 (5.3-18) (ng/l), $p = 0.001$). A trend toward increased NT-proBNP value was reported in RSC patients (1279 (367.3-1186) vs. 551.7 (273-969) (pg/ml), $p = 0.056$). However, no difference in the NT-proBNP/ULN level between both groups was observed. Provocable LVOTG was higher in RSC as compared to non-RSC patients (51 (9.5-105) vs. 13.6 (7.5-31) (mmHg), $p = 0.04$). Furthermore, more patients with RSC had prognostically unfavourable increased septal thickness to left LV diameter at the end diastole ratio. Patients with RSC were associated with an increased level of hs-TnI, and the only trend observed in this group was for the higher NT-proBNP levels. RSC seems to be an alerting factor for the risk of ischemic events. Not resting but only provocable LVOTG was higher in RSC as compared to non-RSC patients.

1. Introduction

Monitoring of biomarkers including troponin (Tn) and N-terminal pro-B-type NT-pronatriuretic peptide (NT-proBNP) might be utilized in the clinical evaluation, management, and prognosis of patients with hypertrophic cardiomyopathy (HCM) [1]. Recently reported papers have studied the importance of very short time synchronization in the sampling of echocardiographic parameters and cardiac biomarkers in HCM [2, 3]. The strategy of these studies was based on performing transthoracic echocardiography (TTE) and evaluation of hs-troponin I and NT-proBNP as close to each other as possible. Such tactic guarantees that currently detected ischemia is related to actual myocardial functional/dynamic status with provoked left ventricular outflow tract gradient (LVOTG) as an equivalent. This protocol is crucial to obtain reliable results of this unstable

parameter. Provocation of higher LVOTG is strongly associated with increased myocardial oxygen consumption inducing ischemia [4, 5]. The strategy of simultaneous measurement of the relationship between gradient provocation and ischemia induction was confirmed in invasive studies [4, 5]. Thus, the potential relationship between current ischemia (probably frequently repeated in past history) and echocardiographic stabile septal configuration predisposing to myocardial ischemia (possibly even during all the life span) should be evaluated. This echocardiographic abnormal configuration is reversed septal curvature (RSC) visualized in 4-chamber apical view. Importantly, a pathomorphological study revealed that RSC occurs more frequently in young than in elderly victims of sudden cardiac death (SCD) [6]. This fact might suggest that majority of patients with RSC configuration died prematurely probably due to ischemia-provoked ventricular fibrillation. In a
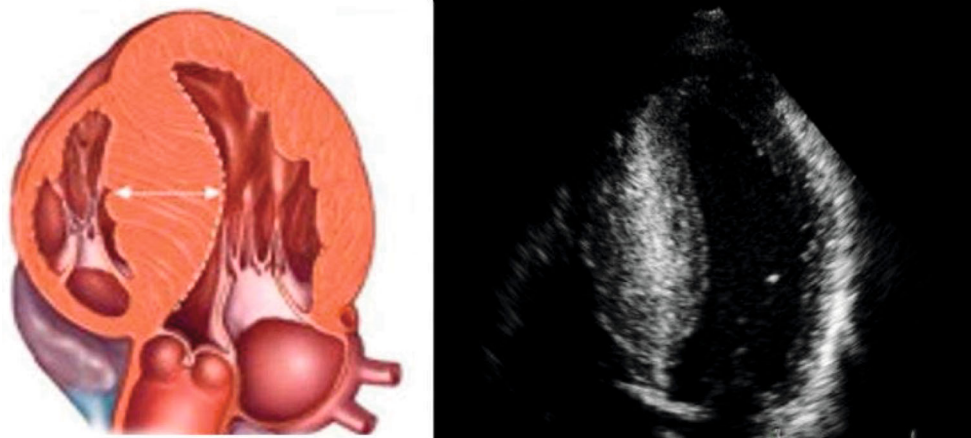
Figure 1: Reversed septal curvature. Predominant midseptal convexity toward left ventricle cavity; crescent-shaped cavity.

previous study, RSC was considered as a risk factor for SCD in HCM [7]. Thus, we sought to compare both RSC and non-RSC groups in terms of the biomarker level and echocardiographic parameters, including LVOTG.

2. Materials and Methods

The group of adult 56 consecutive patients with HCM was enrolled to study analysis after several exclusions. The study protocol was approved by the local ethics committee board (Bioethics Committee of Jagiellonian University KBET/119/B/2017). All included patients provided written informed consent to participate in the study. The study protocol conforms to the ethical guidelines of the 1975 Declaration of Helsinki with later amendments. All analysed patients fulfilled diagnostic criteria for HCM [8]. The standard definition in adult patients was used to recognize HCM with TTE parameter evaluation ([8]. Patients with ($n = 40$) or without ($n = 16$) prescribed treatment (newly diagnosed patients referred to our ambulatory clinic) were examined by TTE with LVOT gradient provocation by two natural stimuli (orthostatic test and the Valsalva test) [8–10]. Exclusion criteria were as follows: ST-segment or non-ST-segment elevation myocardial infarction (current or previous), significant coronary stenosis in recent coronary angiography, previous alcohol septal ablation, dilated LV cavity and decreased LV contractibility, atrial fibrillation, and arterial hypertension. Only patients with LV ejection fraction > 50% were enrolled. Furthermore, renal failure is a typical extracardiac factor related to TnI elevation. To overcome potential bias related to this factor, patients with elevated serum creatinine levels resulting in estimated glomerular filtration rate < 60 ml/min/1.73 m^2 were excluded from the study group.

We performed genetic analysis with positive findings only in part of our patients [11]. According to Bos et al. [12], univariate and multivariate analyses demonstrated echocardiographic RSC, age at diagnosis < 45 years, maximal LVWT ≥ 20 mm, family history of HCM, and family history of SCD to be positive predictors of the positive genetic test while hypertension was a negative predictor. All our patients

had at least one above-mentioned predictor of the positive genetic test, and the negative predictor was excluded.

Several storage diseases were excluded using the following criteria. Fabry disease was excluded by the absence of clinical signs and symptoms: acroparesthesis, angiokeratomas, anhydrosis, and renal dysfunction—proteinuria and lower filtration rate. Finally, in suspected patients, enzymatic analysis was performed. Pompe or Danon diseases were excluded by the following exclusive criteria: (1) patients below 18 years of age, (2) muscle weakness, skeletal myopathy, and (3) elevation of creatine kinase. Apart from storage disease, patients treated with steroids or tacrolimus were excluded.

Only patients with coronary microvessel disease, which might be common in HCM at any age, were enrolled in the study group (inclusion criteria: normal/near-normal coronary arteries or no indication of coronary arteriography). Almost all patients with CCS III class ($n = 9/10$) and one with CCS IV ($n = 1/1$) underwent coronary angiography. Most of the patients have not undergone coronary angiography (young, without angina, and without risk factors for CAD—especially without diabetes mellitus). The probability of CAD was low; thus, there was no clinical indication to perform coronary angiography. Diabetes mellitus is associated with silent ischemia from epicardial coronary arteries; thus, it was necessary to exclude painless macrovascular disease [13]. All included patients were compared according to septal curvature assessed in 4-chamber apical view. There were 39 patients in the subgroup with nonreversed septal curvature (non-RSC) and 17 patients with RSC (Figure 1).

In the non-RSC subgroup, there were basic septal, neutral (no convex/no concave toward LV cavity), and no apical variant. Additionally, we analysed the ratio of septal thickness divided by LV diameter at end diastole moment (STD/LVEDD). This ratio was calculated using echocardiographic parameters measured in long-axis parasternal view. STD was measured also in short-axis parasternal view (if STD was greater than 2 mm (few cases), the patient was excluded) [7]. Patients were also excluded if maximal LV thickness was located out of the septal sector (2 patients). These patients after comprehensive analysis

were rediagnosed as Fabry disease. This parameter is linked to an unfavourable prognosis when the result is above 0.5 [7]. Furthermore, both RSC and non-RSC groups were compared in terms of the level of high-sensitivity troponin I (hs-TnI), NT-proBNP (absolute value), and NT-proBNP/ULN (value normalized for sex and age). A cut-off value of 19 ng/l was used according to the manufacturer's instructions (biometry VIDAS® high-sensitivity troponin I). This value represents the 99th percentile of a presumably healthy population. High-sensitivity troponin tests were performed with the use of the VIDAS high-sensitivity troponin I (TNHS). The test is capable of measuring cardiac troponin I concentration in the range of 4.9-40,000.00 pg/ml (ng/1) without the need for dilution. The level of NT-proBNP was evaluated with the use of an Elecsys proBNP II Cobas e601 system. The test is able to measure the NT-proBNP concentration in the range of 5–35,000 pg/ml without the need for dilution. The NT-proBNP levels were presented as absolute values and standardized to sex and age on the basis of the manufacturer's guidelines (http://www.rochecanada.com/content/dam/roche_canada/en_CA/documents/package_inserts/ProBNPII-04842464190-EN-V9-CAN.pdf). The value of NT-proBNP above the 95th percentile for age and gender (the ULN) was considered abnormal. Therefore, the results were expressed as the ratio of the NT-proBNP to age- and sex-matched ULN. Rate > 1.0 was considered to be abnormal [14]. This standardization of NT-proBNP provides a normal distribution of data, whereas absolute values were distributed abnormally. Thus, there was no need for logarithmic transformation for artificial calculation. Standard descriptive statistics were used. Quantitative variables were expressed as the mean and standard deviation (SD) (normally distributed data—Kolmogorov-Smirnov) or median and interquartile range (IQR) (abnormal distribution of data). Categorical variables were presented with counts and as percentages (Fisher exact or Chi-squared test). Differences between two groups were evaluated using an independent t-test or Mann-Whitney-Wilcoxon test dependent on distribution of data. The results were considered significant at p value of 0.05 or lower. All statistical analyses were performed using STATISTICA v 13 software (StatSoft, Inc., Kraków, Poland).

3. Results

The study group included 30 men and 26 women. The mean age of all patients was 45 ± 6 (years). Most of them was on treatment—31 (55%) on beta-blockers, 19 (34%) on verapamil, and 6 (11%) on diuretics. Baseline clinical data is presented in Table 1. Almost all patients with CCS III class ($n = 9/10$) and one with CCS IV ($n = 1/1$) underwent coronary angiography. RSC was related to CCS III/IV. A higher level of hs-TnI was observed in RSC patients as compared to the non-RSC group. A trend toward increased NT-proBNP value was reported in RSC patients. However, no difference in the NT-proBNP/ULN level was observed between both groups (Table 2). In TTE parameters, the RSC group was characterized by a higher value of provocable LVOTG as compared to non-RSC patients; however, similar resting LVOT was observed. In M-mode measurements, STD

TABLE 1: Baseline characteristics of the patients.

NYHA	
Class I	6 (11%)
Class II	26 (46%)
Class III/IV	24 (43%)
CCS	
Class I	25 (45%)
Class II	20 (36%)
Class III/IV	11 (19%)
Syncope (n)	23 (41%)
Sudden death in family history (n)	22 (39%)
NSVT in Holter (n)	24 (43%)
EF (%)	62.5 ± 10.2
Mitral regurgitation trace	
Mild	40 (71%)
Moderate/severe	16 (29%)
Tricuspid regurgitation trace	
Mild	38 (68%)
Moderate/severe	18 (32%)
Systolic pulmonary artery pressure (mmHg)	35.4 ± 14.7
Maximum LV thickness (mm)	22.6 ± 4.9
Resting LVOT gradient ≥ 30 mmHg (n)	14
Provocable LVOT gradient ≥ 30 mmHg (n)	12
Left atrial diameter (cm), mean (SD)	4.89 ± 0.81

Data are presented as the number (percentage) or mean and standard deviation. CCS: Canadian Cardiovascular Society; EF: ejection fraction; LVOT: left ventricular outflow tract; LV: left ventricular; NSVT: nonsustained ventricular tachycardia; NYHA: New York Heart Association.

was greater and LVEDD was smaller in RSC vs. non-RSC; thus, STD/LVEDD > 0.5 was more frequently reported in the RSC subgroup (Table 2). There was a higher rate of nsVT, syncope, and family history of SCD in the RSC group (Table 2).

Patients with non-RSC had more than twice lower risk of SCD according to the ESC calculator (3.09 (1.9-4.76) vs. 8.83 (4.37-12.35) (%/5 years), $p = 0.002$) (Table 2). In addition, in the RSC subgroup, majority of patients were at high risk of SCD according to the ESC risk calculator (>6%/5 years vs. <4%/5 years: 53% vs. 18%, $p = 0.007$).

4. Discussion

The results of our analysis suggest that patients with RSC were associated with an increased level of hs-TnI. Additionally, a trend was observed in this group for the higher NT-proBNP but not in NT-proBNP levels. RSC seems to be an alerting, morphological sign related to ischemic events. Only provocable LVOTG was higher in RSC as compared to non-RSC patients. Furthermore, more patients with RSC had a prognostically unfavourable increased STD/LVEDD ratio [7]. In a pioneered paper by Lever et al., the RSC with crescent LV cavity size was detected only in younger HCM patients [15]. Analysing the relationship between age and RSC in a pathomorphological study [6], advanced

Table 2: Comparison of patients with reversed septal curvature and nonreversed septal curvature.

	RSC ($n = 17$)	Non-RSC ($n = 39$)	p value
hs-TnI (ng/l)	102 (29.2-214.7)	8.7 (5.3-18)	0.001
NT-proBNP (pg/ml)	1279 (367.3-1186)	551.7 (273-969)	0.056
NT-proBNP/ULN	6.51 ± 4.87	4.59 ± 4.23	0.14
LVOTG at rest (mmHg)	10 (6.47-52)	8.2 (5.4-21)	0.3
LVOTG provocable (mmHg)	51 (9.5-105)	13.6 (7.5-31)	0.04
STD (mm)	24.1 ± 5.3	19.8 ± 3.4	0.02
LVEDD (mm)	35.3 ± 6.6	42.1 ± 5.2	0.001
STD/LVEDD > 0.5	14/17 (82%)	9/39 (18%)	0.001
EF (%)	61.2 ± 9.8	63.4 ± 9.5	0.7
Systolic pulmonary artery pressure (mmHg)	38.3 ± 16.6	33.7 ± 13.5	0.3
nsVT	11/17 (65.7%)	13/39 (33.3%)	0.02
Syncope	11/17 (65%)	12/39 (31%)	0.02
Family history of SCD	10/17 (59%)	12/39 (31%)	0.04
Risk of SCD at 5 years (%)	8.83 (4.37-12.35)	3.09 (1.9-4.76)	0.002

Data are presented as the mean and standard deviation or median and interquartile range. EF: ejection fraction; LVEDD: left ventricular end-diastolic diameter; LVOTG: left ventricular outflow tract gradient; nsVT: nonsustained ventricular tachycardia; SCD: sudden cardiac death; STD: septal thickness at end diastole.

abnormality in myocardial architecture (strongly related to reversed RSC) was common in patients who died at a mean age of 25 years. In contrast, most of the patients who were older than 65 years when they died had a normal circular unit surrounding the LV cavity as a morphological marker of non-RSC. Hypothetically, SCD may be related to RSC via repetitive ischemic episodes. To evaluate the cumulative effect of both increased septal hypertrophy and decreased LV cavity size, we used the proportion of two TTE parameters measured at end diastole (the ratio of septal thickness to left ventricular diastolic diameter (STD/LVEDD)). In searching for other morphological substrates that culminate in the STD/LVEED ratio as SCD risk factors, we hypothesised that a small LV cavity might be a predictor of SCD because it is often linked with several risk factors (from different guidelines) for SCD, syncope [16], abnormal blood pressure response to exercise [17], and massive LV hypertrophy [18]. A narrow LV cavity easily predisposes to hypotensive mediated syncope during LV low input-low output failure triggered by tachycardia [19]. It was postulated that the combination of low filling volume and nonsustained ventricular tachycardia (nsVT) might lead to sudden depression of cardiac output with severe hypotension [19]. Thus, ventricular fibrillation might be triggered as the cumulative effect of myocardial ischemia (due to hypotension mediated reduction of coronary perfusion) and electrical instability. In a recently published study [20], authors have defined two subgroups of HCM patients: the first subgroup had RSC morphology with more fibrosis, but less resting obstruction, whereas the second subgroup presented non-RSC configuration with more frequent obstruction occurrence and less fibrosis. The authors postulated the need for further investigation comparing these subgroups to search for risk factors for SCD. This reasonable conception had been partially verified in the year 2005 in a small-scale study [7] where RSC had been recognized as a risk cofactor for SCD. In our opinion,

the lack of provoked obstruction in all included patients might limit observed results. The European Society of Cardiology (ESC) risk score of SCD recommended the use of maximal-provocable LVOT gradient rather than the resting one [8]. Importantly, in this study, we have documented that the maximized value of provocable LVOT gradient was associated with an increased level of high-sensitivity troponin [4]. In another study [20], the positive troponin test corresponded with a higher ESC risk score of SCD as compared to patients with a negative troponin test estimated according to the SCD calculator (including provocable LVOT gradient as a component) ($6.38\% \pm 4.17\%$ vs. $3.81\% \pm 3.23\%$, $p < 0.05$). Furthermore, the authors stated that TTE examination should be performed as close as possible to the moment of enrollment. It created unfavourable delay for biomarker assessment. In contrast, we stressed that TTE and biomarker sampling/measurement must be close to each other as possible [2, 3]. The strategy of simultaneous measurement of the relationship between gradient provocation and ischemia induction was also effectively used in the invasive study [4, 5]. The pathophysiological mechanism behind ischemia in RSC is still elusive. However, RSC patients have a higher volume of postcontrast hyperenhancement in MRI study suggesting a greater amount of ischemical necrosis [19]. The RSC generating catenoid shape of the septum might lead to septal immobility because a ventricular segment with a net zero curvature would develop internal tension with no isometric contraction. Adjacent fiber tracts with opposite curvatures would develop maximum tension without motion. This process is connected with high energy consumption/demand and easily provokes myocardial ischemia [21].

There were patients with ($n = 40$) or without ($n = 16$) prescribed treatment (newly diagnosed patients referred to our ambulatory clinic). Our group was mixed as concerned to therapy. After our study assessment, the therapy was

introduced or improved especially in NYHA III/IV. The number of patients is too low to assess the relationship with RSC.

5. Limitations

The most important limitation of this study is the relatively small number of patients related to several exclusion criteria. Most of the patients have not met clinical indications for coronary angiography (young, without angina pectoris, and without risk factors for CAD). The risk for CAD was low; thus, coronary angiography was not indicated (unfortunately, multislice coronary computed tomography was not performed). The strategy of noninvasive identification of subgroups with a low likelihood of obstructive CAD is effective [22]. Slightly higher troponin might be not a result of myocardial ischemia; however, very detailed exclusion criteria and use of the high-sensitivity troponin I test may assure that troponin was released by ischemic event. There is a possible bias related to insufficient sample size. We were not able to calculate multivariable regression analysis.

The next problem related to the small number of patients is the fact that the value of NT-proBNP was elevated in both subgroups, but differences were on the border of statistical significance.

Thus, the result of this study is rather hypothesis-generating than causative. However, a study with a large group of patients might be able to achieve statistically significant differences.

6. Conclusion

Ischemia detected by an elevated troponin level in HCM patients might be strongly related to abnormal septal configuration. RSC as an unchangeable (during many years) feature seems to be an alerting signal of risk of ischemic events. The RSC subgroup was linked to a higher rate of nsVT, syncope, and family history of SCD.

Data Availability

All data used to support the findings of this study are available from the corresponding author upon request: Paweł Petkow Dimitrow, 2nd Department of Cardiology, Jagiellonian University Medical College, Jakubowskiego 2 Str., 30-688 Krakow, Poland, e-mail: dimitrow@mp.pl.

Conflicts of Interest

The authors declare no conflict of interest.

Authors' Contributions

Conceptualization, project administration, and resources were handled by R.RS. and P.DP.; data curation, formal analysis, investigation, methodology, software, validation, visualization, writing of original draft, and writing (review and editing) were taken care of by R.RS., T.T., and P.DP.; and supervision was made by P.DP.

References

[1] D. W. Kehl, A. Buttan, R. J. Siegel, and F. Rader, "Clinical utility of natriuretic peptides and troponins in hypertrophic cardiomyopathy," *International Journal of Cardiology*, vol. 218, pp. 252–258, 2016.

[2] R. Rajtar-Salwa, A. Gębka, A. Dziewierz, and P. P. Dimitrow, "Hypertrophic cardiomyopathy: the time-synchronized relationship between ischemia and left ventricular dysfunction assessed by highly sensitive troponin I and NT-proBNP," *Disease Markers*, vol. 2019, Article ID 6487152, 8 pages, 2019.

[3] R. Hładij, R. Rajtar-Salwa, and P. P. Dimitrow, "Troponin as ischemic biomarker is related with all three echocardiographic risk factors for sudden death in hypertrophic cardiomyopathy (ESC Guidelines 2014)," *Cardiovascular Ultrasound*, vol. 15, no. 1, p. 24, 2017.

[4] R. O. Cannon 3rd, W. H. Schenke, B. J. Maron et al., "Differences in coronary flow and myocardial metabolism at rest and during pacing between patients with obstructive and patients with nonobstructive hypertrophic cardiomyopathy," *Journal of the American College of Cardiology*, vol. 10, no. 1, pp. 53–62, 1987.

[5] R. O. Cannon 3rd, C. L. McIntosh, W. H. Schenke, B. J. Maron, R. O. Bonow, and S. E. Epstein, "Effect of surgical reduction of left ventricular outflow obstruction on hemodynamics, coronary flow, and myocardial metabolism in hypertrophic cardiomyopathy," *Circulation*, vol. 79, no. 4, pp. 766–775, 1989.

[6] T. Kuribayashi and W. C. Roberts, "Myocardial disarray at junction of ventricular septum and left and right ventricular free walls in hypertrophic cardiomyopathy," *The American Journal of Cardiology*, vol. 70, no. 15, pp. 1333–1340, 1992.

[7] P. P. Dimitrow and J. S. Dubiel, "Echocardiographic risk factors predisposing to sudden cardiac death in hypertrophic cardiomyopathy," *Heart*, vol. 91, no. 1, pp. 93-94, 2005.

[8] Authors/Task Force members, P. M. Elliott, A. Anastasakis et al., "2014 ESC guidelines on diagnosis and management of hypertrophic cardiomyopathy," *European Heart Journal*, vol. 35, no. 39, pp. 2733–2779, 2014.

[9] P. P. Dimitrow, M. Bober, J. Michałowska, and D. Sorysz, "Left ventricular outflow tract gradient provoked by upright position or exercise in treated patients with hypertrophic cardiomyopathy without obstruction at rest," *Echocardiography*, vol. 26, no. 5, pp. 513–520, 2009.

[10] P. P. Dimitrow and R. Rajtar-Salwa, "Obstructive form of hypertrophic cardiomyopathy-left ventricular outflow tract gradient: novel methods of provocation, monitoring of biomarkers, and recent advances in the treatment," *BioMed Research International*, vol. 2016, Article ID 1575130, 8 pages, 2016.

[11] M. Lipari, E. Wypasek, M. Karpiński et al., "Identification of a variant hotspot in MYBPC3 and of a novel CSRP3 autosomal recessive alteration in a cohort of Polish patients with hypertrophic cardiomyopathy," *Polish Archives of Internal Medicine*, vol. 130, no. 2, pp. 89–99, 2020.

[12] J. M. Bos, M. L. Will, B. J. Gersh, T. M. Kruisselbrink, S. R. Ommen, and M. J. Ackerman, "Characterization of a phenotype-based genetic test prediction score for unrelated patients with hypertrophic cardiomyopathy," *Mayo Clinic Proceedings*, vol. 89, no. 6, pp. 727–737, 2014.

[13] A. Gębka, R. Rajtar-Salwa, A. Dziewierz, and P. Petkow-Dimitrow, "Painful and painless myocardial ischemia detected by elevated level of high-sensitive troponin in patients with

hypertrophic cardiomyopathy," *Advances in Interventional Cardiology*, vol. 14, no. 2, pp. 195–198, 2018.

[14] J. L. Blackshear, R. E. Safford, C. S. Thomas et al., "Platelet function analyzer 100 and brain natriuretic peptide as biomarkers in obstructive hypertrophic cardiomyopathy," *The American Journal of Cardiology*, vol. 121, no. 6, pp. 768–774, 2018.

[15] H. M. Lever, R. F. Karam, P. J. Currie, and B. P. Healy, "Hypertrophic cardiomyopathy in the elderly. Distinctions from the young based on cardiac shape," *Circulation*, vol. 79, no. 3, pp. 580–589, 1989.

[16] C. A. Nienaber, S. Hiller, R. P. Spielmann, M. Geiger, and K. H. Kuck, "Syncope in hypertrophic cardiomyopathy: multivariate analysis of prognostic determinants," *Journal of the American College of Cardiology*, vol. 15, no. 5, pp. 948–955, 1990.

[17] P. M. Elliott, J. R. Gimeno Blanes, N. G. Mahon, J. D. Poloniecki, and W. J. McKenna, "Relation between severity of left-ventricular hypertrophy and prognosis in patients with hypertrophic cardiomyopathy," *The Lancet*, vol. 357, no. 9254, pp. 420–424, 2001.

[18] P. Spirito, P. Bellone, K. M. Harris, P. Bernabo, P. Bruzzi, and B. J. Maron, "Magnitude of left ventricular hypertrophy and risk of sudden death in hypertrophic cardiomyopathy," *The New England Journal of Medicine*, vol. 342, no. 24, pp. 1778–1785, 2000.

[19] S. Neubauer, P. Kolm, C. Y. Ho et al., "Distinct subgroups in hypertrophic cardiomyopathy in the NHLBI HCM registry," *Journal of the American College of Cardiology*, vol. 74, no. 19, pp. 2333–2345, 2019.

[20] R. Rajtar-Salwa, R. Hładij, and P. P. Dimitrow, "Elevated level of troponin but not N-terminal probrain natriuretic peptide is associated with increased risk of sudden cardiac death in hypertrophic cardiomyopathy calculated according to the ESC guidelines 2014," *Disease Markers*, vol. 2017, Article ID 9417908, 5 pages, 2017.

[21] K. J. Silverman, G. M. Hutchins, J. L. Weiss, and G. W. Moore, "Catenoidal shape of the interventricular septum in idiopathic hypertrophic subaortic stenosis: two dimensional echocardiographic confirmation," *The American Journal of Cardiology*, vol. 49, no. 1, pp. 27–32, 1982.

[22] J. Reeh, C. B. Therming, M. Heitmann et al., "Prediction of obstructive coronary artery disease and prognosis in patients with suspected stable angina," *European Heart Journal*, vol. 40, no. 18, pp. 1426–1435, 2019.

Research Article

MicroRNA-216a Promotes Endothelial Inflammation by Smad7/IκBα Pathway in Atherosclerosis

Shujun Yang [ID],[1,2] **Yu Chen** [ID],[1] **Xuenan Mi** [ID],[1] **Shuyuan Zhang** [ID],[1] **Yunyun Yang** [ID],[1] **Rutai Hui** [ID],[1] and **Weili Zhang** [ID][1]

[1]*State Key Laboratory of Cardiovascular Disease, FuWai Hospital, National Center for Cardiovascular Diseases, Peking Union Medical College & Chinese Academy of Medical Sciences, Beijing, China*
[2]*Xiamen Cardiovascular Hospital, Xiamen University, Xiamen, China*

Correspondence should be addressed to Weili Zhang; zhangweili1747@yahoo.com

Background. The endothelium is the first line of defence against harmful microenvironment risks, and microRNAs (miRNAs) involved in vascular inflammation may be promising therapeutic targets to modulate atherosclerosis progression. In this study, we aimed to investigate the mechanism by which microRNA-216a (miR-216a) modulated inflammation activation of endothelial cells. *Methods*. A replicative senescence model of human umbilical vein endothelial cells (HUVECs) was established, and population-doubling levels (PDLs) were defined during passages. PDL8 HUVECs were transfected with miR-216a mimics/inhibitor or small interfering RNA (siRNA) of SMAD family member 7 (Smad7). Real-time PCR and Western blot assays were performed to detect the regulatory role of miR-216a on Smad7 and NF-κB inhibitor alpha (IκBα) expression. The effect of miR-216a on adhesive capability of HUVECs to THP-1 cells was examined. MiR-216a and Smad7 expression *in vivo* were measured using human carotid atherosclerotic plaques of the patients who underwent carotid endarterectomy ($n = 41$). *Results*. Luciferase assays showed that Smad7 was a direct target of miR-216a. Smad7 mRNA expression, negatively correlated with miR-216a during endothelial aging, was downregulated in senescent PDL44 cells, compared with young PDL8 HUVECs. MiR-216a markedly increased endothelial inflammation and adhesive capability to monocytes in PDL8 cells by promoting the phosphorylation and degradation of IκBα and then activating NF-κB signalling pathway. The effect of miR-216a on endothelial cells was consistent with that blocked Smad7 by siRNAs. When inhibiting endogenous miR-216a, the Smad7/IκBα expression was rescued, which led to decreased endothelial inflammation and monocytes recruitment. In human carotid atherosclerotic plaques, Smad7 level was remarkably decreased in high miR-216a group compared with low miR-216a group. Moreover, miR-216a was negatively correlated with Smad7 and IκBα levels and positively correlated with interleukin 1 beta (IL1β) expression *in vivo*. *Conclusion*. In summary, our findings suggest a new mechanism of vascular endothelial inflammation involving Smad7/IκBα signalling pathway in atherosclerosis.

1. Introduction

Atherosclerosis, a chronical inflammatory disorder, is a critical pathogenesis underlying cardiovascular diseases. Endothelial inflammation and dysfunction play a pivotal role in various stages of atherosclerosis, which can be induced by conventional risk factors such as aging, obesity, smoking, hypertension, hyperglycaemia, and hyperlipidemia [1]. Except for these risk factors, a growing body of evidence indicates that microRNAs (miRNAs) are potentially epigenetic factors in regulating the progression of vascular endothelial senescence, inflammatory response, and atherosclerosis [2, 3].

The miRNAs, single-stranded, small noncoding RNAs comprising of approximately 22 nucleotides can bind to the complementary sequence in the $3'$ untranslated region ($3'$ UTR) of their specific target messenger RNAs (mRNAs) and regulate the translational suppression or destabilization of these mRNAs [4]. MicroRNA-216a (miR-216a) is highly conserved among various species including human, mouse, rat, and zebrafish. Several studies have demonstrated that

miR-216a has important roles in vascular endothelial aging, inflammation, and autophagy defects in atherosclerosis [5–7]. Our previous work showed that plasma miR-216a level increases in aged patients with coronary artery disease compared with healthy controls; experimental results further showed that stable expression of miR-216a can contribute to a premature senescence-like phenotype in human endothelial cells, inhibit endothelial proliferation, and activate inflammatory responses by inhibiting SMAD family member 3 (Smad3) expression [5]. The miR-216a overexpression is also involved in the loss of autophagic function by targeting beclin 1 during endothelial cell aging [6]. Wang et al. further reported that miR-216a-mediated repressive effects on autophagy and survival can be abrogated by the long noncoding RNA (lncRNA) MALAT1 in human endothelial cells [7].

Besides, miR-216a plays important regulatory roles in macrophage polarization and foam cells formation during atherosclerosis development [8, 9]. Our previous study found that miR-216a can promote M1 macrophage polarization and lipid uptake ability *via* targeting Smad3/NF-κB pathway *in vitro* and accelerate atherosclerotic plaque development in a mouse model [8]. Plasma miR-216a is highly expressed in coronary artery disease patients with venerable plaques compared with the patients with stable plaques, indicating that miR-216a may be a potential biomarker for atherosclerotic diseases [8]. Gong et al. reported that miR-216a motivates cholesterol efflux by targeting cystathionine gamma-lyase (CSE) in macrophage cells [9].

The effects of miR-216a on endothelial functions may be differential due to the alternative targeting genes under certain microenvironments. The bioinformatics prediction analysis showed that there is a potential miR-216a-binding site within the 3′UTR of SMAD family member 7 (Smad7) gene. Smad7, a major negative inhibitor of transforming growth factor beta (TGFβ) signal pathway, plays complex regulatory roles in inflammatory processes. Some studies showed that Smad7 can block the protective, anti-inflammatory effect of TGFβ *via* regulating the Smad2/3 expression and subsequently inducing NF-κB activation in human intestinal lamina propria mononuclear cells or in macrophages [10, 11]. However, inconsistent findings existed. For example, Smad7 retains the NF-κB inhibitor alpha (IκBα) expression; inhibits NF-κB-activated genes such as tumour necrosis factor alpha (TNFα), interleukin 1 beta (IL1β), and intercellular adhesion molecule 1 (ICAM1); and thereafter plays an anti-inflammatory role in several tumour cell lines [12, 13].

To date, the molecular mechanisms of miR-216a in vascular endothelial cells have not been comprehensively explored. In this study, we aimed to investigate whether miR-216a could modulate the activation and inflammatory responses of endothelial cells by targeting Smad7 *in vitro* and further examined the relationship between miR-216a and Smad7 expression *in vivo* in human carotid atherosclerotic plaques.

2. Materials and Methods

2.1. Cell Culture and miRNA or siRNA Transfection. Primary human umbilical vein endothelial cells (HUVECs) were cul-

tured in endothelial cell medium (ScienCell, San Diego, CA, USA) containing 5% fetal bovine serum and 1% penicillin/-streptomycin, and the replicative senescence model was established. Population-doubling levels (PDLs) were calculated during the passages according to an equation reported previously (1), in which Ch is the number of cells at harvest and Cs is the number of cells seeded [14]. Consequently, PDL8 and PDL44 HUVECs were defined as young and aging cells, respectively.

$$PD = \log_2\left(\frac{Ch}{Cs}\right). \tag{1}$$

To explore the regulatory role of miR-216a in target gene expression, PDL8 HUVECs were transfected with 100 nM miR-216a mimics or miR-216a inhibitor (GenePharma, Suzhou, China) using the lipofectamine 3000 reagent (Invitrogen, Carlsbad, CA, USA) and harvested at 48 h posttransfection. To determine the effects of Smad7 on endothelial cells, Smad7 was silenced *via* transfection of 40 nM small interfere RNAs (siRNAs) (Invitrogen, Carlsbad, CA, USA). The following siRNA of Smad7 was used: sense 5′ CAGC GGCCCAAUGACCACGAGUUUA 3′, and antisense 5′ UAAACUCGUGGUCAUUGGGCCGCUG 3′.

2.2. Assays for Endothelial Cell Adhesion Activity. The capacity of endothelial adhesion to monocytes was examined in PDL8 HUVECs. Confluent endothelial monolayers were established in 24-well plate before incubation for 48 h with miR-216a mimics/inhibitor or Smad7 siRNA in the presence of lipofectamine 3000 reagent. THP-1 monocytes (Zhong Qiao Xin Zhou Biotechnology, Shanghai, China) were labelled with CellTracker™ CM-Dil (Life Technologies, Carlsbad, CA, USA) and added to 24-well plates containing HUVEC monolayers (1×10^5 THP-1 cells/well). After incubation at 37°C for 30 min, cells were gently washed twice with PBS to remove nonadherent monocytes. The number of THP-1 cells attached to HUVEC surface was quantified throughout 5 random fields.

2.3. Real-Time PCR for mRNA and miRNA Expression Analysis. The mRNA expression of ICAM1, IL1β, and Smad7 was analysed by real-time PCR. The total RNAs of HUVECs were extracted by TRIzol reagent (Invitrogen, Carlsbad, CA, USA) in accordance with the manufacturer's instruction; then, 1 μg RNA was used to synthesize cDNA using PrimeScript Reverse Transcriptase assay (Takara, Dalian, China). Real-time PCR was performed with SYBR Green qPCR mix (YEASEN, Shanghai, China) utilizing the ABI ViiA7™ System with 384-Well Block (Applied Biosystems, Foster City, CA, USA). A relative expression was determined by the $\Delta\Delta$Ct method, and GAPDH gene was applied as the internal reference. Primers for real-time PCR were listed as following: ICAM1 forward 5′ TCTGTGTCCCC CCTCAAAAGTC 3′and reverse 5′ GGGTCTCTATGCCC AACAA 3′; IL1β forward 5′ CAGCTACGAATCTCCG ACCAC 3′ and reverse 5′ GGCAGGGAACCAGCATCTT C 3′; Smad7 forward 5′ ACTCCAGATACCCGATGGA

TTT 3$'$ and reverse 5$'$ CCTCCCAGTATGCCACCAC 3$'$; GAPDH forward 5$'$ GAAGGTGAAGGTCGGAGTCA 3$'$ and reverse 5$'$ GGAAGATGGTGATGGGATTTC 3$'$.

Total RNAs extracted from HUVECs or human carotid plaque tissues by Trizol reagent were used to examine the miR-216a expression using miScript II reverse transcription kit and miScript SYBR Green PCR kit (QIAGEN, Hilden, Germany) by real-time PCR on the ABI ViiA7™ System. The miR-216a level was normalized to U6 small nuclear RNA.

2.4. Luciferase Reporter Assay. There exists a putative miR-216a binding sequence between 1,230 and 1,236 base pairs (bps) in the 3$'$UTR of Smad7 (ENSG00000101665). Primers were designed to amplify the Smad7 3$'$UTR sequence: forward 5$'$ GCCAAGCTTTCTTCTTCTCGTCCTCGTT 3$'$ and reverse 5$'$ GCCGAGCTCTAGGTGATAACACCCAT AGA 3$'$. The Smad7 3$'$UTR amplicons, with the length of 1,134 bps, were inserted into pMIR-REPORT™ Luciferase vectors (Ambion, Austin, TX, USA).

To determine the regulatory effect of miR-216a on the mRNA expression of Smad7, the luciferase reporter assays were performed in HEK293T cells (China Infrastructure of Cell Line Resources, Beijing, China). Cells were cotransfected with 100 ng Smad7 3$'$UTR or 3$'$UTR mutant plasmid in 96-well plates and 50 nM miR-216a mimics or negative control (NC) ($n = 8$ per group) using Lipofectamine 3000 (Invitrogen, Carlsbad, CA, USA). After 2 days, the firefly and renilla luciferase activities were detected with the Dual Luciferase Reporter Assay System (Promega, Madison, WI, USA) utilizing an UniCel DxC 800 Synchron Analyzer (Backman, CA, USA). Renilla luciferase activity was used to normalize firefly luciferase activity.

2.5. Western Blot Analysis. The role of miR-216a in protein expression of Smad7, IκBα, and phosphorylated IκBα was investigated using Western blot. PDL8 HUVECs were lysed by RIPA lysis buffer (Beyotime Biotechnology, Shanghai, China) containing both of protease and phosphatase inhibitors (Roche, Mannheim, Germany). Protein concentrations of cell lysates were assessed by the Pierce BCA Protein Assay Kit (Invitrogen, Carlsbad, CA, USA). For each sample, 50 μg of protein was loaded and electrophoresed using 10% SDS-PAGE gel and subsequently transferred to the nitrocellulose membrane (Millipore, MA, USA). After blocked by 5% BSA, membranes were incubated with primary antibodies and then corresponding secondary antibodies. Primary antibodies were rabbit polyclonal anti-Smad7 (Proteintech, Chicago, IL, USA), anti-IκBα, anti-Phospho-IκBα (Ser32), and anti-GAPDH (Cell Signaling Technology, USA), in which GAPDH was used as an internal reference. Secondary antibody was anti-rabbit (1 : 5000) labelled with horseradish peroxidase. The protein bands were visualized using the FluorChem™ R System (ProteinSimple, CA, USA), and proteins were quantified by the AlphaView Software.

2.6. Human Carotid Atherosclerotic Plaques. The human carotid atherosclerotic plaques were obtained from patients undergoing the carotid endarterectomy surgery ($n = 41$),

and clinical characteristics of patients are shown in Table 1. Tissues were minced and embedded into RNAlater™ Stabilization Solution (Ambion, Carlsbad, CA, USA), then stored at -80°C.This study was approved by the ethics committee of the FuWai Hospital.

2.7. Statistical Analysis. The quantitative variables were presented as means ± S.D. or medians and interquartile ranges (IQRs), while the categorical variables were quantified as absolute counts (percentages). Group differences were analysed by Student t-test, one-way ANOVA, or Mann–Whitney nonparametric test for the quantitative variables, where appropriate. The χ^2 test was utilized to compare the categorical variables. The Pearson's correlation analysis was performed to evaluate the correlation between miR-216a levels and the mRNA expression of Smad7, IκBα, and IL1β in human atherosclerotic plaques. The SPSS Statistics 20.0 software (SPSS Inc, Chicago, USA) was used, and statistical significance was considered when $P < 0.05$.

3. Results

3.1. Smad7 Was a Direct Target of miR-216a. Compared with that expression in young PDL8 HUVECs, Smad7 mRNA was found to be downregulated by 47% ($P = 0.03$) in senescent PDL44 cells, which was negatively correlated with the miR-216a expression during endothelial aging (Figure 1(a)). The computational miRNA target analysis by TargetScan Release 7.1 from miRNA databases indicated that Smad7 was a potential target gene of miR-216a, containing a candidate miR-216a binding site between 1,230 and 1,236 bps in the 3$'$UTR (Figure 1(b)). Next, the luciferase reporter vectors of Smad7 3$'$UTR and 3$'$UTR mutant were constructed. Cotransfection of miR-216a mimics with Smad7 3$'$UTR vector inhibited the luciferase activity by 91% in HEK293T cells ($P < 0.001$), whereas the luciferase reporter carrying Smad7 3$'$UTR mutant did not respond to regulation of miR-216a (Figure 1(c)).

The regulatory role of miR-216a in the Smad7 protein expression was assessed in PDL8 HUVECs. Overexpression of miR-216a resulted in remarkable downregulation of the Smad7 protein expression by 50% ($P = 0.02$), while antago-miR-216a, a synthetic inhibitor of endogenous miR-216a, significantly increased the Smad7 protein expression by 19% ($P = 0.03$; Figure 1(d)). Furthermore, miR-216a overexpression enhanced IκBα phosphorylation by 27% ($P = 0.01$) and subsequently reduced the IκBα protein level by 41% ($P = 0.004$; Figure 1(e)), which indicated the proinflammatory role of miR-216a in downregulating Smad7 and IκBα in endothelial cells.

3.2. miR-216a Promoted Monocytes Adhesion to Endothelial Cell Monolayers. To investigate whether miR-216a regulated endothelial inflammation by targeting Smad7, the mRNA expression levels of IL1β and ICAM1 were examined in PDL8 HUVECs. The results showed that miR-216a overexpression increased the IL1β and ICAM1 expression by 29% ($P = 0.04$) and 66% ($P = 0.03$) (Figure 2(a)), while miR-216a inhibition suppressed the mRNA expression levels of

TABLE 1: Clinical characteristics of patients who underwent carotid endarterectomy.

Characteristics	Low miR-216a group ($n = 21$)	High miR-216a group ($n = 20$)	P
Age, years	65.6 ± 8.8	62.9 ± 9.0	0.33
Male, n (%)	18 (85.7%)	17 (85.0%)	0.95
BMI, kg/m^2	25.4 ± 3.2	24.7 ± 2.2	0.46
Hypertension, n (%)	18 (87.5%)	14 (70%)	0.22
Hyperlipidemia, n (%)	6 (31.6%)	10 (58.8%)	0.20
Diabetic mellitus, n (%)	14 (70.0%)	9 (45.0%)	0.11
Cigarette smoking, n (%)	13 (61.9%)	13 (68.4%)	0.21
Alcohol intake, n (%)	2 (9.5%)	7 (35.0%)	0.09
Systolic BP, mmHg	138 ± 19	139 ± 15	0.83
Diastolic BP, mmHg	82 ± 9	83 ± 10	0.76
Fasting glucose, mmol/L	6.50 ± 1.74	5.97 ± 1.44	0.31
Total cholesterol, mmol/L	4.91 ± 1.38	4.95 ± 1.16	0.93
Triglyceride, mmol/L	1.63 (1.31-2.06)	1.45 (1.26-1.91)	0.76
HDL-C, mmol/L	1.12 ± 0.52	1.05 ± 0.27	0.59
LDL-C, mmol/L	2.88 ± 1.21	2.89 ± 0.90	0.99
hsCRP, mg/L	8.92 ± 17.38	5.28 ± 5.92	0.50

BMI: body mass index; BP: blood pressure; HDL-C: high-density lipoprotein cholesterol; LDL-C: low-density lipoprotein cholesterol; hsCRP: high sensitive C-reaction protein.

IL1β and ICAM1 by 33% ($P = 0.002$) and 41% ($P = 0.05$), respectively (Figure 2(b)). The THP-1 cell adhesion assay showed that miR-216a increased the adhesion ability of THP-1 monocytes to endothelial cells by 66% ($P = 0.004$) in PDL8 HUVECs with transfection of miR-216a mimics (Figure 2(c)), whereas inhibition of endogenous miR-216a reduced endothelial adhesion ability to THP-1 cells by 27% ($P = 0.003$; Figure 2(d)).

3.3. miR-216a Enhanced Endothelial Inflammation via Smad7/IκBα Pathway. As mentioned above, miR-216a was found to downregulate the Smad7 expression, while simultaneously increasing the expression of NF-κB response genes like IL1β and ICAM1, which subsequently enhances the endothelial adhesive ability to monocytes. To further investigate the molecular mechanism by which miR-216a regulated endothelial inflammation via the target Smad7, siRNAs of Smad7 were transfected into PDL8 cells. It was found that the Smad7 mRNA expression was significantly suppressed by 78% ($P = 0.01$) after inhibition of endogenous Smad7 by siRNAs, while the IL1β and ICAM1 expression increased remarkably by 4.0-fold ($P = 0.03$) and 2.5-fold ($P = 0.007$), respectively (Figure 3(a)). The Smad7 protein expression was downregulated considerably by 75% ($P = 0.002$; Figure 3(b)); subsequently, the phosphorylation level of IκBα was increased by 66% ($P = 0.01$), and the total protein level of IκBα was reduced by 79% ($P < 0.001$) in HUVECs when silencing Smad7 (Figure 3(c)). These results supported that Smad7 plays an anti-inflammatory role through inhibiting the phosphorylation and degradation of IκBα in endothelial cells.

Next, endogenous miR-216a and Smad7 in HUVECs were inhibited by cotransfection with miR-216a inhibitor and Smad7 siRNA. We found that miR-216a inhibition rescued the downregulation of Smad7 and IκBα protein levels by 58% ($P = 0.05$) and 56% ($P = 0.003$), respectively (Figure 3(d)). Under the condition of silencing Smad7, the endothelial adhesive ability to monocytes was suppressed by miR-216a inhibitor by 30% ($P < 0.001$; Figure 3(e)). All these results suggested that miR-216a promoted endothelial inflammation by directly regulating the Smad7/IκBα pathway.

3.4. miR-216a Was Negatively Related with Smad7 Level in Human Atherosclerotic Plaques. The regulatory effect of miR-216a on endothelial inflammation suggested a significant role of miR-216a in the pathogenesis of atherosclerosis. To assess the impact of miR-216a in vivo, miR-216a and Smad7 mRNA levels were examined in atherosclerotic plaques from the patients who underwent the carotid endarterectomy. The patients were stratified into the low miR-216a group ($n = 21$) or high miR-216a group ($n = 20$), according to the median of miR-216a expression level (1.91, IQR, 0.80-4.14). Compared with that expression in the low miR-216a group, miR-216a levels increased by 7.4-fold ($P < 0.001$), and the Smad7 mRNA expression markedly decreased by 30% ($P = 0.02$) in the high miR-216a group (Figure 4(a)). Moreover, we found that miR-216a was negatively correlated with Smad7 ($R = -0.43$, $P = 0.005$) and its downstream IκBα ($R = -0.34$, $P = 0.03$) based on Pearson's correlation analysis. On the contrary, miR-216a was positively correlative with IL1β ($R = 0.36$, $P = 0.02$) (Figure 4(b)). These results were indicative of the regulatory effect of miR-216a on Smad7/IκBα pathway in human atherosclerotic plaques.
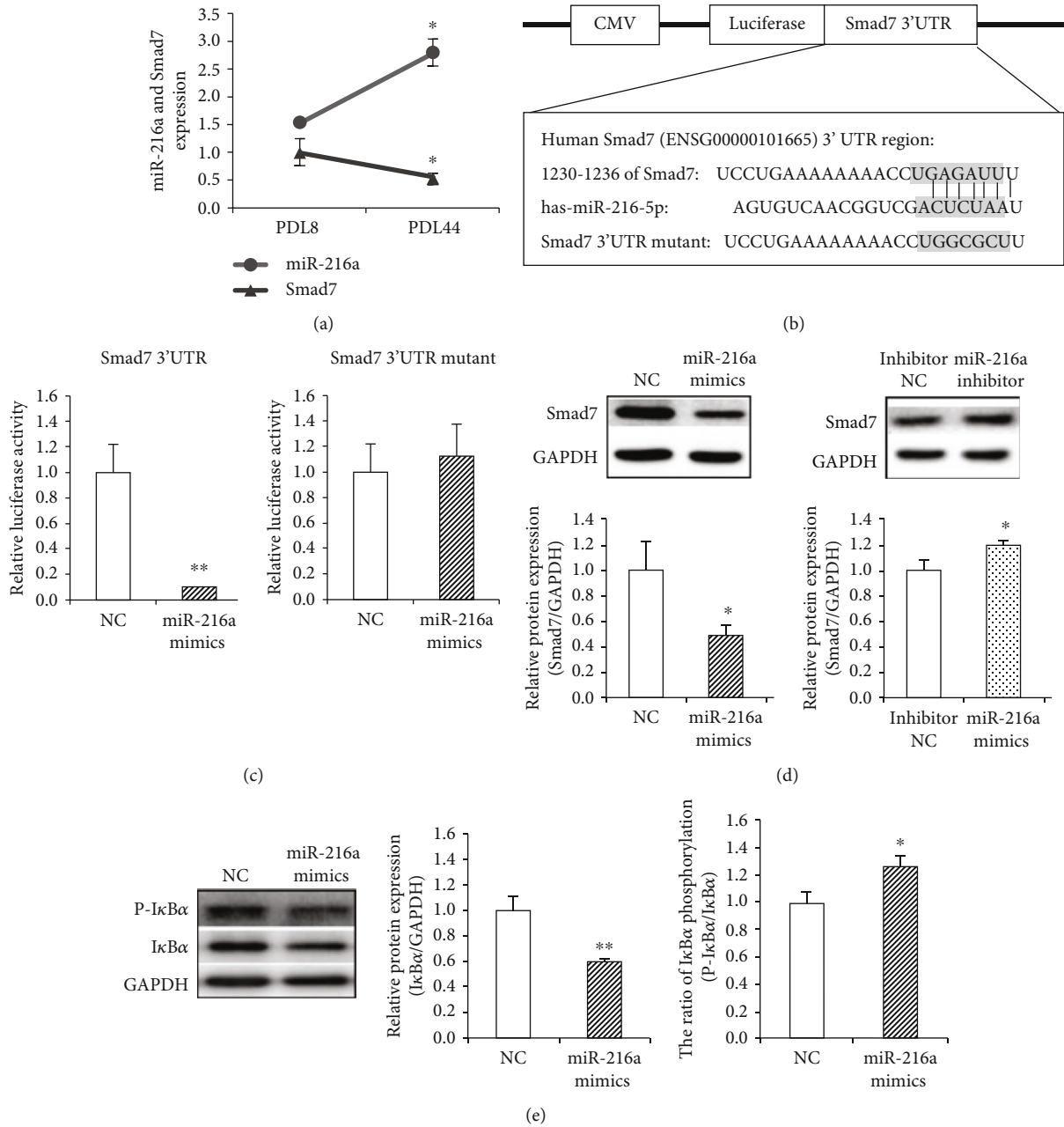
FIGURE 1: Smad7 was a direct target of miR-216a. (a) Compared with young PDL8 HUVECs, senescent PDL44 cells exhibited upregulated miR-216a and downregulated Smad7 ($n = 5$). (b) Schematic diagram of the potential binding site of miR-216a within Smad7 3′UTR and the luciferase plasmids. (c) miR-216a inhibited the luciferase activity of Smad7 3′UTR vector but not Smad7 3′UTR mutant vector in HEK293T cells ($n = 8$). (d) Overexpression of miR-216a suppressed the Smad7 protein expression; conversely, miR-216a inhibitor upregulated Smad7 protein level in PDL8 cells ($n = 5$). (e) The total protein expression of IκBα was reduced, and the proportion of IκBα phosphorylation (phosphorylated IκBα/total IκBα) was increased in PDL8 cells with transfection of miR-216a ($n = 5$). $^*P < 0.05$, $^{**}P < 0.01$.

4. Discussion

In the current study, we provided *in vitro* evidence that miR-216a promoted endothelial inflammation and the adhesion ability of monocytes to endothelial cells by directly targeting Smad7/IκBα signalling pathway and subsequently increasing expression of NF-κB response genes such as IL1β and ICAM1. In human carotid atheroscle-rotic plaque tissues, the Smad7 mRNA expression mark-edly decreased in the high miR-216a group in comparison with that in the low miR-216a group. Our findings extended the knowledge of miR-216a on endothe-lial inflammation involving Smad7/IκBα pathway *in vitro* and *in vivo*.

The miR-216a may exert various effects on endothelial functions according to its different target genes. Our

(a)

(b)

(c)

(d)
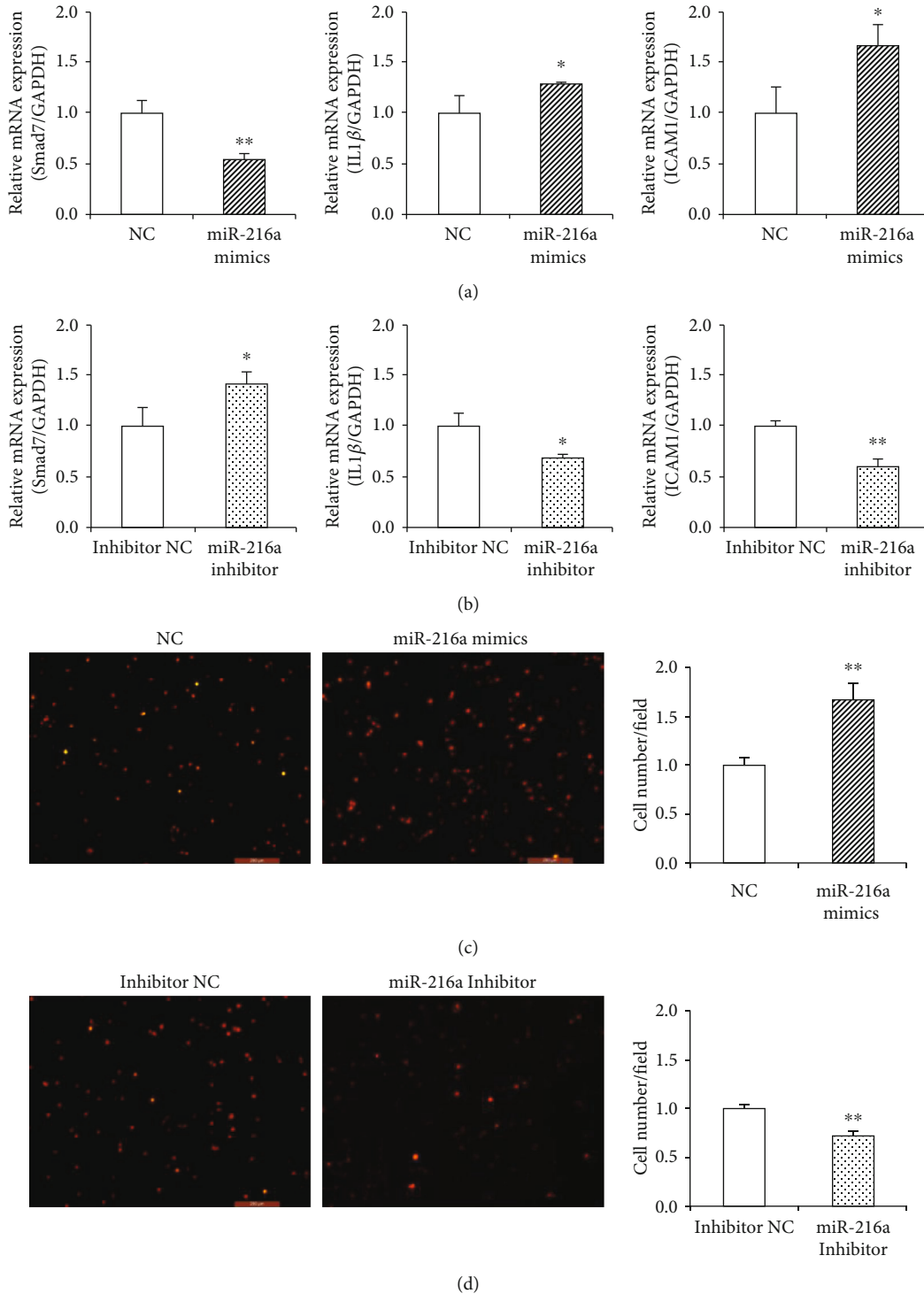
FIGURE 2: miR-216a promoted monocytes adhesion to HUVEC monolayers. (a, b) Smad7 mRNA expression was inhibited by miR-216a mimics and increased by miR-216a inhibitor. Simultaneously, mRNA levels of IL1β and ICAM1 were upregulated by miR-216a and inhibited by miR-216a inhibitor in PDL8 HUVECs. (c, d) The endothelial adhesion ability of PDL8 HUVECs to THP-1 monocytes was increased by miR-216a mimics, whereas decreased by miR-216a inhibitor. Scale bars: 200 μm. $n = 5$ for each group; $^{*}P < 0.05$, $^{**}P < 0.01$.

previous work showed that miR-216a induces endothelial aging and promotes inflammatory process *via* directly inhibiting Smad3/IκBα signalling pathway [5]. In this study, bioinformatics analysis predicted that Smad7 might be an alternative target gene of miR-216a. Our further experiments confirmed Smad7 as a direct target gene of miR-216a; overexpression of miR-216a remarkably down-regulated the mRNA and protein expression of Smad7, while inhibition of miR-216a significantly upregulated the expression of Smad7 in endothelial cells.

(a)

(b)

(c)

(d)

(e)
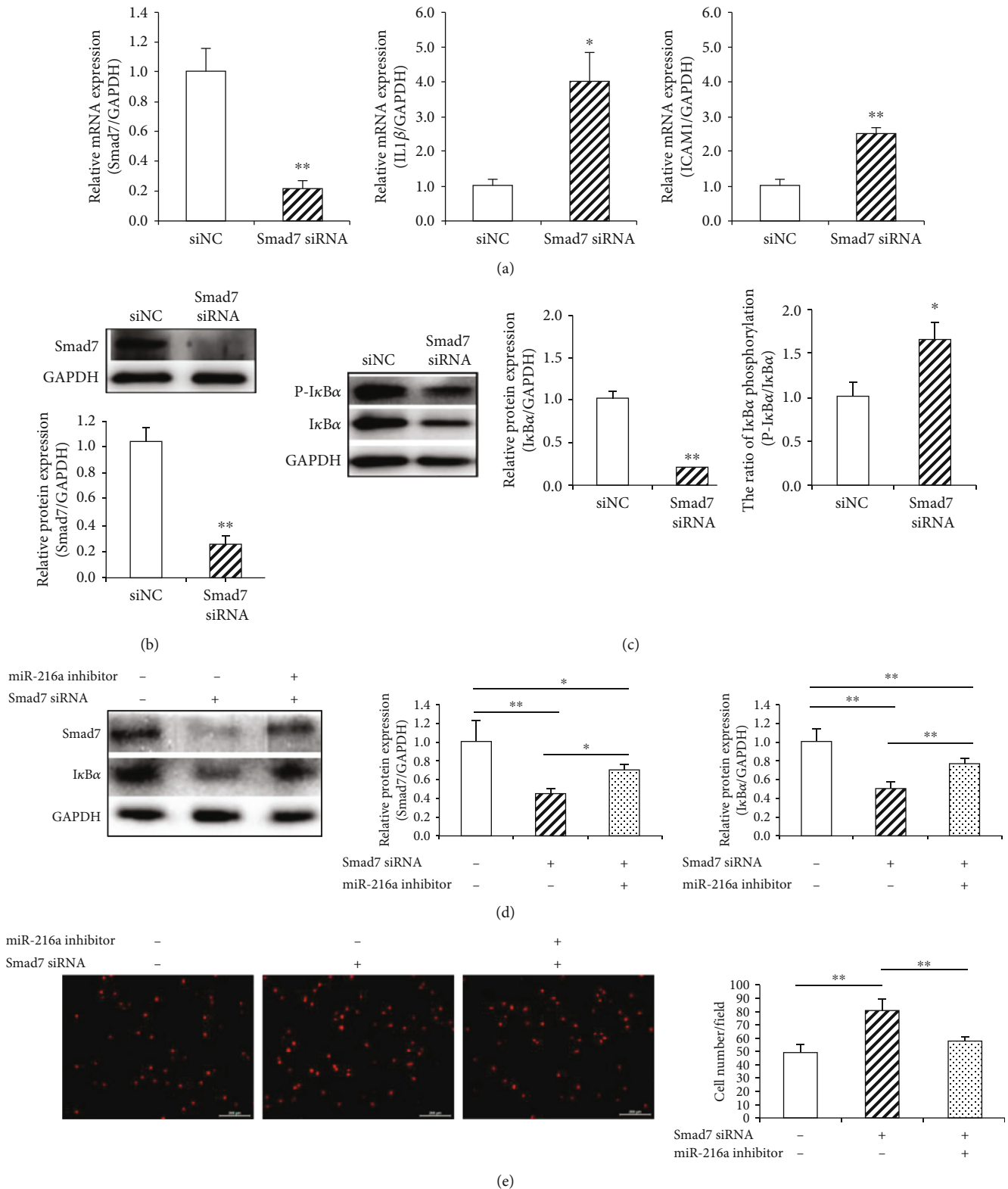
FIGURE 3: miR-216a enhanced endothelial inflammation *via* Smad7/IκBα pathway. (a) Knockdown of Smad7 with siRNA resulted in the downregulation of the Smad7 mRNA expression and the remarkable upregulation of IL1β and ICAM1 mRNA levels in PDL8 HUVECs. (b) Smad7 protein level in HUVECs was inhibited by its siRNA. (c) The total IκBα expression was reduced, and the proportion of IκBα phosphorylation was increased after silencing Smad7. (d) The protein expression of Smad7 and IκBα was rescued by miR-216a inhibitor when endogenous Smad7 was silenced. (e) The capacity of endothelial adhesive to THP-1 monocytes was increased by miR-216a inhibitor after silencing Smad7. Scale bars: 200 μm. $n = 5$ for each group; $^{*}P < 0.05$, $^{**}P < 0.01$.
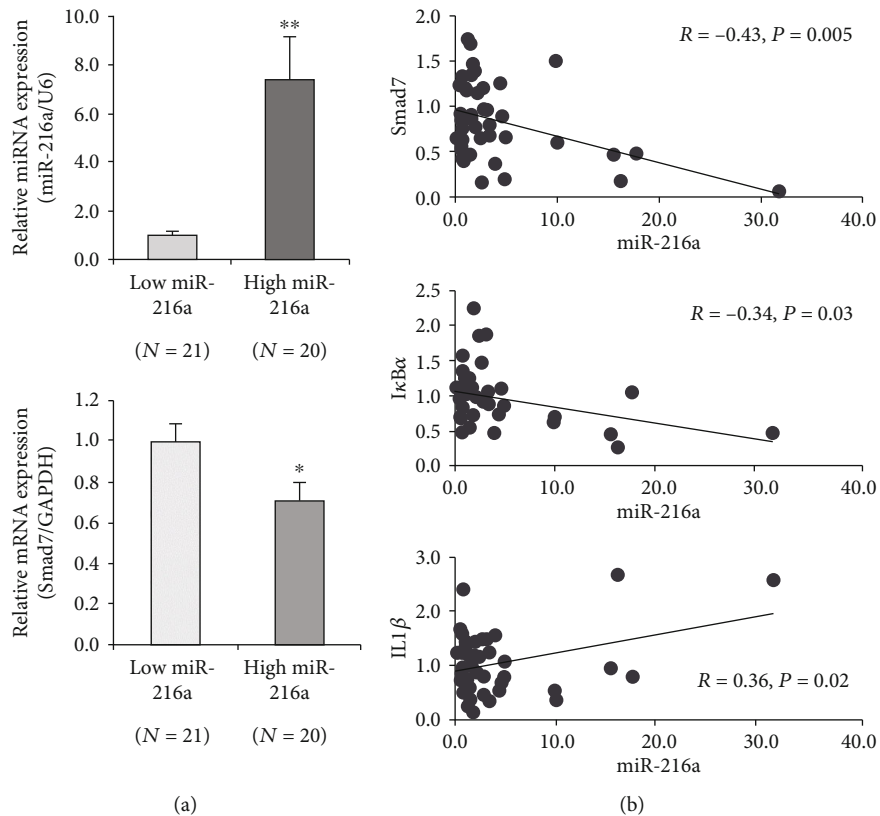
Figure 4: miR-216a was negatively related with the Smad7 expression in human atherosclerotic plaques. (a) The patients undergoing the carotid endarterectomy were stratified into two groups according to the median of the miR-216a expression in their carotid plaques ($n = 41$). The Smad7 expression was downregulated in the high miR-216a group ($n = 20$), compared to the low miR-216a group ($n = 21$). (b) miR-216a was negatively correlated with Smad7 and IκBα, whereas positively correlated with IL1β in human carotid atherosclerotic plaques by Pearson's correlation analysis. $^*P < 0.05$, $^{**}P < 0.01$.

Smad7 is not only the major negative inhibitor of TGFβ signal pathway but also functions as a key mediator of the crosstalk between proinflammatory and anti-inflammatory pathways. Smad2/3 signalling pathway is known as the canonical mediator of TGFβ and responsible for its anti-inflammatory effect. Smad7 can form a stable complex with TGFβ type I receptor and exert a proinflammatory effect; the underlying mechanism of which is to inhibit Smad2/3 pathway, reduce IκBα expression, and then result in NF-κB activation in human intestinal lamina propria mononuclear cells or in macrophages [10, 11]. On the other hand, Smad7 also exerts an anti-inflammatory effect by inhibiting phosphorylation of IκBα and thus suppressing NF-κB-activated genes in human head and neck squamous cell carcinoma lines or in mouse skin [12, 13]. To date, the effects of Smad7 have been extensively studied in inflammatory bowel diseases and tumour cells, but its role in vascular cells and atherosclerosis is still unclear. A recent study reported that low expression of Smad7 leads to activation of NF-κB pathway and upregulation of proinflammatory cytokines (such as TNFα and IL1β) in human vascular smooth muscle cells [15]. Here, our study demonstrated that Smad7 functioned as an important anti-inflammatory regulator in human vascular endothelial cells.

We found that inhibition of the Smad7 expression mediated by miR-216a could enhance IκBα phosphorylation, afterwards induce IκBα degradation and activate NF-κB response inflammation in the endothelial cells. This is consistent with previous studies that Smad7 blocks the recruitment of TGF-activated kinase and thereafter inhibits IκBα phosphorylation and proteasomal degradation [13]. When endogenous miR-216a was suppressed by its synthetic inhibitor, the Smad7/IκBα expression was rescued, which decreased endothelial inflammation and adhesive ability to monocytes. Moreover, in human carotid atherosclerosis plaque tissues, Smad7 mRNA expression level markedly decreased in the high miR-216a group in comparison with the low miR-216a group, suggesting a negative regulation of miR-216a on the Smad7 expression within human atherosclerotic lesions. In support with our study, Sandusky et al. reported that the Smad7 expression is significantly lower in the human coronary plaque endothelium than in normal vascular endothelium [16]. These data indicated that the reduction of the Smad7 expression mediated by miR-216a can activate vascular endothelial inflammatory responses and may accelerate atherosclerosis development.

As shown in our previous work, plasma miR-216a is specifically increased in aged patients with coronary artery disease and in patients with coronary artery vulnerable plaques [5, 8]. In this study, we provided new evidence that

miR-216a was positively correlated with the IL1β expression in carotid atherosclerotic plaques, which could give more accurate information about miR-216a as a biomarker for vascular inflammation and atherosclerosis. Additionally, miR-216a is found to be upregulated both in the myocardium tissues and the plasma of heart failure patients compared with healthy controls [17], and the consistent result of plasma miR-216a in heart failure was recently reported by Ding et al. [18]. Thus, miR-216a may be a promising biomarker for vascular dysfunctions including endothelial senescence and inflammatory responses, atherosclerotic diseases, and heart failure.

5. Conclusions

In summary, we provided *in vitro* evidence that miR-216a promotes endothelial inflammation and enhances the adhesion ability of monocytes to endothelial cells by directly targeting the Smad7/IκBα pathway. Consistently, the negative correlation between miR-216a and Smad7 is validated in human carotid plaques. These findings illuminate a new regulatory role of miR-216a in endothelial inflammation involving Smad7/IκBα pathway, which suggests that miR-216a is a potential therapeutic target and a biomarker for atherosclerosis.

Data Availability

The data used to support the findings of this study are available from the corresponding author on reasonable request.

Conflicts of Interest

The authors declare that there is no conflict of interest regarding the publication of this paper.

Acknowledgments

References

[1] F. Paneni, C. Diaz Cañestro, P. Libby, T. F. Lüscher, and G. G. Camici, "The aging cardiovascular system: understanding it at the cellular and clinical levels," *Journal of the American College of Cardiology*, vol. 69, no. 15, pp. 1952–1967, 2017.

[2] B. Rizzacasa, F. Amati, F. Romeo, G. Novelli, and J. L. Mehta, "Epigenetic modification in coronary atherosclerosis: JACC review topic of the week," *Journal of the American College of Cardiology*, vol. 74, no. 10, pp. 1352–1365, 2019.

[3] Q. Cao, J. Wu, X. Wang, and C. Song, "Noncoding RNAs in vascular aging," *Oxidative Medicine and Cellular Longevity*, vol. 2020, Article ID 7914957, 14 pages, 2020.

[4] D. P. Bartel, "MicroRNAs: target recognition and regulatory functions," *Cell*, vol. 136, no. 2, pp. 215–233, 2009.

[5] S. Yang, X. Mi, Y. Chen et al., "MicroRNA-216a induces endothelial senescence and inflammation via Smad3/IκBα pathway," *Journal of Cellular and Molecular Medicine*, vol. 22, no. 5, pp. 2739–2749, 2018.

[6] R. Menghini, V. Casagrande, A. Marino et al., "MiR-216a: a link between endothelial dysfunction and autophagy," *Cell Death & Disease*, vol. 5, no. 1, article e1029, 2014.

[7] K. Wang, C. Yang, J. Shi, and T. Gao, "Ox-LDL-induced lncRNA MALAT1 promotes autophagy in human umbilical vein endothelial cells by sponging miR-216a-5p and regulating Beclin-1 expression," *European Journal of Pharmacology*, vol. 858, article 172338, 2019.

[8] S. Yang, J. Li, Y. Chen et al., "MicroRNA-216a promotes M1 macrophages polarization and atherosclerosis progression by activating telomerase via the Smad3/NF-κB pathway," *Biochimica et Biophysica Acta - Molecular Basis of Disease*, vol. 1865, no. 7, pp. 1772–1781, 2019.

[9] D. Gong, H. P. Cheng, W. Xie et al., "Cystathionine γ-lyase(C-SE)/hydrogen sulfide system is regulated by miR-216a and influences cholesterol efflux in macrophages via the PI3K/AKT/ABCA1 pathway," *Biochemical and Biophysical Research Communications*, vol. 470, no. 1, pp. 107–116, 2016.

[10] G. Monteleone, J. Mann, I. Monteleone et al., "A failure of transforming growth factor-beta1 negative regulation maintains sustained NF-kappaB activation in gut inflammation," *The Journal of Biological Chemistry*, vol. 279, no. 6, pp. 3925–3932, 2004.

[11] L. E. Smythies, R. Shen, D. Bimczok et al., "Inflammation anergy in human intestinal macrophages is due to Smad-induced IκBα expression and NF-κB inactivation," *The Journal of Biological Chemistry*, vol. 285, no. 25, pp. 19593–19604, 2010.

[12] C. Freudlsperger, Y. Bian, S. Contag Wise et al., "TGF-β and NF-κB signal pathway cross-talk is mediated through TAK1 and SMAD7 in a subset of head and neck cancers," *Oncogene*, vol. 32, no. 12, pp. 1549–1559, 2013.

[13] S. Hong, S. Lim, A. G. Li et al., "Smad7 binds to the adaptors TAB2 and TAB3 to block recruitment of the kinase TAK1 to the adaptor TRAF2," *Nature Immunology*, vol. 8, no. 5, pp. 504–513, 2007.

[14] R. Menghini, V. Casagrande, M. Cardellini et al., "MicroRNA 217 modulates endothelial cell senescence via silent information regulator 1," *Circulation*, vol. 120, no. 15, pp. 1524–1532, 2009.

[15] L. H. Wei, N. X. Chao, S. Gao et al., "Homocysteine induces vascular inflammatory response via SMAD7 hypermethylation in human umbilical vein smooth muscle cells," *Microvascular Research*, vol. 120, pp. 8–12, 2018.

[16] G. Sandusky, D. T. Berg, M. A. Richardson, L. Myers, and B. W. Grinnell, "Modulation of thrombomodulin-dependent activation of human protein C through differential expression of endothelial Smads," *The Journal of Biological Chemistry*, vol. 277, no. 51, pp. 49815–49819, 2002.

[17] J. Tao, J. Wang, C. Li et al., "MiR-216a accelerates proliferation and fibrogenesis via targeting PTEN and SMAD7 in human cardiac fibroblasts," *Cardiovascular Diagnosis and Therapy*, vol. 9, no. 6, pp. 535–544, 2019.

[18] H. Ding, Y. Wang, L. Hu et al., "Combined detection of miR-21-5p, miR-30a-3p, miR-30a-5p, miR-155-5p, miR-216a and miR-217 for screening of early heart failure diseases," *Bioscience Reports*, vol. 40, no. 3, 2020.

Research Article

Accurate Noninvasive Assessment of Myocardial Iron Load in Advanced Heart Failure Patients

Przemysław Leszek [1], **Barbara Sochanowicz,**[2] **Kamil Brzóska,**[2] **Leszek Kraj,**[3]
Mariusz Kuśmierczyk,[1] **Witold Śmigielski,**[1] **Tomasz M. Rywik,**[1]
Małgorzata Sobieszczańska-Małek,[1] **Piotr Rozentryt,**[4,5] **and Marcin Kruszewski**[2,6]

[1]*The National Cardinal Stefan Wyszynski Institute of Cardiology, 04-628 Warszawa, Alpejska 42, Poland*
[2]*Center of Radiobiology and Biological Dosimetry, Institute of Nuclear Chemistry and Technology, ul. Dorodna 16, 03-195 Warszawa, Poland*
[3]*Department of Hematology, Oncology and Internal Diseases, The Medical University of Warsaw, 1A Banacha Str., 02-097 Warsaw, Poland*
[4]*3rd Department of Cardiology, School of Medicine with the Division of Dentistry in Zabrze, Silesian Centre for Heart Disease, Medical University of Silesia in Katowice, 41-800 Zabrze Marii Skłodowskiej-Curie 9, Poland*
[5]*Department of Toxicology and Health Protection, School of Public Health in Bytom, Medical University of Silesia, Katowice, 41-902 Bytom, Piekarska 18, Poland*
[6]*Department of Medical Biology and Translational Research, Institute of Rural Health, ul. Jaczewskiego 2, 20-090 Lublin, Poland*

Correspondence should be addressed to Przemysław Leszek; przemyslaw.leszek@ikard.pl

Background. Heart failure patients presenting with iron deficiency can benefit from systemic iron supplementation; however, there is the potential for iron overload to occur, which can seriously damage the heart. Therefore, myocardial iron (M-Iron) content should be precisely balanced, especially in already failing hearts. Unfortunately, the assessment of M-Iron via repeated heart biopsies or magnetic resonance imaging is unrealistic, and alternative serum markers must be found. This study is aimed at assessing M-Iron in patients with advanced heart failure (HF) and its association with a range of serum markers of iron metabolism. *Methods*. Left ventricle (LV) myocardial biopsies and serum samples were collected from 33 consecutive HF patients (25 males) with LV dysfunction (LV ejection fraction 22 (11) %; NT-proBNP 5464 (3308) pg/ml) during heart transplantation. Myocardial ferritin (M-FR) and soluble transferrin receptor (M-sTfR1) were assessed by ELISA, and M-Iron was determined by Instrumental Neutron Activation Analysis in LV biopsies. Nonfailing hearts ($n = 11$) were used as control/reference tissue. Concentrations of serum iron-related proteins (FR and sTfR1) were assessed. *Results*. LV M-Iron load was reduced in all HF patients and negatively associated with M-FR ($r = -0.37$, $p = 0.05$). Of the serum markers, sTfR1/logFR correlated with ($r = -0.42$; $p = 0.04$) and predicted (in a step-wise analysis, $R^2 = 0.18$; $p = 0.04$) LV M-Iron. LV M-Iron load (μg/g) can be calculated using the following formula: $210.24 - 22.869 \times$ sTfR1/logFR. *Conclusions*. The sTfR1/logFR ratio can be used to predict LV M-Iron levels. Therefore, serum FR and sTfR1 levels could be used to indirectly assess LV M-Iron, thereby increasing the safety of iron repletion therapy in HF patients.

1. Introduction

Iron plays a crucial role in oxygen transport and storage, cardiac and skeletal muscle metabolism, energy production, and protein synthesis [1]. Iron deficiency (ID) is a common comorbidity in cardiac patients, particularly in heart failure (HF) patients, resulting in further detrimental effects [2]. Recent clinical studies have demonstrated that in HF patients presenting with ID, iron supplementation can lead to significant clinical improvement [3–5]. As such, the 2016

European Society of Cardiology (ESC) HF guidelines state that iron replacement therapy should be considered in HF patients with ID [6]. This clinical benefit of intravenous (iv) iron supplementation in HF patients seems to be independent of the presence of anemia [1, 7]. Despite these benefits, an excess of iron could potentially exert harmful effects; for example, improperly shielded iron ions can catalyze the production of reactive free radicals (due to the rapid oxidation-reduction cycling between Fe^{3+} and Fe^{2+} states), resulting in oxidative damage [8–12]. Therefore, patient iron levels should be closely monitored during iron replacement therapy.

Myocardial iron (M-Iron) metabolism has also been shown to be strongly related to left ventricle (LV) remodeling in HF [13, 14]. Indeed, based on an experimental rat model, we know that ID-anemia leads to molecular heart remodeling and, finally, LV dilatation [1]. These findings align with our data on human explanted hearts, which show a significant reduction in M-Iron load in failing LVs [13–15]. Hence, iron replenishment may be beneficial for the heart [16–18]. Conversely, low iron concentrations have been shown to exert positive effects by stimulating inducible nitric oxidase synthase (iNOS) activity and nitric oxide (NO) production, which promote cell survival in cardiomyocytes [17]. As iron replenishment can exert both beneficial and detrimental effects on a failing myocardium, depending on the actual M-Iron content, proper characterization of the M-Iron load is a key, especially in HF subjects. However, to date, there are no standardized criteria for monitoring the effectiveness and safety of iv iron treatment on the myocardium.

This study is aimed at assessing M-Iron load in the failing LV in relation to serum markers of iron metabolism to develop an indirect method of M-Iron assessment without performing a heart biopsy. This noninvasive assessment should increase the safety of iron supplementation in HF patients.

2. Material and Methods

2.1. Study Population and Protocol. The protocol was approved by the Local Ethics Committee. Each patient participating in the study signed an informed consent form after a detailed explanation of the study principles. The study group comprised 33 consecutive patients referred to orthotopic heart transplantation (OHT). Myocardial studies were performed in failing ventricular myocardium obtained during transplantation.

2.2. Study Protocol. All clinical assessments and blood sampling were performed just before OHT.

Two-dimensional, M-mode, and color Doppler transthoracic echocardiography was performed at rest according to the recommendations of the American Society of Echocardiography. Right heart catheterization, hemodynamic and cardiac output measurements, and resistance calculations were performed just before OHT.

Blood counts were determined with an automatic counter (Sysmex K4500), as follows: red blood cell (RBC) count (normal range, male/female: 4.6–6.2/4.2–5.4 million/μl),

hematocrit (Hct: 42–52/37–47%), mean corpuscular volume (MCV: d80–99 fl), hemoglobin (Hb: 14–18/12–16 g/dl), and mean corpuscular hemoglobin (MCH: 27–32 pg).

Body iron status and biochemical assessment were evaluated in serum using the Clinical Chemistry System Olympus 680 (Olympus Life Science) as follows: serum iron (normal range, male/female: 70–180/60–180 μg/dl), transferrin (200–360 mg/dl), transferrin saturation (TSAT, calculated from serum iron/transferrin: 15–45%), total iron-binding capacity (TIBC, calculated from iron: 210–340/260–390 μg/dl), and unsaturated iron-binding capacity (UIBC, calculated from TIBC and iron: 140–180/200–210 μg/dl). The COBAS Integra® 800 System (Roche Diagnostic) was used to evaluate soluble transferrin receptor (sTfR: 2.2–5.0/1.9–4.4 mg/l), high-sensitivity C-reactive protein (hsCRP, normal range: 0–0.5 mg/dl), sodium (136–145 mmol/l), and creatinine (62–106/44–80 μmol/l). The ARCHITECT® Immunochemistry Diagnostics Platform (Abbott Laboratories) was used to determine ferritin (FR, normal range, male/female: 4.63–204/21.81–274.66 ng/ml). Chemiluminescent IMMULITE 2000 (Siemens Healthcare Diagnostics) was used to measure erythropoietin (EPO, normal range, 3.7–29.5 mIU/ml). The Cobas e411R analyzer (Roche Diagnostic) was used to determine N-terminal pro-B-type natriuretic peptide (NT-proBNP, normal range, 0–125 pg/ml). Tumor Necrosis Factor-alpha (TNFα) levels were assayed by an enzyme-linked immunosorbent assay (ELISA, normal ranges < 8 pg/ml) according to the manufacturer's instructions (Human TNF-alpha, R&D System Inc., USA).

The estimated total dose required for iron repletion (TIRD) was assessed by the Ganzoni formula: TIRD (mg) = body weight (kg) × (target Hb – actual Hb in g/l) × 2.4* + iron depot (mg)** (*the factor 2.4 = 0.0034 × 0.07 × 10 000; **iron depot : <35 kg body weight : iron depot = 15 mg/kg body weight;≥35 kg body weight : iron depot = 500 mg).

2.3. Myocardial Assessments. Tissue samples of the LV free wall were taken at the time of explantation (avoiding scarred, fibrotic, or adipose tissue, endocardium, epicardium, or great vessels), rinsed immediately, blotted dry, frozen in liquid nitrogen, and kept at -80°C until use.

2.3.1. Myocardial Ferritin (M-FR) and Myocardial Soluble Transferrin Receptor (M-sTfR1) Assessment. In total, 80–100 mg of cardiac tissue was homogenized using an Ultra-Turrax T25 homogenizer in buffer with a Complete Protease Inhibitor Cocktail. Homogenate was filtered through two layers of gauze and centrifuged at 10,000 × g for 10 min. The supernatant was collected, portioned, rapid frozen in liquid nitrogen, and stored at -75°C. The total protein concentration was determined by the Bradford method. M-FR (kit from Alpha Diagnostic International Inc., San Antonio, TX, USA) and M-sTfR1 (kit from BioVendor GmbH, Heidelberg, Germany) were assayed by ELISA according to the manufacturer's instructions.

2.3.2. Myocardial Total Iron (M-Iron) Assessment. M-Iron was assayed by Instrumental Neutron Activation Analysis

TABLE 1: Clinical characteristics of the study group.

	Heart failure patients ($n = 33$)
Age (yrs)	51 (6.5)
Men/women, n	25/8
Etiology: idiopathic/ischemic/other, n	10/21/2
NYHA functional class: III/IV, n	15/18
LVESV (ml)/LVEDV (ml)/LVEF (%)	189 (95)/245 (83)/22 (11)
RVD (mm)	32 (10)
Mean PWP/mean PAP (mmHg)	23 (9)/33 ± 13
PVR/SVR (W.u.)	3.36 (1.2)/21.9 (6.2)
CI (l/min/m^2)	1.93 (0.64)
Red blood cells (ml/μl)/hematocrit (%)	4.5 (0.6)/39.7 (5.3)
Mean corpuscular volume (fl)	88.4 (7.1)
Hemoglobin (g/dl)/mean corpuscular hemoglobin (pg)	13.2 (1.7)/29.5 (2.5)
Serum iron (μg/dl)	62 (32)
Serum transferrin (mg/dl)/transferrin saturation (%)	240 (47)/19.5 (10.6)
Total iron-binding capacity/unsaturated iron-binding capacity (μmol/l)	288 (56)/41 (11)
Serum soluble transferrin receptor (mg/l)	3.2 (2.6)
Serum ferritin (ng/ml)	156 (122)
Erythropoietin (mIU/ml)	29.5 (44.4)
TIRD (see Material and Methods) (mg)	808 (323)
NT-proBNP (pg/ml)	5464 (3308)
TNFα (pg/ml)	15.8 (9.7)
hsCRP (mg/dl)	0.72 (0.3)
Serum sodium (mEq/l)	138 (2.5)
Serum creatinine (μmol/l)	108 (35)

LVESV/LVEDV: left ventricle volume end-diastolic/systolic; LVEF: left ventricle ejection fraction; RVD: right ventricle diastolic size; PWP: mean pulmonary wedge pressure; PAP: mean pulmonary artery pressure; PVR: pulmonary vascular resistance; SVR: systemic vascular resistance; CI: cardiac index; TIRD: total iron dose required for iron repletion calculated using the Ganzoni formula (see Material and Methods); NT-proBNP: N-terminal pro-B-type natriuretic peptide; TNFα: Tumor Necrosis Factor-alpha; hsCRP: high-sensitivity C-reactive protein.

(INAA). In brief, frozen samples were lyophilized (Freeze-mobile 12XL, Virtis Company, New York, US), weighed, and packaged in HDPE snap-cap capsules (Faculteit Biologie, Vrije Universiteit, Amsterdam, Holland). The certified reference material NIST 1577c Bovine Liver (National Institute of Standards and Technology (NIST), US) was used for quality control. Samples and standards were irradiated at the neutron flux of 10^{14} cm^{-2} s^{-1} for 50 min in a nuclear reactor MARIA (Świerk, Poland). After three weeks of cooling, the gamma-ray emission of the samples and standards was measured with the GENIE-2000 Canberra Gamma Spectrometry System and the GENIE 2000 software (Canberra Industries, Inc., Meriden, US).

2.4. Statistical Analysis. Data are expressed as means (SD) or as medians (IQR) for data that were not normally distributed. The test for normality for each analyzed parameter was performed using the Shapiro-Wilk test. Pearson correlation matrices were used to establish univariate correlations among M-Iron and other parameters. A stepwise multiple regression analysis was employed to assess the strongest model of independent predictors of M-Iron.

3. Results

3.1. Baseline Characteristics of the Study Group. The study group consisted of 33 consecutive, symptomatic HF patients (25 males), with a mean age of 48 years, who were referred for OHT. The study group presented with LV dilatation or dysfunction (LVESV 189 (95) ml; LVEDV 245 (83) ml; LVEF 22 (11) %), RV enlargement (RVD 32 (10) mm), pulmonary hypertension (PVR 3.36 (1.2) W.u.), and significant neurohumoral (NT-proBNP 5464 (3308) pg/ml) and proinflammatory (TNFα 15.8 (9.7) pg/ml; hsCRP 0.72 (0.3) mg/dl) activation (Table 1).

3.2. Iron- and HF-Related Parameters Associated with M-Iron in the Failing LV. M-Iron load at the cellular level was recently shown to be reduced in the failing heart, without significant changes in the expression of M-FR and M-sTfR1 [13, 14]. However, in patients with M-Iron deficiency, M-Iron reduction is accompanied by decreased M-FR expression [13, 14].

In our current calculations, based on Pearson's correlation matrices, we found that in the failing LV myocardium,

TABLE 2: Association between myocardial iron load and iron handling proteins in the failing left ventricle.

	M-FR	M-sTfR1
LV M-Iron	$r = 0.01$	$r = -0.37$
	$p = 0.94$	$p = 0.05$

LV M-Iron: left ventricle myocardial iron load; M-FR: myocardial ferritin; M-sTfR1: myocardial soluble transferrin receptor.

M-Iron load was negatively associated with M-sTfR1 but not M-FR (Table 2).

Although serum sTfR1 tended to correlate negatively with M-Iron, only the sTfR1/logFR ratio was significantly negatively associated with M-Iron. However, we did not confirm any correlation between M-Iron and other parameters routinely utilized for iron metabolism assessment (Table 3). Furthermore, we did not prove any association among M-Iron and TIRD calculated according to the Ganzoni formula or other RBC-related parameters, except RBC number (Table 3). Finally, neither the degree of LV dysfunction nor the level of neurohumoral or proinflammatory activation (i.e., two parameters frequently used to assess the severity of HF) was associated with M-Iron (Table 3).

3.3. Predictive Value of the sTfR1/logFR Ratio in Assessing M-Iron Load.

Among all iron- and RBC-related parameters described above, only the sTfR1/logFR ratio was an independent predictor of M-Iron (Figure 1).

Based on our calculations and obtained correlations after the mathematical transformation, the formula for LV M-Iron calculations is LV M-Iron load $(\mu g/g) = 210.24 - 22.869 \times sTfR1/logFR$.

We previously compared M-Iron content in LV myocardium from HF and non-HF subjects [14] and found that the normal LV iron content ranges from 200 to 300 $\mu g/g$. Therefore, using the above equation, the normal M-Iron ranges from 200 $\mu g/g$, which corresponds to a sTfR1/logFR of 0.753, and 300 $\mu g/g$, which corresponds to a sTfR1/logFR of 0.01.

4. Discussion

ID (with or without anemia) is common in chronic diseases, and iv iron supplementation is now often used in cardiology, oncology, hematology, and nephrology patients [1, 3–7, 19, 20]. However, an excess of iron in the body leads to dysfunctions of many organs, including the heart. Thalassemia, sickle cell anemia, and hemochromatosis are the most frequently occurring diseases with altered iron homeostasis, leading to uncontrolled iron entry and progressive tissue damage due to intracellular oxidative stress arising from the excessive production of free radicals [8–10, 12]. Therefore, when supplementing iron (especially iv), monitoring of iron stores is necessary to avoid overcorrection, which may lead to M-Iron overload.

Bone marrow biopsy assessment is the most accurate method to define ID (i.e., the depletion of iron in bone marrow stores) [21, 22]. However, performing a bone marrow biopsy simply to define ID is not appropriate. Similarly, a heart biopsy cannot be used routinely to evaluate the M-Iron load. Therefore, in real life, ID is defined based on laboratory assessments, including serum FR levels of <100 $\mu g/l$ or between 100 and 299 $\mu g/l$ when TSAT is <20% [23, 24]. Nevertheless, although this definition is widely accepted and the examinations are easy to perform, they do not accurately reflect the iron load in the body [25].

Regarding M-Iron, there is a general agreement that the M-Iron load is reduced in a failing LV [13–15]. Moreover, in HF patients with ID, the expression of the main iron storage protein, M-FR, is also reduced [13, 14]. Although we found no significant correlation between M-Iron and M-FR in our study, it is important to note that M-FR expression is not exclusively related to M-Iron load but also to inflammation and oxidative stress that accompanies the HF syndrome [24].

Only a few studies have evaluated changes in the expression of M-TfR1, the main protein responsible for iron acquisition, albeit with conflicting results. While Maeder et al. reported a reduction of M-TfR1 expression at the mRNA level in HF [15], we were unable to prove this finding at the protein level [13, 14]. However, we found a significant negative correlation between M-Iron load in the failing LV myocardium and M-TfR1 protein expression that is in agreement with the known role of TfR1 in iron metabolism.

Although there are undoubtedly links between M-Iron, M-FR, and M-TfR1 at the cellular level in the failing myocardium, our work proves that traditionally used clinical serum markers for body iron stores, such as TSAT and FR, do not reflect the actual M-Iron status. Serum FR has been commonly used as a clinical biomarker of ID since the early 1970s [26]. FR is produced in response to an increase in cellular iron content and reflects the storage compartment of cellular iron. However, increased levels of FR are observed at the onset of acute and chronic diseases [24, 26]. Thus, the diagnostic utility of FR in the HF population may be compromised by a false-positive increase in FR in these conditions. In turn, transferrin is a negative acute-phase reactant, and reduced TSAT levels are also observed in chronic conditions [27]. Moreover, TSAT levels show circadian fluctuations and are related to sleep quality [28]. Indeed, Nanas et al. [21] previously defined ID based on bone morrow assessment and proved that serum FR was not a reliable marker of ID in HF patients. In the case of iron deficiency for hematopoiesis, RBC correlates with the classic biochemical parameters of iron metabolism (TSAT, TIBC, and FR) in the blood serum. In this study, LV M-Iron does not correlate with these biochemical parameters. Interestingly, we observed a negative correlation between LV M-Iron and RBC, which proves the compartmentalization of iron in different tissues. However, the exact mechanisms that regulate the interaction between these compartments are unclear.

As the currently used serum markers are not satisfactory, and the direct assessment of M-Iron content by heart biopsies or frequent magnetic resonance imaging examination is not realistic, alternative serum markers must be found for the reliable assessment of M-Iron content. Our results validated the parameters commonly used for iron load

TABLE 3: Associations between myocardial iron load in the failing left ventricle and commonly used iron, red blood cell, and heart failure (HF) severity parameters.

(a) Associations with iron-related serum parameters

	Iron	Transferrin	TSAT	TIBC	UIBC	sTfR1	FR	sTfR1/logFR
LV M-Iron	$r = -0.07$	$r = -0.17$	$r = -0.03$	$r = -0.19$	$r = -0.15$	$r = -0.38$	$r = 0.13$	$r = -0.42$
	$p = 0.77$	$p = 0.54$	$p = 0.90$	$p = 0.38$	$p = 0.49$	$p = 0.07$	$p = 0.54$	$p = 0.04$

(b) Associations with red blood cell-related parameters

	TIRD	RBC	Hb	Hct	MCV	MCH	MCHC	Weight	EPO
LV M-Iron	$r = 0.16$	$r = -0.39$	$r = -0.22$	$r = -0.22$	$r = 0.23$	$r = 0.32$	$r = 0.11$	$r = -0.20$	$r = -0.29$
	$p = 0.42$	$p = 0.04$	$p = 0.25$	$p = 0.26$	$p = 0.25$	$p = 0.10$	$p = 0.56$	$p = 0.31$	$p = 0.18$

(c) Associations with HF severity-related parameters

	LVESV	LVEDV	LVEF	RVD	mPWP	PVR	NT-proBNP	hsCRP	TNFα	Serum sodium	Creatinine clearance
LV M-Iron	$r = -0.26$	$r = -0.19$	$r = -0.18$	$r = -0.32$	$r = 0.23$	$r = 0.19$	$r = -0.22$	$r = -0.02$	$r = 0.09$	$r = -0.12$	$r = -0.03$
	$p = 0.20$	$p = 0.32$	$p = 0.36$	$p = 0.21$	$p = 0.54$	$p = 0.17$	$p = 0.34$	$p = 0.93$	$p = 0.69$	$p = 0.38$	$p = 0.85$

LV M-Iron: left ventricle myocardial iron load. Iron-related serum parameters: iron: serum iron; TSAT: transferrin saturation; TIBC: total iron-binding capacity; UIBC: unsaturated iron-binding capacity; sTfR1: soluble transferrin receptor 1; FR: ferritin. Red blood cell-related parameters: TIRD: total iron dose required for iron repletion calculated using the Ganzoni formula; RBC: red blood cells; Hb: hemoglobin; Hct: hematocrit; MCV: mean corpuscular volume; MCH: mean corpuscular hemoglobin; MCHC: mean corpuscular hemoglobin concentration; EPO: erythropoietin. Heart failure severity-related parameters: LVESV/LVEDV: left ventricle volume end-diastolic/systolic; LVEF: left ventricle ejection fraction; RVD: right ventricle diastolic size; mPWP: mean pulmonary wedge pressure; PVR: pulmonary vascular resistance; NT-proBNP: N-terminal pro-B-type natriuretic peptide; hsCRP: high-sensitivity C-reactive protein; TNFα: Tumor Necrosis Factor-alpha.
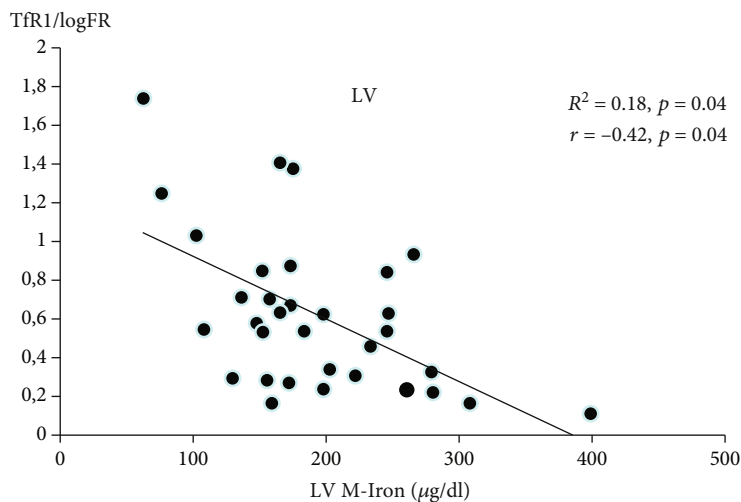
FIGURE 1: Independent predictors of myocardial iron load (M-Iron) (in failing left ventricle). LV M-Iron: left ventricle myocardial iron load; sTfR1/log FR: serum soluble transferrin receptor 1/log ferritin.

assessment and demonstrated that the M-iron load can be assessed more accurately based on serum sTfR1, particularly by calculating the sTfR1/logFR ratio. Circulating sTfR1 is produced by the proteolytic cleavage in direct proportion to the cellular receptor content [29]. sTfR1 levels reflect the total body mass of receptors, whereas the rate of their synthesis is closely linked to the iron requirements of the cells. In contrast to FR and TSAT, acute-phase reactions do not influence the sTfR1 serum level [30]. The most common cause of elevated serum sTfR1 levels is erythropoiesis in the bone marrow [29]; however, it can be released from other tissues, including cardiac [31]. As sTfR1 and FR levels reflect the functional and storage iron compartments, respectively, the sTfR1/logFR ratio has been suggested as a parameter for estimating iron status in the human body [32, 33]. Indeed, Enko et al. showed that the sTfR1/logFR ratio is superior to sTfR1,

FR, and TSAT in predicting functional ID in hospitalized patients, irrespective of the acute-phase reaction [25, 34]. Our results also show the accuracy of sTfR1/logFR in the proper characterization of M-Iron load and homeostasis.

In the HF population, iron repletion and the total iron repletion dose (TIRD) required for supplementation for an individual ID patient is usually calculated using the Ganzoni formula and relies on the subject's weight and Hb value [35]. However, besides the RBC count, we (and others [36]) found no association between M-iron and TIRD or the other RBC-related parameters in the Ganzoni formula.

Iron repletion therapy is usually tailored based on the presence of ID criteria (i.e., serum FR and TSAT levels) [4, 37]. We show that among all frequently used iron/RBC parameters, only sTfR1/logFR is an independent predictor of M-Iron. We determined that the best formula for LV M-Iron calculations is LV M-Iron load (μg/g) = 210.24 − 22.869 × sTfR1/logFR. Therefore, when referring to the LV M-Iron load in HF and non-HF patients, we postulate that iv iron repletion therapy may be additionally tailored by the noninvasive M-Iron calculation based on the above formula. This formula allows the LV M-Iron content to be approximated at each stage of iv iron supplementation in a noninvasive way.

There are some limitations to our study. In particular, the presented work is based on a limited, but representative, homogeneous population of patients with advanced HF (33 patients) subjected to heart transplantation. Despite this, the population size is comparable to the size of the population on which the fundamental formula for iron deficiency calculations was established by Ganzoni (30 patients). Nonetheless, prospective longitudinal studies involving follow-up measurements of proposed parameters are needed for improved data modeling.

In summary, among the commonly used serum markers for iron turnover assessment, only the sTfR1/logFR ratio is an independent predictor of LV M-Iron. In this study, we present a formula that enables the indirect assessment of LV M-Iron, which will help increase the safety of iron repletion therapy in HF patients.

Data Availability

The data are not freely available, due to restricted access to human data related to legal (GDPR) and ethical concerns.

Conflicts of Interest

There are no potential conflicts of interest, including related consultancies, shareholdings, and funding grants.

Acknowledgments

References

[1] E. A. Jankowska, S. von Haehling, S. D. Anker, I. C. Macdougall, and P. Ponikowski, "Iron deficiency and heart failure: diagnostic dilemmas and therapeutic perspectives," *European Heart Journal*, vol. 34, no. 11, pp. 816–829, 2013.

[2] P. Moliner, E. A. Jankowska, D. J. van Veldhuisen et al., "Clinical correlates and prognostic impact of impaired iron storage versus impaired iron transport in an international cohort of 1821 patients with chronic heart failure," *International Journal of Cardiology*, vol. 243, pp. 360–366, 2017.

[3] S. D. Anker, J. Comin Colet, G. Filippatos et al., "Ferric carboxymaltose in patients with heart failure and iron deficiency," *The New England Journal of Medicine*, vol. 361, no. 25, pp. 2436–2448, 2009.

[4] G. Filippatos, D. Farmakis, J. C. Colet et al., "Intravenous ferric carboxymaltose in iron-deficient chronic heart failure patients with and without anaemia: a subanalysis of the FAIR-HF trial," *European Journal of Heart Failure*, vol. 15, no. 11, pp. 1267–1276, 2013.

[5] P. Ponikowski, D. J. van Veldhuisen, J. Comin-Colet et al., "Beneficial effects of long-term intravenous iron therapy with ferric carboxymaltose in patients with symptomatic heart failure and iron deficiency†," *European Heart Journal*, vol. 36, no. 11, pp. 657–668, 2015.

[6] P. Ponikowski, A. A. Voors, S. D. Anker et al., "2016 ESC guidelines for the diagnosis and treatment of acute and chronic heart failure: the task force for the diagnosis and treatment of acute and chronic heart failure of the European Society of Cardiology (ESC)developed with the special contribution of the Heart Failure Association (HFA) of the ESC," *European Heart Journal*, vol. 37, no. 27, pp. 2129–2200, 2016.

[7] N. Ebner, E. A. Jankowska, P. Ponikowski et al., "The impact of iron deficiency and anaemia on exercise capacity and outcomes in patients with chronic heart failure. Results from the studies investigating co-morbidities aggravating heart failure," *International Journal of Cardiology*, vol. 205, pp. 6–12, 2016.

[8] C. J. Murphy and G. Y. Oudit, "Iron-overload cardiomyopathy: pathophysiology, diagnosis, and treatment," *Journal of Cardiac Failure*, vol. 16, no. 11, pp. 888–900, 2010.

[9] P. Gujja, D. R. Rosing, D. J. Tripodi, and Y. Shizukuda, "Iron overload cardiomyopathy: better understanding of an increasing disorder," *Journal of the American College of Cardiology*, vol. 56, no. 13, pp. 1001–1012, 2010.

[10] S. K. Das, W. Wang, P. Zhabyeyev et al., "Iron-overload injury and cardiomyopathy in acquired and genetic models is attenuated by resveratrol therapy," *Scientific Reports*, vol. 5, no. 1, article 18132, 2015.

[11] G. Y. Oudit, H. Sun, M. G. Trivieri et al., "L-type Ca2+ channels provide a major pathway for iron entry into cardiomyocytes in iron-overload cardiomyopathy," *Nature Medicine*, vol. 9, no. 9, pp. 1187–1194, 2003.

[12] M. Kruszewski, "Labile iron pool: the main determinant of cellular response to oxidative stress," *Mutation Research*, vol. 531, no. 1-2, pp. 81–92, 2003.

[13] P. Leszek, B. Sochanowicz, M. Szperl et al., "Myocardial iron homeostasis in advanced chronic heart failure patients," *International Journal of Cardiology*, vol. 159, no. 1, pp. 47–52, 2012.

[14] P. Leszek, B. Sochanowicz, K. Brzóska et al., "Does myocardial iron load determine the severity of heart insufficiency?," *International Journal of Cardiology*, vol. 182, pp. 191–193, 2015.

[15] M. T. Maeder, O. Khammy, C. dos Remedios, and D. M. Kaye, "Myocardial and systemic iron depletion in heart failure implications for anemia accompanying heart failure," *Journal of the American College of Cardiology*, vol. 58, no. 5, pp. 474–480, 2011.

[16] S. Haddad, Y. Wang, B. Galy et al., "Iron-regulatory proteins secure iron availability in cardiomyocytes to prevent heart failure," *European Heart Journal*, vol. 38, no. 5, pp. 362–372, 2017.

[17] J. P. Munoz, M. Chiong, L. García et al., "Iron induces protection and necrosis in cultured cardiomyocytes: role of reactive oxygen species and nitric oxide," *Free Radical Biology & Medicine*, vol. 48, no. 4, pp. 526–534, 2010.

[18] Y. Naito, T. Tsujino, M. Matsumoto, T. Sakoda, M. Ohyanagi, and T. Masuyama, "Adaptive response of the heart to long-term anemia induced by iron deficiency," *American Journal of Physiology. Heart and Circulatory Physiology*, vol. 296, no. 3, pp. H585–H593, 2009.

[19] A. T. Deak, K. Troppan, and A. R. Rosenkranz, "Anemia management in cancer patients with chronic kidney disease," *European Journal of Internal Medicine*, vol. 36, pp. 13–19, 2016.

[20] L. Peyrin-Biroulet, N. Williet, and P. Cacoub, "Guidelines on the diagnosis and treatment of iron deficiency across indications: a systematic review," *The American Journal of Clinical Nutrition*, vol. 102, no. 6, pp. 1585–1594, 2015.

[21] J. N. Nanas, C. Matsouka, D. Karageorgopoulos et al., "Etiology of anemia in patients with advanced heart failure," *Journal of the American College of Cardiology*, vol. 48, no. 12, pp. 2485–2489, 2006.

[22] K. S. Phiri, J. C. J. Calis, D. Kachala et al., "Improved method for assessing iron stores in the bone marrow," *Journal of Clinical Pathology*, vol. 62, no. 8, pp. 685–689, 2009.

[23] J. B. Wish, "Assessing iron status: beyond serum ferritin and transferrin saturation," *Clinical Journal of the American Society of Nephrology*, vol. 1, Supplement 1, pp. S4–S8, 2006.

[24] M. B. Zimmermann, "Methods to assess iron and iodine status," *The British Journal of Nutrition*, vol. 99, Supplement 3, pp. S2–S9, 2008.

[25] D. Enko, H. Wagner, G. Kriegshäuser, C. Kimbacher, R. Stolba, and G. Halwachs-Baumann, "Assessment of human iron status: a cross-sectional study comparing the clinical utility of different laboratory biomarkers and definitions of iron deficiency in daily practice," *Clinical Biochemistry*, vol. 48, no. 13-14, pp. 891–896, 2015.

[26] M. Worwood, "The laboratory assessment of iron status–an update," *Clinica Chimica Acta*, vol. 259, no. 1-2, pp. 3–23, 1997.

[27] M. E. Elsayed, M. U. Sharif, and A. G. Stack, "Transferrin saturation: a body iron biomarker," *Advances in Clinical Chemistry*, vol. 75, pp. 71–97, 2016.

[28] S. M. H. A. Araujo, V. M. S. Bruin, E. F. Daher, C. A. M. Medeiros, G. H. Almeida, and P. F. C. Bruin, "Quality of sleep and day-time sleepiness in chronic hemodialysis: a study of 400 patients," *Scandinavian Journal of Urology and Nephrology*, vol. 45, no. 5, pp. 359–364, 2011.

[29] A. Pagani, M. Vieillevoye, A. Nai et al., "Regulation of cell surface transferrin receptor-2 by iron-dependent cleavage and release of a soluble form," *Haematologica*, vol. 100, no. 4, pp. 458–465, 2015.

[30] A. Koulaouzidis, E. Said, R. Cottier, and A. A. Saeed, "Soluble transferrin receptors and iron deficiency, a step beyond ferritin. A systematic review," *Journal of Gastrointestinal and Liver Diseases*, vol. 18, no. 3, pp. 345–352, 2009.

[31] S. Guo, D. M. Frazer, and G. J. Anderson, "Iron homeostasis: transport, metabolism, and regulation," *Current Opinion in Clinical Nutrition and Metabolic Care*, vol. 19, no. 4, pp. 276–281, 2016.

[32] R. Castel, M. G. Tax, J. Droogendijk et al., "The transferrin/log(ferritin) ratio: a new tool for the diagnosis of iron deficiency anemia," *Clinical Chemistry and Laboratory Medicine*, vol. 50, no. 8, pp. 1343–1349, 2012.

[33] I. Infusino, F. Braga, A. Dolci, and M. Panteghini, "Soluble transferrin receptor (sTfR) and sTfR/log ferritin index for the diagnosis of iron-deficiency anemia a meta-analysis," *American Journal of Clinical Pathology*, vol. 138, no. 5, pp. 642–649, 2012.

[34] E. J. Lee, E. J. Oh, Y. J. Park, H. K. Lee, and B. K. Kim, "Soluble transferrin receptor (sTfR), ferritin, and sTfR/log ferritin index in anemic patients with nonhematologic malignancy and chronic inflammation," *Clinical Chemistry*, vol. 48, no. 7, pp. 1118–1121, 2002.

[35] A. M. Ganzoni, "Kinetics and regulation of erythrocyte production. Experimental studies on normal and anemic rats," *Experimentelle Medizin, Pathologie und Klinik*, vol. 31, pp. 1–94, 1970.

[36] M. Tkaczyszyn, J. Comín-Colet, A. A. Voors et al., "Iron deficiency and red cell indices in patients with heart failure," *European Journal of Heart Failure*, vol. 20, no. 1, pp. 114–122, 2018.

[37] P. Ponikowski, G. Filippatos, J. C. Colet et al., "The impact of intravenous ferric carboxymaltose on renal function: an analysis of the FAIR-HF study," *European Journal of Heart Failure*, vol. 17, no. 3, pp. 329–339, 2015.

Review Article
Th17/Treg Imbalance and Atherosclerosis

Xin He [iD],[1] **Bo Liang** [iD],[1] and **Ning Gu** [iD][2]

[1]*Nanjing University of Chinese Medicine, Nanjing, China*
[2]*Nanjing Hospital of Chinese Medicine Affiliated to Nanjing University of Chinese Medicine, Nanjing, China*

Correspondence should be addressed to Ning Gu; guning@njucm.edu.cn

Xin He and Bo Liang contributed equally to this work.

Atherosclerosis is nowadays recognized as a chronic inflammatory disease of large arteries. In recent years, cellular and molecular biology studies on atherosclerosis confirmed that the occurrence and development are related to inflammation and autoimmunity. A variety of immune cells, cytokines, and transcription factors are involved in this process. Current studies found that T helper cell 17, regulatory T cells, and their cytokines play an important role in the development of atherosclerosis and vulnerable plaque rupture. Here, we provide a review of the up-to-date applications of T helper cell 17, regulatory T cells, cytokines, and their balance in the prognosis and therapy of atherosclerosis.

1. Introduction

Atherosclerosis, a pathological condition that underlies several important adverse vascular events, including coronary artery disease (CAD), stroke, and peripheral arterial disease, is responsible for most of the cardiovascular morbidity and mortality in the world today [1]. CAD is the further development of atherosclerosis, and its main pathological process is the activation of inflammatory reactions and the coagulation system [2]. A variety of inflammatory cells and cytokines contribute to the thinning of the fibrous cap and enlargement of the lipid core, thus promoting the formation and rupture of vulnerable plaques. Pathogenesis of atherosclerosis includes lipid infiltration, damage response, monocular macrophage invasion, and inflammation response [3]. Currently, atherosclerosis is considered to be a vascular wall chronic inflammatory disease and involves cellular immune responses. T cells predominantly populate atherosclerotic lesions with an enrichment in the fibrous cap [4, 5]. In terms of adaptive immune response, CD4$^+$ T helper cell 1 (Th1) and T helper cell 2 (Th2) are regarded as important factors regulating immune balance. Suppression of Th1 function or enhancement of Th2 function has been proven to reduce atherogenesis in *apolipoprotein E (ApoE)*$^{-/-}$ or l*ow-density lipoprotein receptor (Ldlr)*$^{-/-}$ mice [6–8]. In a mouse model resistant to atherosclerosis, an increase of Th2 protects against early fatty streak development [9]. However, increased evidences indicated that T helper cell 17 (Th17) and regulatory T cells (Treg) are highly involved in atherogenesis [10]. T cells present during all stages of the disease are essential to the development of atherosclerotic plaque. Among them, Th17-mediated proinflammatory responses aggravate atherosclerosis while Treg play a key atheroprotective role by limiting inflammation and counterbalancing plaque formation [11]. Recently, studies found that the Th17/Treg balance could control inflammation and may play an important role in the plaque stability. Therefore, the balance between Th17 and Treg may be important for the development and prevention of atherosclerosis. Here, we critically review the related cytokines, transcription factor, Th17, Treg, and their imbalance in atherosclerosis in order to contribute to the knowledge concerning atherosclerosis pathogenesis.

2. Cytokines

Cytokines are small molecular polypeptides or glycoproteins synthesized and secreted by a variety of tissue cells (mainly immune cells). Cytokines can mediate the interaction between cells and have a variety of biological functions. Emerging evidences show that the interleukin (IL) and transforming growth factor-β (TGF-β) families, two kinds of cytokines, play an important role in the occurrence and development of atherosclerosis [12, 13].

2.1. IL-10. IL-10 is an inhibitory cytokine produced by activated lymphocytes and monocytes, thought to be protective against the development and progression of atherosclerosis. IL-10 suppresses antigen presenting capacity, dendritic cell activity, and T cell proliferation, as well as negatively regulates proinflammatory cytokine production [14, 15]. It is an anti-inflammatory cytokine, deficiency of which increases atherosclerosis in atherosclerosisprone mice [16]. Mallat et al. showed that IL-10 deficiency in C57BL/6 mice fed an atherogenic cholate-containing diet promotes early atherosclerotic lesion formation, characterized by increased infiltration of inflammatory cells, particularly activated T cells, and by increased production of proinflammatory cytokines [17]. Data suggests that a higher level of IL-10 at the time of an acute coronary syndrome event is protective against risk for future cardiovascular events [18, 19]. Animal data suggest that IL-10 prevents atherosclerotic plaque development, improves plaque stability, and promotes lesion size reduction [8, 20, 21]. Studies evidenced that IL-10 can inhibit minimally oxidized low-density lipoprotein-induced monocyte-endothelium interaction [16] and increase actin filament rearrangement in macrophages, and induces the uptake of high-density lipoprotein and low-density lipoprotein by fluid-phase endocytosis [22], thus inhibiting atherosclerotic lesion formation in mice fed an atherosclerotic diet. Systemic or local overexpression of IL-10 by adenoviral gene transfer in a model of collar-induced atherosclerosis in $Ldlr^{-/-}$ mice was found highly efficacious in preventing atherosclerosis [23], and overexpression of IL-10 by activated T lymphocytes reduced atherosclerosis in $Ldlr^{-/-}$ mice [8]. More recently, using a model of chimeric $Ldlr^{-/-}$ mice in which bone marrow cells were deficient for IL-10, we provided evidence that leukocyte-derived IL-10 is instrumental in the prevention of atherosclerotic lesion development and in the modulation of cellular and collagen plaque composition, at least in part, through a systemic immune response modulation [7].

2.2. IL-17. In immune, endothelial, and stromal cells, IL-17 induces the secretion of the proinflammatory cytokine IL-6, granulocyte colony-stimulating factor, and granulocyte-macrophage colony-stimulating factor, as well as chemokines, all of which can be proatherogenic [24]. By contrast, IL-6 and TGF-β induce a subtype of Th17 cells that produces IL-10 concomitantly with IL-17, and IL-10 can be atheroprotective [16, 25, 26]. ApoE is a protein in plasma and plays a vital role in lipid metabolism. It had been confirmed that lack of ApoE resulted in accumulation in plasma of cholesterol-rich remnants and thus induced atherosclerosis. So, the

$ApoE^{-/-}$ mouse is widely used in the research for atherosclerosis as it can manifest pathological features of human atherosclerosis [27, 28]. Experimental studies in $ApoE^{-/-}$ mice on the role of IL-17 yielded discrepant results, with some studies suggesting that IL-17A is proatherogenic [40] and others atheroprotective [29] and a further study suggesting that IL-17 has no effect on atherosclerosis [30]. Some studies in mouse models of atherosclerosis demonstrated that IL-17 can promote plaque stability by increasing the production of type I collagen by vascular smooth muscle cells (VSMC) [49, 61]. Moreover, IL-17 signaling activates various downstream pathways, which include nuclear factor kappaB (NF-κB) and mitogen-activated protein kinases to induce various mediators with relevance to atherosclerosis. The NF-κB transcription factor was discovered 30 years ago and has since emerged as the master regulator of inflammation and immune homeostasis. It achieves this status by means of the large number of important pro- and anti-inflammatory factors under its transcriptional control. NF-κB has a central role in inflammatory diseases such as atherosclerosis. NF-κB is an evolutionarily conserved transcription factor that provides a means to achieve inducible, specific, and regulated immune responses [31]. The proinflammatory nature of the transcriptional targets of NF-κB and their inherent potential for damage to host tissue necessitates tight control of NF-κB activation and transcriptional activity. The consequences of uncontrolled, inappropriate, or dysregulated inflammation are manifested in a range of diseases including atherosclerosis. Many studies identified additional mechanisms, mostly involving posttranslational modification of the NF-κB subunits, that regulate NF-κB-mediated transcriptional responses. An array of posttranslational modifications is identified including phosphorylation, ubiquitination, acetylation, glycosylation, and nitrosylation, all of which directly affect NF-κB transcriptional activity [32]. A study showed that IL-17 can promote the expression of vascular cell adhesion molecule-1 in aortic VSMC by inducing activation of NF-κB, which is important for the development of atherosclerosis. Therefore, these signaling pathways might be therapeutic targets for treatment of IL-17-mediated inflammation [33]. IL-17 alone often stimulates a weak response, but it may synergize with different cytokines like tumor necrosis factor-α, interferon-γ, granulocyte-macrophage colony stimulating factor (GM-CSF), IL-1β, and IL-22 to increased production of inflammatory mediators such as IL-6 and IL-8, leading to increased and prolonged proinflammatory response [34]. On the other hand, the antiatherogenic impact of IL-17 may be referring to its inhibitory action on vascular cell adhesion molecule-1 expression and inflammatory adhesion molecules on fibroblasts and VSMC [35]. Besides, elevated systemic levels of the acute phase C-reactive protein are predictors of future cardiovascular events. The results, confirmed in primary human hepatocytes and coronary artery smooth muscle cells, demonstrate for the first time that IL-17 is a potent inducer of C-reactive protein expression via p38 mitogen-activated protein kinase and extracellular regulated protein kinase 1/2-dependent NF-κB and CCAAT/enhancer binding protein β activation and suggest that IL-17 may mediate chronic inflammation, atherosclerosis, and thrombosis [36].

In some clinical studies, it is shown that plasma IL-17 levels and the number of peripheral Th17 cells are increased in patients with unstable angina or acute myocardial infarction compared with patients with stable angina and healthy individuals [37, 38]. Erbel et al. administered *in vivo* IL-17-blocking antibody in $ApoE^{-/-}$ mice and found that functional blockade of IL-17 reduced atherosclerotic lesion improvement and lowered plaque vulnerability, cellular infiltration, and tissue activation [39]. They concluded that IL-17 plays a pivotal role in atherogenesis.

Retinoic-related orphan receptor- (ROR-) γt is an isoform of ROR-γ that belongs to the retinoid acid-related orphan receptor subgroup; it is best known as the regulator of Th17 cells and more broadly the transcription factor controlling IL-17 production in other cells [40, 41]. ROR-γt plays a crucial role in the induction of autoimmune tissue injuries and inflammation [42]. ROR-γt cooperates with other transcriptional factors, including signal transducer and activator of transcription 3 and runt-related transcription factor 1, to induce IL-17 expression; the transcription factor basic leucine zipper transcription factor controls the differentiation Th17 cells by regulating the expression of ROR-γt [43, 44]. Ubiquitinylation and deubiquitinylation is an inverse process that can regulate protein stability dynamically. It is found that TGF-β plus IL-6 which are important signals for Th17 differentiation could enhance the deubiquitinylation mediated by Ubiquitin-Specific Peptidase 4, which could promote ROR-γt function, suggesting that Ubiquitin-Specific Peptidase 4 may play a role in Th17 development [45]. Transcription factors are also involved in the regulation of ROR-γt. A study established that Forkhead Box P3 (Foxp3) can inhibit ROR-γt transcriptional activity during Th17 differentiation [46].

Recently, a study demonstrated that loss of the immune-regulatory factor tripartite motif containing 21 (Trim21) influences the atheromatous process. Trim21, as a ubiquitin E3 ligase, is the effector ligase in the ubiquitination cascade; the main role has been implicated in immune processes. The research showed that Trim21-deficient bone marrow transplanted into $Ldlr^{-/-}$ mice fed a hypercholesterolemic diet would develop larger atherosclerotic plaques with significantly higher collagen content. $Ldlr^{-/-}$ mice are one of the most widely used genetically engineered animals in the field of atherosclerosis. Compared with $ApoE^{-/-}$ mice, the lipoprotein profile of $Ldlr^{-/-}$ mice is closer to humans, which is helpful to infer the relationship between lipoprotein changes and human atherosclerosis and hyperlipidemia [47]. The data showed that TRIM21 deficiency promotes IL-17 expression, smooth muscle cell levels increased, and protein expression levels of interferon-γ and matrix metalloproteinases (MMPs) decreased in mice. The result indicated that Trim21 affects atherosclerosis by regulating the Th17 response, promoting plaque fibrosis and stability [48].

Furthermore, the detrimental effects of a high-salt diet on human health have received much attention in the past few years. It has been well established that high dietary salt intake is related to cardiovascular diseases; most studies discussing the mechanism for the detrimental effect of high salt demonstrated a pivotal involvement of pathogenic Th17 cells. In

humans, GM-CSF expression was shown to be inhibited by the IL-23/ROR-γt/Th17 axis [49]. A study indicated that high sodium concentrations increased the differentiation of murine and human Th17 cells and induced a highly pathogenic phenotype, characterized by an increased expression of the surface receptors IL-23 receptor and chemokine receptor C-C motif chemokine receptor 6 and the upregulation of GM-CSF, IL-2, and tumor necrosis factor-α. This plays an important role in the occurrence and development of atherosclerosis [50]. In addition to the increased induction of proinflammatory Th17 cells, excess dietary sodium intake can impact autoimmunity by reducing the number of Treg and inhibiting the function of Treg.

2.3. IL-35. IL-35, a novel functional cytokine of Treg comprised of the IL-12p35 subunit and the other subunit Epstein-Barr virus-induced gene 3, regulates the activity of CD4$^+$ T cells and macrophages, thereby playing a critical role in atherosclerosis [51]. In a study, researchers examined the expression of IL-35 during early atherosclerosis and found that IL-35 blocks lysophosphatidylcholine-induced mitochondrial reactive oxygen species, which are required for the induction of site-specific histone 3 lysine 14 acetylation, increased binding of proinflammatory transcription factor activator protein-1 in the promoter of intercellular adhesion molecule-1, and induction of intercellular adhesion molecule-1 transcription in human aortic endothelial cells. It indicated that IL-35 is induced during atherosclerosis development and inhibits mitochondrial reactive oxygen species-histone 3 lysine 14 acetylation-activator protein-1-mediated endothelial cell activation [52]. Recently, Huang et al. found that in $ApoE^{-/-}$ mice, IL-12p35 deficiency reduces the level of IL-35, inhibits the generation and function of Treg, exacerbates Th17/Treg imbalance, promotes atherosclerosis, but stabilizes the plaque [51]. In animal studies, treatment with recombinant human IL-35 led to an increase in both circulating and local Treg levels and a reduction in the plaque size in $ApoE^{-/-}$ mice, suggesting that IL-35 attenuates atherosclerosis via upregulating Treg immune response [53]. Taken together, these results indicated that IL-35 exerts an antiatherosclerotic effect and facilitates stability of the vulnerable plaques by increasing Treg levels.

2.4. TGF-β. TGF-β is a potent anti-inflammatory, immune-suppressive, and profibrotic cytokine, with major effects on the biology of VSMC [54]. The anti-inflammatory and profibrotic properties of TGF-β highly suggest the potential anti-atherogenic role for this cytokine. Recent advances in the study of atherosclerosis point to an important role of TGF-β signaling in the protection against excessive plaque inflammation, loss of collagen content, and induction of regulatory immunity [54]. Specific abrogation of TGF-β receptor 2 signaling in T cells aggravates atherosclerosis and causes an inflammatory and destabilized plaque phenotype [55]. Overexpressing TGF-β in hearts of $ApoE^{-/-}$ mice decreases lesion size, reduces T cell infiltration, and increases collagen production in the plaques, demonstrating the critical role of TGF-β for VSMC matrix production and plaque stability in atherosclerosis [56]. TGF-β-triggered signals are transduced

by proteins belonging to the SMAD family [57]. Immunohistochemistry and reverse transcription-polymerase chain reaction analysis of human plaques reveal SMAD family member 2, SMAD family member 3, and SMAD family member 4 expression in macrophages of fibrofatty lesions and in VSMC of fibrous caps [58]. Mallat et al. also detected phosphorylated SMAD family member 2 in the aortic sinus of $ApoE^{-/-}$ mice, indicative of TGF-β activity in atherosclerotic lesions [59]. SMAD family member 7 (Smad7) is viewed as a major inhibitory regulator of TGF-β signaling. Bone marrow from mice with a T cell-specific deletion of Smad7, a potent inhibitor of TGF-β signaling, was transplanted into hypercholesterolemic $Ldlr^{-/-}$ mice. Smad7-deficient mice had significantly larger atherosclerotic lesions that contained large collagen-rich caps, consistent with a more stable phenotype [60]. Taken together, these results show that abrogation of TGF-β signaling in T cells increases atherosclerosis and suggest that TGF-β reduces atherosclerosis by dampening T cell activation [55, 61]. The important role of TGF-β signaling in atherosclerosis suggests that regulatory pathways in adaptive immunity are essential in modulation of the development and progression of atherosclerosis.

3. Foxp3

Foxp3 is a marker of human Treg, which is critical for anti-inflammatory responses and for maintaining immune tolerance mainly by regulating the secretion of the anti-inflammatory cytokine IL-10 [62]. TGF-β plus T cell receptor stimulation triggers naive $CD4^+$ $CD25^-$ $Foxp3^-$ T cells to differentiate into $Foxp3^+$ Tregs, via a SMAD-dependent pathway in mice [63, 64]. It has been reported that a number of factors can influence the expression of Foxp3 including conserved noncoding DNA sequence at the Foxp3 gene locus and transcription factors such as NF-κB, nuclear factor of activated T cells, SMAD family member 3, signal transducers, and activators of transcription 5 [65]. Using transgenic mice with increased or decreased NF-κB activity, Long et al. showed that the T cell receptor-induced NF-κB pathway upregulates Foxp3 expression [66]. A clinical study showed that CD31 signal transduction mediated by recruitment and activation of tyrosine phosphatases, resulting in attenuated Foxp3 expression leads to impaired secretion of inhibitory cytokines and subsequent suppressor function of Treg cells [11]. According to a study, Foxp3 can be regulated by various posttranscriptional modifications including ubiquitinylation, acetylation, and phosphorylation, which can influence both its stability and function [65]. An Foxp3 E3 ligase STIP1 homology and u-box containing protein 1 (STUB1) was recently identified by Chen et al., and it targets Foxp3 to degradation by promoting K48-linked polyubiquitinylation of Foxp3 in a heat shock protein 70-dependent manner. Based on the role STUB1 plays in regulating the stability of Foxp3, targeting STUB1 may be beneficial in the inflammation conditions of atherosclerosis [67]. Li et al. found that TGF-β could increase the acetylated level of Foxp3 and promote the recruitment of Foxp3 to IL-2 promoter. Inversely, IL-6 treatment reverses this effect, suggesting that the inflammatory signals downregulate Treg function par-

tially through regulating Foxp3 acetylation. Further, histone deacetylation inhibitor treatment abolished the decreased acetylation of Foxp3 by TGF-β and IL-6, suggesting that TGF-β and IL-6 may upregulate histone deacetylation to deacetylate Foxp3 [68].

4. Immune Cells

4.1. Th17. In the past decade, increasing attention has been focused on a subset of $CD4^+$ T cells, commonly known as Th17 cells. Th17, the third subpopulation of Th cells, plays critical roles in the development of autoimmunity and allergic reactions and recently has been thought to be key regulators of inflammation and thus may potentially contribute to the immunopathogenesis of atherosclerosis [69, 70]. Th17 cells are characterized by expression of the Th17-defining transcription factor nuclear receptor retinoic-related orphan receptor- (ROR-) γt. Th17 cells are activated by IL-23, and IL-17 is their main secreted cytokine [24].

4.2. Treg. Naturally arising Treg cells, most of which are produced by the normal thymus as a functionally mature T cell subpopulation, play key roles in the maintenance of immunologic self-tolerance and negative control of a variety of physiological and pathological immune responses. Treg can be divided into natural Treg and inducible Treg and plays a significantly protective role in atherosclerosis by limiting inflammation and stabilizing plaque. Treg cells exert their atheroprotective properties by secreting IL-10 and TGF-β and by suppressing the proliferation of proinflammatory effector T cells [71]. In mice, Treg cells protect against atherosclerosis [72]. Similarly, clinical data suggest a strong inverse relationship between Treg cells and atherosclerosis, whereby Treg cell numbers and IL-10, a cytokine secreted by Treg cells, are lower in patients with myocardial infarction than in patients with stable angina or individuals without coronary artery disease [73, 74]. Studies showed that the generation of Treg cells induced by immunity can reduce atherosclerosis in mice [75–77].

4.3. Th17/Treg Imbalance. The Th17/Treg is a newly balanced pair which plays an important role in the development of atherosclerosis and plague rupture [78]. Various signals, factors, epigenetic modifications, metabolic pathways, and microbiota are shown to regulate the plasticity between Tregs and Th17 cells [65]. A clinical study showed that the Th17/Treg imbalance might act synergistically with microinflammation on immune-mediated atherosclerosis and contribute to the high incidence of adverse cardiovascular events [79]. Compared with healthy people, the number of Th17 in the peripheral blood of CAD patients and IL-17, IL-6, IL-23, and ROR-γt levels increased significantly; the number of Treg, IL-10, TGF-β, and Foxp3 and the ratio of Treg and Th17 decreased significantly. The results showed that patients with CAD had significant Th17/Treg imbalance, suggesting the potential role of Th17/Treg imbalance in plaque instability and CAD episodes [37]. Numerous animal studies have proven that reversing the imbalance of Th17/Treg significantly attenuated atherosclerosis by drugs.

Peroxisome proliferator-activated receptors could regulate Th17 and Treg plasticity by enhancing Foxp3 expression and decreasing ROR-γt and IL-17A expression. Pioglitazone, an agonist of peroxisome proliferator-activated receptors, could stabilize atherosclerotic plaque by inducing protein phosphorylation, decreasing IL-17, and increasing Foxp3 cells, improving Th17/Treg balance in the spleen of $ApoE^{-/-}$ mice [80]. The Angong Niuhuang pill, a Chinese traditional medicine, has been proven to protect atherosclerotic $ApoE^{-/-}$ mice by regulating Th17/Treg balance, inhibiting chronic inflammation, reducing plaque collagen fibers, and reducing inflammatory cell infiltration, which are probably related to regulating ROR-γt and Foxp3 expression [81]. In addition, a recent clinical study shows that after statin treatment, the number of Th17 and accumulation of IL-17, IL-6, and IL-23 decreased and the number of Treg and accumulation of IL-10 and TGF-β increased in the peripheral blood in CAD patients. It indicated that statin therapy could ameliorate the Th17 and Treg functional imbalance in patients with CAD. Thus, Th17/Treg imbalance plays an important role in the development of atherosclerosis and plaque instability. Drug therapy can reverse the Th17/Treg imbalance, delaying the progress of atherosclerosis and stabilizing plaque.

5. Conclusion

Atherosclerosis is the main cause of most cardiovascular and cerebrovascular diseases. The activation of immunity is closely related to atherosclerosis; at the same time, the imbalance of regulatory and pathogenic immunity may promote the development of atherosclerosis. The balance between pro- and anti-inflammatory cytokines has emerged as a major determinant of atherosclerosis. Therefore, exploring the Th17/Treg imbalance could provide a new idea and target for the treatment of atherosclerosis.

Data Availability

The data used to support the findings of this study are included within the article.

Conflicts of Interest

The authors declare that they have no conflicts of interest.

Authors' Contributions

Xin He and Bo Liang contributed to this article equally as first authors.

Acknowledgments

References

[1] S. L. Lai, R. Marin-Juez, and D. Y. R. Stainier, "Immune responses in cardiac repair and regeneration: a comparative point of view," *Cellular and Molecular Life Sciences*, vol. 76, no. 7, pp. 1365–1380, 2019.

[2] A. V. Khera and S. Kathiresan, "Genetics of coronary artery disease: discovery, biology and clinical translation," *Nature Reviews. Genetics*, vol. 18, no. 6, pp. 331–344, 2017.

[3] Q. Li, Y. Kuang, J. Qiu, X. Zhang, Y. Ruan, and Z. Li, "The correlation between plasma tissue factor and interleukin 18 and their significance in patients with acute coronary syndrome," *Cardiovascular Toxicology*, vol. 15, no. 3, pp. 276–282, 2015.

[4] L. Jonasson, J. Holm, O. Skalli, G. Bondjers, and G. K. Hansson, "Regional accumulations of T cells, macrophages, and smooth muscle cells in the human atherosclerotic plaque," *Arteriosclerosis*, vol. 6, no. 2, pp. 131–138, 1986.

[5] G. K. Hansson, L. Jonasson, B. Lojsthed, S. Stemme, O. Kocher, and G. Gabbiani, "Localization of T lymphocytes and macrophages in fibrous and complicated human atherosclerotic plaques," *Atherosclerosis*, vol. 72, no. 2-3, pp. 135–141, 1988.

[6] E. Laurat, B. Poirier, E. Tupin et al., "In vivo downregulation of T helper cell 1 immune responses reduces atherogenesis in apolipoprotein E-knockout mice," *Circulation*, vol. 104, no. 2, pp. 197–202, 2001.

[7] S. Potteaux, B. Esposito, O. van Oostrom et al., "Leukocyte-derived interleukin 10 is required for protection against atherosclerosis in low-density lipoprotein receptor knockout mice," *Arteriosclerosis, Thrombosis, and Vascular Biology*, vol. 24, no. 8, pp. 1474–1478, 2004.

[8] L. J. Pinderski, M. P. Fischbein, G. Subbanagounder et al., "Overexpression of interleukin-10 by activated T lymphocytes inhibits atherosclerosis in LDL receptor-deficient mice by altering lymphocyte and macrophage phenotypes," *Circulation Research*, vol. 90, no. 10, pp. 1064–1071, 2002.

[9] S. A. Huber, P. Sakkinen, C. David, M. K. Newell, and R. P. Tracy, "T helper-cell phenotype regulates atherosclerosis in mice under conditions of mild hypercholesterolemia," *Circulation*, vol. 103, no. 21, pp. 2610–2616, 2001.

[10] A. K. Robertson and G. K. Hansson, "T cells in atherogenesis," *Arteriosclerosis, Thrombosis, and Vascular Biology*, vol. 26, no. 11, pp. 2421–2432, 2006.

[11] L. Huang, Y. Zheng, X. Yuan et al., "Decreased frequencies and impaired functions of the CD31+ subpopulation in Treg cells associated with decreased FoxP3 expression and enhanced Treg cell defects in patients with coronary heart disease," *Clinical and Experimental Immunology*, vol. 187, no. 3, pp. 441–454, 2017.

[12] A. Grebe, F. Hoss, and E. Latz, "NLRP3 inflammasome and the IL-1 pathway in atherosclerosis," *Circulation Research.*, vol. 122, no. 12, pp. 1722–1740, 2018.

[13] M.-J. Goumans and P. Ten Dijke, "TGF-β signaling in control of cardiovascular function," *Cold Spring Harbor Perspectives in Biology*, vol. 10, no. 2, p. a022210, 2018.

[14] A. O'Garra, F. J. Barrat, A. G. Castro, A. Vicari, and C. Hawrylowicz, "Strategies for use of IL-10 or its antagonists in human disease," *Immunological Reviews*, vol. 223, no. 1, pp. 114–131, 2008.

[15] M. Saraiva and A. O'Garra, "The regulation of IL-10 production by immune cells," *Nature Reviews. Immunology*, vol. 10, no. 3, pp. 170–181, 2010.

[16] L. J. Pinderski Oslund, C. C. Hedrick, T. Olvera et al., "Interleukin-10 blocks atherosclerotic events in vitro and in vivo," *Arteriosclerosis, Thrombosis, and Vascular Biology*, vol. 19, no. 12, pp. 2847–2853, 1999.

[17] Z. Mallat, S. Besnard, M. Duriez et al., "Protective role of interleukin-10 in atherosclerosis," *Circulation Research*, vol. 85, no. 8, pp. e17–e24, 1999.

[18] D. F. Zhang, X. T. Song, Y. D. Chen et al., "Prognostic performance of interleukin-10 in patients with chest pain and mild to moderate coronary artery lesions-an 8-year follow-up study," *Journal of Geriatric Cardiology*, vol. 13, no. 3, pp. 244–251, 2016.

[19] C. Heeschen, S. Dimmeler, C. W. Hamm et al., "Serum level of the antiinflammatory cytokine interleukin-10 is an important prognostic determinant in patients with acute coronary syndromes," *Circulation*, vol. 107, no. 16, pp. 2109–2114, 2003.

[20] G. Caligiuri, M. Rudling, V. Ollivier et al., "Interleukin-10 deficiency increases atherosclerosis, thrombosis, and low-density lipoproteins in apolipoprotein E knockout mice," *Molecular Medicine*, vol. 9, no. 1-2, pp. 10–17, 2003.

[21] X. Han, S. Kitamoto, H. Wang, and W. A. Boisvert, "Interleukin-10 overexpression in macrophages suppresses atherosclerosis in hyperlipidemic mice," *The FASEB Journal*, vol. 24, no. 8, pp. 2869–2880, 2010.

[22] D. Lucero, P. Islam, L. A. Freeman et al., "Interleukin 10 promotes macrophage uptake of HDL and LDL by stimulating fluid-phase endocytosis," *Biochimica et Biophysica Acta - Molecular and Cell Biology of Lipids*, vol. 1865, no. 2, p. 158537, 2020.

[23] J. H. Thüsen, J. Kuiper, M. L. Fekkes, P. Vos, T. J. C. Berkel, and E. A. L. Biessen, "Attenuation of atherogenesis by systemic and local adenovirus-mediated gene transfer of interleukin-10 in LDLr -/- mice," *The FASEB Journal*, vol. 15, no. 14, pp. 1–19, 2001.

[24] M. J. McGeachy, D. J. Cua, and S. L. Gaffen, "The IL-17 family of cytokines in health and disease," *Immunity*, vol. 50, no. 4, pp. 892–906, 2019.

[25] M. J. McGeachy, K. S. Bak-Jensen, Y. Chen et al., "TGF-beta and IL-6 drive the production of IL-17 and IL-10 by T cells and restrain T(H)-17 cell-mediated pathology," *Nature Immunology*, vol. 8, no. 12, pp. 1390–1397, 2007.

[26] Y. Lee, A. Awasthi, N. Yosef et al., "Induction and molecular signature of pathogenic TH17 cells," *Nature Immunology*, vol. 13, no. 10, pp. 991–999, 2012.

[27] E. de Franca, J. G. B. Alves, and M. H. Hutz, "Apolipoprotein E polymorphism and its association with serum lipid levels in Brazilian children," *Human Biology*, vol. 76, no. 2, pp. 267–275, 2004.

[28] S. Zhang, R. Reddick, J. Piedrahita, and N. Maeda, "Spontaneous hypercholesterolemia and arterial lesions in mice lacking apolipoprotein E," *Science*, vol. 258, no. 5081, pp. 468–471, 1992.

[29] K. Danzaki, Y. Matsui, M. Ikesue et al., "Interleukin-17A deficiency accelerates unstable atherosclerotic plaque formation in apolipoprotein E-deficient mice," *Arteriosclerosis, Thrombosis, and Vascular Biology*, vol. 32, no. 2, pp. 273–280, 2012.

[30] M. S. Madhur, S. A. Funt, L. Li et al., "Role of interleukin 17 in inflammation, atherosclerosis, and vascular function in apolipoprotein e-deficient mice," *Arteriosclerosis, Thrombosis, and Vascular Biology*, vol. 31, no. 7, pp. 1565–1572, 2011.

[31] J. P. Mitchell and R. J. Carmody, "NF-κB and the transcriptional control of inflammation," *International Review of Cell and Molecular Biology*, vol. 335, pp. 41–84, 2018.

[32] F. Christian, E. L. Smith, and R. J. Carmody, "The regulation of NF-κB subunits by phosphorylation," *Cells*, vol. 5, no. 1, p. 12, 2016.

[33] H. Zhang, J. Chen, X. Liu et al., "IL-17 induces expression of vascular cell adhesion molecule through signalling pathway of NF-κB, but not Akt1 and TAK1 in vascular smooth muscle cells," *Scandinavian Journal of Immunology*, vol. 77, no. 4, pp. 230–237, 2013.

[34] A. Beringer, M. Noack, and P. Miossec, "IL-17 in chronic inflammation: from discovery to targeting," *Trends in Molecular Medicine*, vol. 22, no. 3, pp. 230–241, 2016.

[35] M. S. Madhur, H. E. Lob, L. A. McCann et al., "Interleukin 17 promotes angiotensin II-induced hypertension and vascular dysfunction," *Hypertension*, vol. 55, no. 2, pp. 500–507, 2010.

[36] D. N. Patel, C. A. King, S. R. Bailey et al., "Interleukin-17 stimulates C-reactive protein expression in hepatocytes and smooth muscle cells via p38 MAPK and ERK1/2-dependent NF-kappaB and C/EBPbeta activation," *The Journal of Biological Chemistry*, vol. 282, no. 37, pp. 27229–27238, 2007.

[37] X. Cheng, X. Yu, Y. J. Ding et al., "The Th17/Treg imbalance in patients with acute coronary syndrome," *Clinical Immunology*, vol. 127, no. 1, pp. 89–97, 2008.

[38] S. Hashmi and Q. T. Zeng, "Role of interleukin-17 and interleukin-17-induced cytokines interleukin-6 and interleukin-8 in unstable coronary artery disease," *Coronary Artery Disease*, vol. 17, no. 8, pp. 699–706, 2006.

[39] C. Erbel, L. Chen, F. Bea et al., "Inhibition of IL-17A attenuates atherosclerotic lesion development in apoE-deficient mice," *Journal of Immunology*, vol. 183, no. 12, pp. 8167–8175, 2009.

[40] I. I. Ivanov, B. S. McKenzie, L. Zhou et al., "The orphan nuclear receptor RORγt directs the differentiation program of proinflammatory IL-17+ T helper cells," *Cell*, vol. 126, no. 6, pp. 1121–1133, 2006.

[41] I. I. Ivanov, L. Zhou, and D. R. Littman, "Transcriptional regulation of Th17 cell differentiation," *Seminars in Immunology*, vol. 19, no. 6, pp. 409–417, 2007.

[42] D. Mucida, Y. Park, G. Kim et al., "Reciprocal TH17 and regulatory T cell differentiation mediated by retinoic acid," *Science*, vol. 317, no. 5835, pp. 256–260, 2007.

[43] B. R. Marks, H. N. Nowyhed, J. Y. Choi et al., "Thymic self-reactivity selects natural interleukin 17-producing T cells that can regulate peripheral inflammation," *Nature Immunology*, vol. 10, no. 10, pp. 1125–1132, 2009.

[44] F. Zhang, G. Meng, and W. Strober, "Interactions among the transcription factors Runx1, RORgammat and Foxp3 regulate the differentiation of interleukin 17-producing T cells," *Nature Immunology*, vol. 9, no. 11, pp. 1297–1306, 2008.

[45] J. Yang, P. Xu, L. Han et al., "Cutting edge: ubiquitin-specific protease 4 promotes Th17 cell function under inflammation by deubiquitinating and stabilizing RORγt," *Journal of Immunology*, vol. 194, no. 9, pp. 4094–4097, 2015.

[46] J. Du, C. Huang, B. Zhou, and S. F. Ziegler, "Isoform-specific inhibition of ROR alpha-mediated transcriptional activation by human FOXP3," *Journal of Immunology*, vol. 180, no. 7, pp. 4785–4792, 2008.

[47] R. A. Matthijsen, M. P. de Winther, D. Kuipers et al., "Macrophage-specific expression of mannose-binding lectin controls

atherosclerosis in low-density lipoprotein receptor-deficient mice," *Circulation*, vol. 119, no. 16, pp. 2188–2195, 2009.

[48] S. Brauner, X. Jiang, G. E. Thorlacius et al., "Augmented Th17 differentiation in Trim21 deficiency promotes a stable phenotype of atherosclerotic plaques with high collagen content," *Cardiovascular Research*, vol. 114, no. 1, pp. 158–167, 2018.

[49] R. Noster, R. Riedel, M.-F. Mashreghi et al., "IL-17 and GM-CSF expression are antagonistically regulated by human T helper cells," *Science Translational Medicine*, vol. 6, no. 241, p. 241ra280, 2014.

[50] S. Haase, N. Wilck, M. Kleinewietfeld, D. N. Müller, and R. A. Linker, "Sodium chloride triggers Th17 mediated autoimmunity," *Journal of Neuroimmunology*, vol. 329, pp. 9–13, 2019.

[51] Y. Huang, H. Hu, L. Liu et al., "Interleukin-12p35 deficiency reverses the Th1/Th2 imbalance, aggravates the Th17/Treg imbalance, and ameliorates atherosclerosis in ApoE-/- mice," *Mediators of Inflammation*, vol. 2019, 3152012 pages, 2019.

[52] X. Li, Y. Shao, X. Sha et al., "IL-35 (interleukin-35) suppresses endothelial cell activation by inhibiting mitochondrial reactive oxygen species-mediated site-specific acetylation of H3K14 (histone 3 lysine 14)," *Arteriosclerosis, Thrombosis, and Vascular Biology*, vol. 38, no. 3, pp. 599–609, 2018.

[53] J. Ye, Y. Huang, B. Que et al., "Interleukin-12p35 knock out aggravates doxorubicin-induced cardiac injury and dysfunction by aggravating the inflammatory response, oxidative stress, apoptosis and autophagy in mice," *EBioMedicine*, vol. 35, pp. 29–39, 2018.

[54] D. J. Grainger, "Transforming growth factor β and atherosclerosis: so far, so good for the protective cytokine hypothesis," *Arteriosclerosis, Thrombosis, and Vascular Biology*, vol. 24, no. 3, pp. 399–404, 2004.

[55] A. K. Robertson, M. Rudling, X. Zhou, L. Gorelik, R. A. Flavell, and G. K. Hansson, "Disruption of TGF-beta signaling in T cells accelerates atherosclerosis," *The Journal of Clinical Investigation*, vol. 112, no. 9, pp. 1342–1350, 2003.

[56] A. D. Frutkin, G. Otsuka, A. Stempien-Otero et al., "TGF-[beta]1 limits plaque growth, stabilizes plaque structure, and prevents aortic dilation in apolipoprotein E-null mice," *Arteriosclerosis, Thrombosis, and Vascular Biology*, vol. 29, no. 9, pp. 1251–1257, 2009.

[57] A. Tedgui and Z. Mallat, "Cytokines in atherosclerosis: pathogenic and regulatory pathways," *Physiological Reviews*, vol. 86, no. 2, pp. 515–581, 2006.

[58] N. Kalinina, A. Agrotis, Y. Antropova et al., "Smad expression in human atherosclerotic lesions," *Arteriosclerosis, Thrombosis, and Vascular Biology*, vol. 24, no. 8, pp. 1391–1396, 2004.

[59] Z. Mallat, A. Gojova, C. Marchiol-Fournigault et al., "Inhibition of transforming growth factor-beta signaling accelerates atherosclerosis and induces an unstable plaque phenotype in mice," *Circulation Research*, vol. 89, no. 10, pp. 930–934, 2001.

[60] A. Gisterå, A. K. Robertson, J. Andersson et al., "Transforming growth Factor–β signaling in T cells promotes stabilization of atherosclerotic plaques through an interleukin-17-dependent pathway," *Science Translational Medicine*, vol. 5, no. 196, p. 196ra100, 2013.

[61] O. Ovchinnikova, A. K. Robertson, D. Wågsäter et al., "T-cell activation leads to reduced collagen maturation in atherosclerotic plaques of Apoe(-/-) mice," *The American Journal of Pathology*, vol. 174, no. 2, pp. 693–700, 2009.

[62] S. Sakaguchi, M. Ono, R. Setoguchi et al., "Foxp3+ CD25+ CD4+ natural regulatory T cells in dominant self-tolerance and autoimmune disease," *Immunological Reviews*, vol. 212, no. 1, pp. 8–27, 2006.

[63] E. Bettelli, Y. Carrier, W. Gao et al., "Reciprocal developmental pathways for the generation of pathogenic effector TH17 and regulatory T cells," *Nature*, vol. 441, no. 7090, pp. 235–238, 2006.

[64] X. Luo, K. V. Tarbell, H. Yang et al., "Dendritic cells with TGF-beta1 differentiate naive CD4+CD25- T cells into islet-protective Foxp3+ regulatory T cells," *Proceedings of the National Academy of Sciences of the United States of America*, vol. 104, no. 8, pp. 2821–2826, 2007.

[65] J. Ren and B. Li, "The functional stability of FOXP3 and RORγt in Treg and Th17 and their therapeutic applications," *Advances in Protein Chemistry and Structural Biology*, vol. 107, pp. 155–189, 2017.

[66] M. Long, S. G. Park, I. Strickland, M. S. Hayden, and S. Ghosh, "Nuclear factor-kappaB modulates regulatory T cell development by directly regulating expression of Foxp3 transcription factor," *Immunity*, vol. 31, no. 6, pp. 921–931, 2009.

[67] L. Chen, J. Wu, E. Pier, Y. Zhao, and Z. Shen, "mTORC2-PKBα/Akt1 serine 473 phosphorylation axis is essential for regulation of FOXP3 stability by chemokine CCL3 in psoriasis," *The Journal of Investigative Dermatology*, vol. 133, no. 2, pp. 418–428, 2013.

[68] A. Samanta, B. Li, X. Song et al., "TGF-beta and IL-6 signals modulate chromatin binding and promoter occupancy by acetylated FOXP3," *Proceedings of the National Academy of Sciences of the United States of America*, vol. 105, no. 37, pp. 14023–14027, 2008.

[69] R. E. Eid, D. A. Rao, J. Zhou et al., "Interleukin-17 and interferon-γ are produced concomitantly by human coronary artery-infiltrating T cells and act synergistically on vascular smooth muscle cells," *Circulation*, vol. 119, no. 10, pp. 1424–1432, 2009.

[70] H. Park, Z. Li, X. O. Yang et al., "A distinct lineage of CD4 T cells regulates tissue inflammation by producing interleukin 17," *Nature Immunology*, vol. 6, no. 11, pp. 1133–1141, 2005.

[71] A. C. Foks, A. H. Lichtman, and J. Kuiper, "Treating atherosclerosis with regulatory T cells," *Arteriosclerosis, Thrombosis, and Vascular Biology*, vol. 35, no. 2, pp. 280–287, 2015.

[72] R. Klingenberg, N. Gerdes, R. M. Badeau et al., "Depletion of FOXP3+ regulatory T cells promotes hypercholesterolemia and atherosclerosis," *The Journal of Clinical Investigation*, vol. 123, no. 3, pp. 1323–1334, 2013.

[73] J. George, S. Schwartzenberg, D. Medvedovsky et al., "Regulatory T cells and IL-10 levels are reduced in patients with vulnerable coronary plaques," *Atherosclerosis*, vol. 222, no. 2, pp. 519–523, 2012.

[74] A. Mor, G. Luboshits, D. Planer, G. Keren, and J. George, "Altered status of CD4(+)CD25(+) regulatory T cells in patients with acute coronary syndromes," *European Heart Journal*, vol. 27, no. 21, pp. 2530–2537, 2006.

[75] D. Wolf and K. Ley, "Immunity and inflammation in atherosclerosis," *Circulation Research*, vol. 124, no. 2, pp. 315–327, 2019.

[76] T. Kimura, K. Kobiyama, H. Winkels et al., "Regulatory CD4(+) T cells recognize major histocompatibility complex

class II molecule-restricted peptide epitopes of apolipoprotein B," *Circulation*, vol. 138, no. 11, pp. 1130–1143, 2018.

[77] M. Vila-Caballer, J. M. González-Granado, V. Zorita et al., "Disruption of the CCL1-CCR8 axis inhibits vascular Treg recruitment and function and promotes atherosclerosis in mice," *Journal of Molecular and Cellular Cardiology*, vol. 132, pp. 154–163, 2019.

[78] J. J. Xie, J. Wang, T. T. Tang et al., "The Th17/Treg functional imbalance during atherogenesis in ApoE(-/-) mice," *Cytokine*, vol. 49, no. 2, pp. 185–193, 2010.

[79] J. Zhang, G. Hua, X. Zhang, R. Tong, X. Du, and Z. Li, "Regulatory T cells/T-helper cell 17 functional imbalance in uraemic patients on maintenance haemodialysis: a pivotal link between microinflammation and adverse cardiovascular events," *Nephrology (Carlton, Vic.)*, vol. 15, no. 1, pp. 33–41, 2010.

[80] Y. Tian, T. Chen, Y. Wu et al., "Pioglitazone stabilizes atherosclerotic plaque by regulating the Th17/Treg balance in AMPK-dependent mechanisms," *Cardiovascular Diabetology*, vol. 16, no. 1, p. 140, 2017.

[81] Q. Fan, Y. Liu, J. Rao et al., "Anti-atherosclerosis effect of Angong Niuhuang pill via regulating Th17/Treg immune balance and inhibiting chronic inflammatory on ApoE(-/-) mice model of early and mid-term atherosclerosis," *Frontiers in Pharmacology*, vol. 10, p. 1584, 2020.

Research Article

Catestatin as a New Prognostic Marker in Stable Patients with Heart Failure with Reduced Ejection Fraction in Two-Year Follow-Up

Łukasz Wołowiec ⬤, **Daniel Rogowicz, Joanna Banach, Wojciech Gilewski, Władysław Sinkiewicz, and Grzegorz Grześk**

Department of Cardiology and Clinical Pharmacology, Faculty of Health Sciences, Ludwik Rydygier Collegium Medicum in Bydgoszcz, Nicolaus Copernicus University in Toruń, Poland

Correspondence should be addressed to Łukasz Wołowiec; lordtor111@gmail.com

Background and Purpose. The main goal of the study was to assess the usefulness of plasma concentrations of catestatin as a predictor of a composite endpoint (CE): unplanned hospitalization and death for all causes in patients with HFrEF in the midterm follow-up. *Experimental Approach*. The study group consisted of 52 Caucasian patients in NYHA classes II and III. The control group consisted of 24 healthy volunteers. The biomarkers, whose concentration was assessed before and after physical exertion as well as the variability of their concentration under the influence of the physical exertion, were NT-proBNP, troponin T, and catestatin. *Key Results*. During the 24-month follow-up period, 11 endpoints were recorded. The univariate analysis of the Cox proportional hazard model showed a statistically significant effect of all assessed CST concentrations on the occurrence of CE. In the 24-month follow-up, where the starting concentration of catestatin was compared with other recognized prognostic factors in HF, the initial concentration of catestatin showed statistical significance in CE prognosis as the only parameter tested. *Conclusions*. Plasma concentration of catestatin before and after physical exertion is a valuable prognostic parameter in predicting death from all causes and unplanned hospitalization in the group of patients with HFrEF in the 2-year follow-up.

1. Introduction

The incidence of heart failure (HF) is constantly increasing, due to the aging of the population and as a result of improved survival after acute myocardial infarction (AMI). The prevalence of HF in developed countries is 1-2%, and it is the most common cause of hospitalization among patients >65 years of age [1]. Along with the development of new HF diagnostic and therapeutic methods, it has become important to define and adapt them to a specific group of patients who will benefit most from innovative methods. It results in the growing role of biomarkers in the risk stratification process within the group of HF patients.

Numerous laboratory findings were found to play an important role in defining the group of HF patients with the most serious prognosis. Natriuretic peptides, hyponatremia, C-reactive protein, melanoma cell adhesion molecule (MCAM), procalcitonin, haemoglobin level, or red blood cell distribution width (RDW) are among the most available ones [2–4]. Nonetheless, the search for a new sensitive and specific risk biomarker is still ongoing.

Catestatin (CST) was discovered in 1997, and recent reports on the importance of CST in cardiovascular diseases suggest a cardioprotective role of this peptide. The precursor to CST is chromogranin A (CgA), which is an acidic hydrophilic protein found mainly in the granules of secretory

neuroendocrine cells. CST, apart from chromaffin and noradrenergic cells, is also found in myocardial tissues, where a decrease in CST concentration is found with aging [5].

CST is a 21-amino acid peptide whose inhibitory effect on catecholamine secretion occurs through direct interaction with a nicotinic receptor, reducing the influx of extracellular Na+ ions into pheochromocytes [6]. CST is secreted together with catecholamines and by autocrine action; it inhibits further catecholamine secretion by negative feedback [7–9]. A direct antagonistic effect on beta-adrenergic receptors leading to the diminished hypertensive reaction was also described [10]. Another mechanism of CST cardioprotective properties may be derived from the observed *in vivo* vasodilatation. Beneficial afterload reduction resulting from vasodilatation seems to be multifactorial—histamine-mediated mechanism [11] together with the reduction of reactive oxygen species availability and stimulation of nitric oxide production were described [12].

CST is also known to modify the myocardial response in the Frank-Starling mechanism, which proves that it modulates myocardial function under both basal conditions and increased preload [13]. CST activates the β2-ARs-PI3K-eNOs-NO signaling pathway in endocardial endothelial cells which play a role in myocardial remodeling. In view of the above, it can be assumed that the inhibition of the fibrotic process by CST occurs through increased production of NO [14]. Another antihypertrophic mechanism may be the phenomenon of CST blocking the receptor for endothelin 1 [15].

2. Aim of the Study

The main aim of our study was to assess the usefulness of determining the plasma catestatin concentration (assessed before and after physical exertion) as a predictor of the complex endpoint: unplanned hospitalization and all-cause mortality in the group of patients with HFrEF in a two-year follow-up.

3. Methods

3.1. Study Population. The study was conducted in 2016-2019. The study group consisted of 52 Caucasian patients with HFrEF in NYHA class II-III, who were either treated on an outpatient basis or hospitalized in the Cardiology Department at the Nicolaus Copernicus University Collegium Medicum University Hospital No. 2 in Bydgoszcz for planned medical procedures, some of which were on the elective list of patients waiting for heart transplantation. Outpatient patients were under the care of the Cardiology Clinic and Heart Failure Clinic operating at the department. The diagnosis of HF was based on the criteria of the European Society of Cardiology from 2016. All patients enrolled in the study were hemodynamically stable for at least 3 months, without the need for an intravenous infusion of positive inotropic drugs or intravenous diuretic therapy, and received optimal pharmacological treatment for each patient in accordance with the ESC guidelines. The control group consisted of 24 healthy volunteers.

The study protocol was approved by the Bioethical Committee of the Nicolaus Copernicus University in Toruń at the Collegium Medicum in Bydgoszcz (KB 591/2016). Each patient signed an informed consent form after obtaining detailed information about the purpose and scope of the study.

The study inclusion criteria included age over 18 years and LVEF < 40% assessed during the current hospitalization or up to 6 months earlier. The exclusion criteria were acute coronary syndrome, active neoplastic disease, active infection, fever of unknown etiology, autoimmune diseases, corticosteroid therapy, uncompensated endocrine disorders, chronic obstructive pulmonary disease, severe impairment of renal function (eGFR < 30 ml/kg/min), impairment of liver function (INR without oral anticoagulation > 1.5 or total bilirubin > 1.5 mg% or the upper limit of the norm for ALT exceeded 3 times), chronic inflammatory bowel disease, and recent surgery (<3 months).

3.2. Organization and Course of the Study. All study participants underwent CPET at the time of inclusion in the study. Before and immediately after the end of the study, approximately 10 ml of peripheral blood was collected from participants through venipuncture in the antecubital fossa. Blood was drawn into the vacutainer system tubes containing ethylenediaminetetraacetic acid (EDTA) and tubes without an anticoagulant. Blood samples were centrifuged at 4°C at 3000 rpm for 20 minutes. The resulting plasma samples were placed in Eppendorf tubes and then frozen at -80°C until the CST determination. The remaining samples from the first collection were used to determine other laboratory parameters necessary for proper qualification for the study and necessary in the routine care and treatment of patients with HFrEF. Blood samples in the control group were obtained identically to the study group. The following tests were performed in the local hospital laboratory in all the participants: complete blood count with a leukocyte interest pattern, plasma NT-proBNP concentration with the "ECLIA" electrochemiluminescence method for Elecsys and cobas e analyzers, plasma C-reactive protein (CRP) concentration with the high sensitivity immunoturbidimetric assay for quantitative in vitro determination of CRP in human serum and plasma in Roche/Hitachi cobas c systems, plasma troponin T (TnT, cardiac troponin T) concentration with the electrochemiluminescence method "ECLIA" for Elecsys and cobas e analyzers, plasma creatinine concentration with a calculation of glomerular filtration rate (eGFR calculated according to the sMDRD formula), fasting glucose, and electrolytes.

CEPT was performed in all study participants according to a protocol selected after a preliminary assessment of exertion tolerance by a 6-minute walk test. All major CPET parameters were assessed during the study: VO2peak (max), VE, VE/VO2, VE/VCO2, VO2AT, and OUES.

Due to the fact that CST is a relatively rarely described marker in clinical trials, and there is no range of concentration standards for the general population, the obtained results of the study group were compared with the control group, which included healthy volunteers. Biomarkers whose concentration was assessed before and after exertion, as well

as their concentration variability under the influence of physical exertion, were NT-proBNP, TnT, and CST. The patient observation was carried out by phone every 3 months from the patient's enrollment and covered 24 months.

3.3. CST Determination. Plasma CST concentration was determined by an enzyme immunoassay (ELISA) kit from RayBiotech® (Norcross, GA, USA), catalog number P10645, dilution factor 12x, reproducibility intra-assay: CV < 10%, and inter-assay: CV < 15%. According to the manufacturer, the reactivity with human CST is 100%. The analytical sensitivity of the method (lower detection limit for the test) is 0.5 ng/ml. The results were read with a LABSYSTEMS iEMS READER MF spectrophotometric reader using the Ascent software version 2.6; the marker was evaluated at 450 nm wavelength. The results were read from the calibration curve prepared for the analyzer used in the study [16].

3.4. Statistical Analysis. The results were analyzed using the PQStat software version 1.6.6.202. Analyses were conducted at 0.05 level of significance. Normality was assessed with the Shapiro-Wilk test. In the absence of normal distributions, nonparametric analyses were carried out. Comparisons of quantitative variables in the two groups were conducted with the Student t-test (in case of normal distribution in both groups) or with the Mann-Whitney test (otherwise). Sex, HF etiology, NYHA class, eGFR, taking medicines, the presence of arterial hypertension (AHT), DM, atrial fibrillation (AF), or the presence of an implantable cardioverter-defibrillator (ICD) were compared depending on the occurrence of CE during 12 and 24 months of follow-up using Fisher's test. The analysis of two repeated measures was conducted with paired t-test (in case of normality of differences) or paired Wilcoxon test (otherwise). A multivariate analysis of the simultaneous impact of many types of drugs on quantitative dependent variables was made by the means of linear regression. 95% confidence intervals were reported along with regression parameters.

The relationship between selected parameters was analyzed by estimating Spearman's rank correlation coefficients. The cutoff points for parameters were established based on the ROC curve. The point on the curve lying closest to the top-left corner of the plot was chosen as a cutoff point. The usefulness of the given parameter as a predictor of the endpoint occurrence was assessed with the area under the ROC curve (AUC). The Kaplan-Meier curves were compared with the log-rank (LR) test. The AUC curves were compared with the DeLong test. The usefulness of combinations of cutoff points for two parameters as predictors of the endpoint occurrence was assessed with sensitivity and specificity. The effect of parameters on the endpoint occurrence was verified using the logistic regression and Cox regression models.

CST δ% (variability of CST concentration under the influence of physical effort) was calculated according to the following formula: (CST post (concentration assessed immediately after physical exertion) − CST pre (concentration assessed immediately before physical exertion)) / CST pre × 100.

TnT δ% (variability of TnT concentration under the influence of physical effort) was calculated according to the following formula: (TnT post (concentration assessed immediately after physical exertion) − TnT pre (concentration assessed immediately before physical exertion)) / TnT pre × 100.

NT − proBNP δ% (variability of NT − proBNP concentration under the influence of physical effort) was calculated according to the following formula: (NT − proBNP − post concentration assessed immediately after physical exertion) −NT − proBNP pre (concentration assessed immediately before physical exertion)) / /NT proBNP pre × 100.

4. Results

The study group consisted of 52 Caucasian patients with HFrEF in NYHA class II or III, whose average age was 51.6 ± 9.2 years, and men constituted 90% of the group. Ischemic etiology of heart failure was evident in 30.8% of patients. All patients enrolled in the study were hemodynamically stable without the need for intravenous infusion of positive inotropic drugs and received the optimal pharmacological treatment in accordance with the ESC recommendations. The composite endpoint of the study was unplanned hospitalization and all-cause mortality. During the 12-month follow-up, 6 endpoints were recorded (2 all-cause deaths and 4 unplanned hospitalizations), while in the 24-month period, there were 11 endpoints (2 all-cause deaths and 9 unplanned hospitalizations). During the 12-month follow-up, a statistically significant difference was found in the CST post and CST δ% between patients who reached and did not reach CE. Patients who had CE during 24-month follow-up differed statistically significantly from the other patients in respect of all CST levels evaluated (CST pre, CST post, and CST δ%), more frequent intake of vitamin K antagonists (VKA), and higher creatinine concentrations. The comparison of the study and the control groups is presented in Table 1.

A statistically significant difference in postexertion CS concentration and its percentage change was shown in the general characteristics of the patients depending on reaching CE during the 12-month follow-up. After sub- and maximum physical exertion, a clear decrease in CST concentration was observed in the group in which CE was noted. The general characteristics of the study group with a division depending on the occurrence of CE for the 24-month period are presented in Table 2.

In the present study, no statistically significant difference in plasma CST concentration was found in patients depending on diabetes, atrial fibrillation, heart failure etiology, or the presence of an implantable cardioverter-defibrillator, as shown in Table 3.

Similarly, the linear regression model did not reveal any significant impact of administered medications on baseline, postexertion, and change (δ%) of catestatin plasma concentration.

Plasma CST concentration before exertion was statistically insignificantly lower in the study group compared to the control group. The exertion during the ergospirometry

Table 1: Study group vs. control group.

	Control group ($n = 24$)	Study group ($n = 52$)	p
Age (years)*	**35.7 ± 12.3**	**51.6 ± 9.2**	**<0.0001**
Men	**70.8%**	90.4%	0.04
EF (%)*	**64.8 ± 7**	28.7 ± 7.5	<0.0001
TAPSE (mm)*	**24.8 ± 3**	20.8 ± 3.9	<0.0001
BMI (kg/m^2)*	**23.5 ± 3**	28.7 ± 5.0	<0.0001
GFR >60	100%	84.6%	0.05
Creatinine (mg/dl)**	**0.86 (0.73-0.94)**	**0.96 (0.85-1.08)**	**0.003**
Hgb (g/dl)**	14.75 (13.3-15.4)	14.7 (14.05-15.4)	0.69
HCT (%)**	43.15 (39.87-44.15)	43.03 (41.5-44.72)	0.30
PLT (tys/mm^3)**	**236 (205.75-248.5)**	**205 (165-237.25)**	**0.02**
RDW (%)**	**12.95 (12.5-13.4)**	**13.55 (13-14.1)**	**0.001**
WBC (tys./mm^3)**	**5.42 (4.84-6.10)**	**7.46 (5.95-8.65)**	**<0.0001**
Neutrocytes (%)**	**51.8 (49.95-54.37)**	**56.15 (51.4-64.15)**	**0.0032**
Hs-CRP (mg/l)**	0.92 (0.545-1.435)	1.105 (0.755-2.457)	0.86
TnTpre (μg/l)**	**0.005 (0.004-0.007)**	**0.012 (0.008-0.016)**	**<0.0001**
TnT post (μg/l)**	**0.005 (0.004-0.006)**	**0.012 (0.009-0.018)**	**<0.0001**
TnT δ% **	**23.8 (14.42-31.87)**	**12.3 (4.57-18.35)**	**0.0003**
NT-proBNPpre (pg/ml)**	**33 (23.5-51)**	**441 (181-1080)**	**<0.0001**
NT-proBNP post (pg/ml)**	**44.5 (26.75-60.75)**	**1153 (208-1280)**	**<0.0001**
NT-proBNP δ%**	0 (0-0)	0 (0-8.3)	0.35
V02max/VO2peak (l/kg/min)*	**37.17 ± 7.52**	**18.01 ± 4.96**	**<0.0001**
VE/VC02 (%)*	**30.13 ± 3.84**	**35.40 ± 7.27**	**0.0001**
OUES*	**2.67 ± 0.86**	**1.90 ± 0.75**	**0.0002**
RER*	**1.21 ± 0.10**	**1.03 ± 0.18**	**<0.0001**
CST pre (ng/ml)**	16.6 (14.75-22.20)	15.95 (13.89-18.81)	0.12
CST post (ng/ml)**	9.26 (6.11-140.23)	7.04 (4.97-11.08)	0.13
CST δ%**	-86,56 (-85,8-126,5)	-148 (71-181)	0,08

EF: ejection fraction; TAPSE: tricuspid annular plane systolic excursion; BMI: body mass index; GFR: glomerular filtration rate; Hgb: hemoglobin; HCT: hematocrit; PLT: platelets; RDW: red cell distribution width; WBC: white blood cells; hs-CRP: high-sensitivity C-reactive protein; TnTpre: cardiac troponin T (concentration assessed before physical exertion); TnTpost: concentration assessed immediately after physical exertion; TnT δ%: variability of TnT concentration under the influence of physical effort; NT-proBNP: N-terminal proBNP; VO2max: maximal oxygen consumption; V02peak: peak oxygen uptake; OUES: oxygen uptake efficiency slope; RER: respiratory exchange ratio; CST: catestatin. Statistically significant results are marked in bold. The results in the tables are presented as follows: *means ± standard deviation. **medians (lower quartile – upper quartile).

test did not reveal differences in the catestatin concentration between the study group and the control group. A number of significant differences were observed between the study group and the control group, including age, LVEF, TAPSE, RDW, BMI, creatinine, troponin T, NT-proBNP, and ergospirometric parameters.

Patients who reached the composite endpoint during the 24-month follow-up were characterized by statistically significantly lower levels of catestatin, both assessed before exertion and after sub- and maximum physical exertion. After ergospirometry, a clear decrease in the catestatin concentration was observed in the CE group. Moreover, the group of patients in whom CE was reported more often took the drug from the group of vitamin K antagonists and had a higher creatinine concentration.

Spearman's rank correlation showed significant negative correlations between catestatin assessed after sub- and maximal physical exertion in the study group of patients and biomarkers with an established position in modern cardiology (CST post vs. NT-proBNPpre, $r = -0.18$; CST post vs. TnTpre, $r = -0.33$; CST post vs. TnT post, $r = -0.24$) and no significant correlation between traditional diagnostic and prognostic markers used in HF, such as hs-CRP and NT-proBNP, and plasma CST concentration evaluated before physical exertion. A significant negative correlation was also observed between CST δ% and V02 peak ($r = -0.23$).

In a one-way analysis carried out using the Cox proportional hazard model over a 24-month period, a statistically significant effect of all assessed CST concentrations (CST

TABLE 2: Basic characteristics of the study group depending on end-point occurrence in the 24-month follow-up.

	All ($n = 52$)	End point ($n = 11$; 21.15%)	No end point ($n = 41$; 78.85%)	p
Age (years)*	51.6 ± 9.1	52 ± 9.5	51.5 ± 9.2	0.87
Men	90.4%	100%	87.8%	0.57
EF (%)*	28.7 ± 7.5	27.9 ± 7.6	28.9 ± 7.6	0.72
TAPSE (mm)*	20.8 ± 3.9	19 ± 3.9	21.32 ± 3.8	0.08
Ischaemic aetiology	30.8%	18.18%	34.2%	0.47
BMI (kg/m^2)*	28.7 ± 5.0	27.4 ± 6.2	29.1 ± 4.7	0.31
NYHA class III	25%	18.18%	26.8%	0.71
DMT2	28.9%	36.36%	26.8%	0.71
Insulin	7.7%	9.1%	7.3%	1.00
AHT	34.6%	9.1%	41.5%	0.07
AF	38.5%	36.4%	68.3%	0.08
ICD	51.9%	63.6%	48.8%	0.50
GFR>60	84.6%	81.8%	85.4%	1.00
Creatinine (mg/dl)**	*0.96 (0.85-1.08)*	*1.03 (0.96-1.22)*	*0.99 (0.81-1.05)*	*0.04*
Hgb (g/dl)**	14.7 (14.05-15.4)	14.8 (14.1-14.95)	14.7 (14.1-15.4)	0.85
HCT (%)**	43.55 (41.5-44.7)	43.5 (42.65-45)	43.6 (40.3-44.7)	0.37
PLT (tys./mm^3)**	205 (165-237.2)	221 (149.5-268.5)	201 (172-236)	0.99
RDW (%)**	13.55 (13-14.1)	13.7 (13.2-14.6)	13.5 (13-14.1)	0.50
WBC (tys./mm^3)**	7.46 (5.95-8.65)	7.7 (6.11-8.76)	7.4 (5.68-8.41)	0.52
Neutrocytes (%)**	56.15 (51.4-64.1)	56.3 (51.9-65.85)	56 (51.1-62)	0.82
Hs-CRP (mg/l)**	1.10 (0.75-2.46)	2.16 (0.81-2.27)	0.96 (0.71-2.72)	0.90
TnTpre (μg/l)**	0.012 (0.008-0.016)	0.014 (0.01-0.02)	0.011 (0.008-0.016)	0.12
TnT post (μg/l)**	0.012 (0.009-0.018)	0.013 (0.01-0.019)	0.012 (0.008-0.016)	0.30
TnT δ%**	12.3 (4.57-18.35)	13.5 (7.5-17.65)	11.1 (3.9-18.2)	0.51
NT-proBNPpre(pg/ml)**	441.5 (181-108)	758 (472.5-112)	373 (175-705)	0.11
NT-proBNPpost (pg/ml)**	442 (208-1280)	955 (512-1380)	403 (189-876)	0.10
NT-proBNP δ%**	0 (0-8,3)	0 (-6.25-1.9)	0 (0-8.3)	0.28
V02max/VO2peak (l/kg/min)*	18.01 ± 4.96	18.22 ± 3.73	17.95 ± 5.28	0.88
VE/VC02 (%)*	35.40 ± 7.27	37.02 ± 6.82	34.97 ± 7.40	0.41
OUES*	1.90 ± 0.75	1.51 ± 0.51	2.00 ± 0.78	0.05
RER*	1.03 ± 0.18	1.05 ± 0.13	1.02 ± 0.19	0.67
CST pre (ng/ml)**	*15.95 (13.89-18.8)*	*14.23 (11.05-15.82)*	*16.86 (14.25-19.46)*	*0.03*
CST post (ng/ml)**	*7.04 (4.97-11.08)*	*4.81 (2.20-6.25)*	*7.82 (5.81-63.48)*	*0.002*
CST δ%**	*-148 (71-181)*	*-254 (161-314)*	*-124 (-71-164)*	*0.002*
ACEi	78.9%	72.7%	80.5%	0.68
ARB	23.1%	27.3%	22%	0.70
Statin	82.7%	90.9%	80.5%	0.66
Beta-bloker	100%	100%	100%	-
ASA	40.4%	18.2%	46.3%	0.17
Digoxin	7.7%	9.1%	7.3%	1.00
Spironolakton	44.2%	54.6%	41.5%	0.51
Eplerenon	59.6%	54.6%	61%	0.74
Iwabradyna	11.5%	27.3%	7.3%	0.10
VKA	*34.6%*	*72.7%*	*24.4%*	*0.0048*
NonVKA	5.8%	0%	7.3%	1.00

	All ($n = 52$)	End point ($n = 11$; 21.15%)	No end point ($n = 41$; 78.85%)	p
Amiodaron	7.7%	18.2%	4.9%	0.19
Furosemid	25%	27.3%	24.4%	1.00
Torasemid	36.5%	54.6%	31.7%	0.18
Hydrochlorotiazyd	15.4%	0 (0%)	19.5%	0.18

EF: ejection fraction; TAPSE: tricuspid annular plane systolic excursion; BMI: body mass index; DMT2: diabetes mellitus type 2; AHT: atrial hypertension; AF: atrial fibrillation; ICD: implantable cardioverter-defibrillator; GFR: glomerular filtration rate; Hgb: hemoglobin; HCT: hematocrit; PLT: platelets; RDW: red cell distribution width; WBC: white blood cells; hs-CRP: high-sensitivity C-reactive protein; TnTpre: cardiac troponin T (concentration assessed before physical exertion); TnTpost: concentration assessed immediately after physical exertion; TnT δ%: variability of TnT concentration under the influence of physical effort; NT-proBNP: N-terminal proBNP; VO2max: maximal oxygen consumption; V02peak: peak oxygen uptake; OUES: oxygen uptake efficiency slope; RER: respiratory exchange ratio; CST: catestatin; ACEi: angiotensin-converting-enzyme inhibitors; ARB: angiotensin II receptor blockers; ASA: acetylsalicylic acid; VKA: vitamin K antagonists; nonVKA: nonvitamin K antagonist. Statistically significant results are marked in italics. The results in the tables are presented as follows: *means ± standard deviation. **medians (lower quartile – upper quartile).

TABLE 3: Differences in plasma CST concentration (ng/ml) depending on the clinical conditions of the patients.

	DMT2 ($N = 15$)			No DMT2 ($N = 37$)			
	Mean ± SD	Median	Quartiles	Mean ± SD	Median	Quartiles	p
CST pre	16.88 ± 4.17	16.6	14.59-18.29	16.43 ± 4.88	15.4	13.66-19.46	0.64
CSTpost	49.41 ± 90.15	6.62	5.19-10.32	47.51 ± 84.88	7.49	5.03-11.98	0.70
CST δ%	135.13 ± 411.93	-61.51	-64.53-31.79	176.63 ± 510.16	-56.6	-64.26-43.47	0.49
	AF ($N = 20$)			SR ($N = 32$)			
CST pre	15.72 ± 5.58	15.21	13.44-17.46	17.09 ± 3.97	16.73	14.18-19.28	0.29
CSTpost	55.73 ± 91.7	6.30	4.19-45.73	43.26 ± 82.6	7.64	5.76-10.51	0.33
CST δ%	236.3 ± 573.28	-62.10	-72.09-100.02	119.88 ± 415.52	-56.03	-61.68-41.35	0.21
	DCM ($N = 36$)			ICM ($N = 16$)			
CST pre	16.7 ± 5.09	15.95	14.01-18.59	16.24 ± 3.6	16.16	13.14-19.28	0.80
CSTpost	48.9 ± 89.39	6.89	4.93-10.2	46.17 ± 78.93	7.66	5.34-25.38	0.71
CST δ%	159.99 ± 496.19	-59.98	-65.31-46.1	13.14-19.28	-58.41	-63.09-48.73	0.50
	ICD ($N = 27$)			NO ICD ($N = 25$)			
CST pre	16.1 ± 5.1	16.52	13.07-18.2	17.06 ± 4.16	15.64	14.25-19.22	0.50
CSTpost	63.37 ± 96.47	7.8	5.21-105.22	31.51 ± 70.13	6.76	5.03-9.45	0.33
CST δ%	261.72 ± 558.17	-55.37	-64.54-397.91	59.83 ± 361.36	-60.25	-63.75-51.6	0.20

DMT2: type 2 diabetes; AF: atrial fibrillation; SR: sinus rhythm; DCM: dilated cardiomyopathy; ICM: ischemic cardiomyopathy; ICD: implantable cardioverter-defibrillator.

pre, CST post, and CST δ%) on the occurrence of CE was demonstrated. The effect of other assessed factors turned out to be statistically insignificant. The above results are presented in Table 4.

In a logistic regression analysis carried out over a 12-month follow-up period, no statistically significant effect of CST on CE was shown. In a 24-month follow-up, where the baseline catestatin concentration was compared with other recognized prognostic factors, baseline CST was the only tested parameter to show statistical significance in CE prediction (Table 5).

Table 6 shows the cutoff points determined based on the ROC curves for selected parameters.

Both preexertion catestatin and postexertion catestatin proved to be important CE predictors (Figure 1 and Figure 2).

The cutoff values were then applied to the Kaplan-Meier event-free survival curves, where significant differences in event-free survival were observed between groups with NT-proBNP (post) ≥ cutoff point and CST (post) ≥ cutoff point vs. NT-proBNP ≥cutoff point and CST (post) < cutoff point (Figure 3).

5. Discussion

A review of the current literature indicates that this is the first paper describing the prognostic significance of CST in the group of patients with HFrEF and the second in the group of patients with CHF; the first to assess the prognostic value of CST in the group of hemodynamically stable patients with HF; and the first to assess the change in catestatin

Table 4: One-factor analysis carried out using the Cox proportional hazard model over a 24-month follow-up period.

—	p	HR	(-95%; 95% confidence interval)
CST pre	0.01	0.84	(0.73; 0.96)
CST post	0.026	0.76	(0.59; 0,97)
CST δ%	<0.001	1.0041	(1.0017; 1.0065)
Age (years)	0.94	1	(0.94; 1.07)
Men	0.98	1	(1; 1)
EF	0.71	0.99	(0.91; 1.07)
TAPSE	0.12	0.89	(0.76;1.03)
Ischaemic aetiology	0.38	0.50	(0.11; 2.33)
BMI	0.29	0.93	(0.82; 1.06)
NYHA III	0.58	0.65	(0.14; 3.01)
Insulin	0.91	1.13	(0.14; 8.80)
AF	0.09	2.88	(0.84; 9.85)
ICD	0.45	1.61	(0.47; 5.51)
Hgb	0.86	0.96	(0.58; 1.57)
RDW	0.13	1.27	(0.93; 1.93)
WBC	0.61	1.08	(0.80; 1.47)
Neutrocytes	0.79	1.01	(0.94; 1.98)
TnTpre	0.31	1.28	(0.23; 0.72)
NT-proBNPpre	0.85	1.00	1
NT-proBNP post	0.83	1.00	1
NT-proBNP δ%	0.18	0.96	(0.90; 1.02)
V02max/V02peak	0.85	1.01	(0.90; 1.14)
OUES	0.06	0.41	(0.16; 1.02)
Ve/VCo2	0.44	1.03	(0.96; 1.11)
Hs-CRP	0.61	0.92	(0.65; 1.28)

Table 5: Multivariate analysis carried out using the logistic regression model over a 24-month observation period.

	p	HR	(-95%; 95% confidence interval)
CST pre	0.04	0.74	(0.56; 1.12)
RDW %	0.43	1.24	(0.73; 2.11)
NT-proBNP(pre) pg/ml	0.34	1	(1; 1)
Hs-CRP mg/l	0.79	0.93	(0.53; 1.63)
TnT(pre) × 100	0.44	1.28	(0.68; 2.38)
OUES	0.11	0.25	(0.05; 1.38)

concentration under the influence of short-term physical exertion in humans.

The decision to assess baseline and postexercise CST concentration in the control group was made because of the lack of sufficient information in the literature on normal ranges in the healthy population. Most studies published up to date evaluated CST in asymptomatic patients with risk factors for CHF development and in patients with less severe forms of symptomatic heart failure (NYHA class I and II). The present study would not be complete without the information on CST concentration in healthy individuals. We have also suspected that the difference between healthy people and stable CHF patients on optimal treatment might be minimal or nonexistent which proved to be the case. There is, however, a statistically significant difference in age between the patients and the control group in the present study, which may influence the results. In investigating patients with heart failure, finding the appropriate age-matched control group always poses a significant challenge. It is mostly the result of the high prevalence of both cardiovascular risk factors and asymptomatic hypertension or hyperlipidemia in age-matched individuals. The decision was made to include only completely healthy patients that ultimately resulted in significantly younger control than the study group, which certainly is a limitation of the study. The assessment of CST changes after the cardiopulmonary stress test was included in the protocol, since exertion challenge in the context of the catestatin plasma concentration has never been done neither in patients with heart failure nor in healthy volunteers. The assumption was made that due to compensation mechanisms typically involved in the pathogenesis of heart failure (namely: upregulation of sympathetic nervous system or renin-angiotensin-aldosteron axis activation), CST changes in response to exercise may be completely different in patients than in healthy volunteers. The omission of this part of the study protocol would make the results incomplete and would make a difficult thorough interpretation of the results.

It should be emphasized that the study group of stable patients was carefully selected, which is confirmed by a very low mortality rate -4% and a very low frequency of unplanned hospitalizations, which was recorded only in 17% of the study group in the 24-month follow-up period. The plasma concentrations of traditional diagnostic and prognostic markers used in heart failure assessed before physical exertion are another proof of the homogeneity of the study group. The NT-proBNP concentration was 441.5 pg/ml (181-1080), TnT concentration 0.012 μg/l (0.008-0.016), and hs-CRP concentration 1.10 mg/l (0.75-2.46), while hemoglobin and RDW concentration 14.7 g/dl (14.05-15.4) and 13.55% (13-14.1), respectively, and V02max/VO2peak in the group of patients amounted to 18.01 ± 4.96 l/kg/min.

The only one currently published report assessing the prognostic significance of catestatin is the study by Zhu et al. The authors assessed the CST concentration in various HF phases and the diagnostic utility of CST as a potential biomarker for detecting asymptomatic HF in stage B according to the American Heart Association (AHA). In a group of 300 patients (stage B—$n = 76$, age 68.58 ± 8.63, LVEF 54.95 ± 9.82%), it was shown that the concentration of CST decreased from stage A, through stage B, to stage C. The CST cutoff value for detection of stage B HF was 19.73 ng/ml with 90% sensitivity (higher in this study than for BNP) and a specificity of 50.9%. The CST concentration did not correlate with BNP concentration ($r = 0.107$, $p = 0.150$). According to the authors, asymptomatic patients in HF stage B would benefit most from regular observation and therapeutic

TABLE 6: Determined cutoff points based on the ROC curves for NT-proBNPpre, NT-proBNP post, CST pre, CST post.

Parameter	Cut point	Sensitivity at cut point	Specificity at cut point	Direction	AUC	p^*
NT-proBNP (pre) (pg/ml)	455	81.82%	60.98%	Positive	0.659	0.08
NT-proBNP (post) (pg/ml)	510	81.82%	63.41%	Positive	0.662	0.07
Catestatin (pre) (ng/ml)	16.52	81.82%	56.10%	Negative	0.718	*0.012*
Catestatin (post) (ng/ml)	6.39	81.82%	70.73%	Negative	0.808	*<0.001*

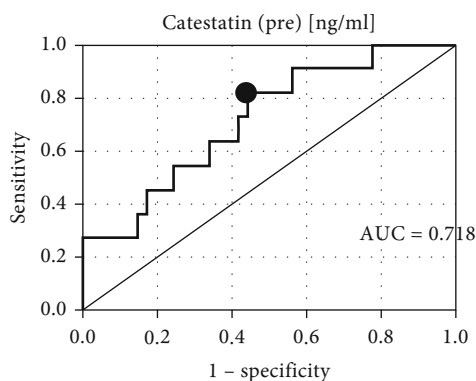*DeLong's method (null hypothesis: AUC = 0.5).

FIGURE 1: The receiver operating characteristic curve for catestatin (pre) at 24 months of follow-up.
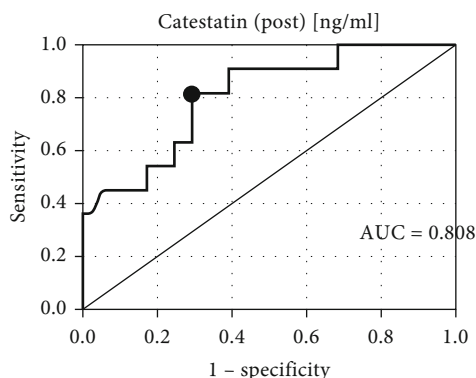

FIGURE 2: The receiver operating characteristic curve for catestatin (post) at 24 months of follow-up.

intervention; as observed in this group, a decrease in catestatin concentration may precede full-blown HF [17].

Comparing the group from our study vs. Zhu et al.—stage C (symptomatic patients), significant differences should be emphasized as to the optimal pharmacological treatment (beta-blocker 100% vs. 86.2%, ACEi or sartan 100% vs. 72.4, spironolactone or eplerenone 100% vs. no data) and the fact that all patients from our study were hemodynamically stable patients, without signs of exacerbation of HF symptoms, whereas AHA stage C encompasses a wide range of symptomatic patients. These 2 factors seem to have a significant impact on the difference in the obtained results. Similar to the presented study, Zhu et al. also failed to show any correlation between the NT-proBNP concentration and CST. In stable patients included in the present study, the

natriuretic peptide concentration was relatively low reflecting the good hemodynamic status of the observed group. The lack of correlation between baseline NT-proBNP and CST may be a result of different mechanisms underlying the production and excretion of both markers. In the present study, statistically significant correlations were observed between postexertion NT-proBNP and CST and between pre- and postexertion troponin and CST. Yet, these correlations were weak; therefore, this phenomenon requires further analysis of large groups of patients to draw any valuable conclusions.

Another study aimed at assessing the CST diagnostic potential in stable and exacerbated HF patients was the analysis by Liu et al. The authors observed no significant differences in the CST levels among NYHA I, NYHA II, and the control group patients; however, the plasma catestatin levels in patients with NYHA III and IV were significantly higher. In the group of patients with medium and severe HF (NYHA III or IV), no significant differences were observed in the CST concentration depending on sex, HFpEF, or HFrEF. Yet, in the group of ICM vs. NICM patients, this difference was significant ($p = 0.002$). The multivariate analysis showed that the NYHA class, ICM, and eGFR independently predicted LogCST in plasma that was independent of the BNP concentration [18].

The result of the above study regarding the lack of a significant relationship between the concentration of natriuretic peptide and catestatin is identical to the presented paper. Liu et al. similarly to the presented analysis showed no significant difference in the plasma catestatin concentration between hemodynamically stable patients (NYHA I and NYHA II) and a group of healthy volunteers. The lack of difference in the plasma CST concentration in the presented analysis depending on the HF etiology may be due to the low ICM percentage in the HF group. Liu et al. showed a significant difference in the CST concentration between the NYHA class II vs. NYHA class III, which is in contrast to the presented analysis. This finding is difficult to interpret as it may be the result of the liberal inclusion criteria to the study group developed by the cited authors. Compared to the presented analysis, the study group of Liu et al. is heterogeneous, since both patients are with HFrEF and HFpEF, hemodynamically stable, and those during the exacerbation of the disease were qualified; moreover, the pharmacological treatment of patients seems to be suboptimal.

In contrast to the presented findings, Peng et al., investigating the heterogenous group of patients with CHF during the 52-month follow-up, observed a significantly higher baseline catestatin concentration in patients who died of all and cardiovascular causes vs. the group with no endpoint
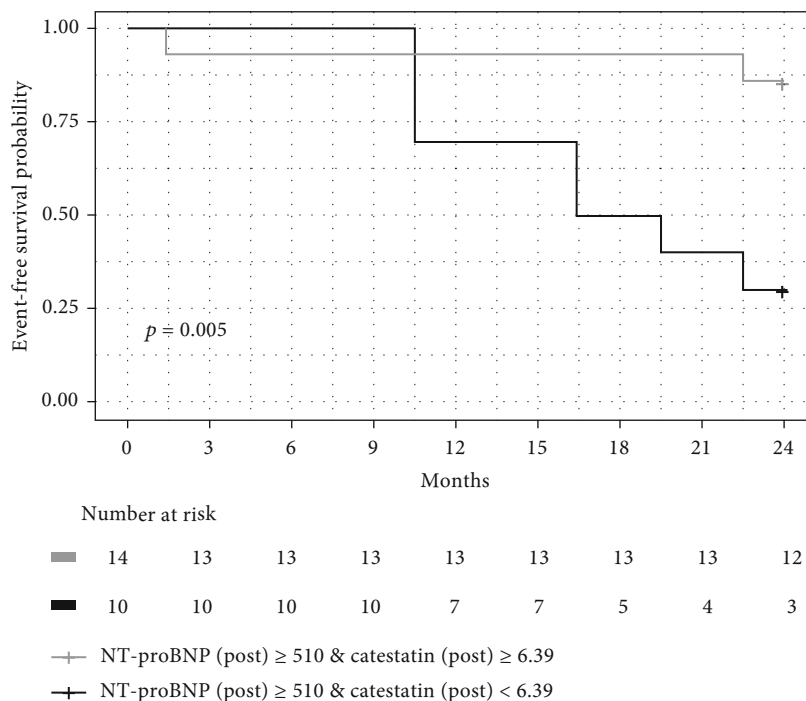
FIGURE 3: The Kaplan-Meier event-free survival curves in groups with NT-pro BNP (post) ≥cutoff point and CST (post) ≥cutoff point vs. NT-proBNP ≥cutoff point and CST (post) < cutoff point for 24 months of follow-up.

recorded. According to Cox multifactorial regression, the plasma catestatin concentration proved to be an independent predictor of death from cardiological reasons, whereas in respect of all-cause deaths, the predictive value of CST was critically insignificant ($p = 0.051$) [19].

Similar to the above-cited Liu et al. paper, the heterogeneity of the group observed in Peng et al. study makes the interpretation of these findings relatively difficult. The authors included in their analysis patients with completely different pathophysiology of heart failure—those with reduced and preserved left ventricular ejection fraction. Although the prognosis for both HF groups may well be equally serious, the reaction for administered treatment is often different reflecting various pathomechanisms involved in the natural history of the disease [20].

The presented study aimed to analyse the prognostic significance of both the CST baseline plasma concentration and concentration after exertion. The ROC analysis indicating the cutoff values of CST-post and constructed accordingly Kaplan-Meier curves of event-free survival revealed that simultaneous assessment of NT-proBNP and CST postexertion allows for the identification of patients with a more severe course of the disease. These individuals may benefit from systematic follow-up and may be candidates for more aggressive treatment. Certainly, evaluating the biochemical markers after sub- or maximal exercise is not always feasible as not every HF patient requires such testing. However, taking into account that the clinical evaluation before a heart transplant usually encompasses a cardiopulmonary exercise stress test, an additional biomarker assessment should not pose any inconvenience. Even in this population of severely ill

patients, stable individuals may not constitute a uniform group, and the identification of those with the poorest prognosis could be helpful.

The limitations of the presented study are as follows:

  (i) Relatively small studied groups

 (ii) No assessment of possible changes in chromogranin A proteolysis disorders in the studied populations [21]

(iii) A significant difference in age between the study and control group

6. Conclusions

(1) The plasma concentration of catestatin before and after physical exertion is a valuable prognostic parameter in predicting the all-cause death and unplanned hospitalization in the group of patients with HFrEF in the 2-year follow-up

(2) Catestatin has no diagnostic value in the diagnosis of patients with compensated heart failure with a reduced left ventricular ejection fraction

(3) The prognostic value of catestatin in the group of patients with HFrEF becomes increasingly important in long-term follow-up

(4) Traditional diagnostic and prognostic markers used in heart failure, such as hs-CRP, TnT, and NT-proBNP, are not related to the plasma concentration of catestatin evaluated before the physical exertion

Data Availability

All data used to support the finding of this study are available from the corresponding author upon request.

Conflicts of Interest

None of the authors have any conflicts of interest.

Authors' Contributions

Łukasz Wołowiec contributed to the study conception and design, acquisition of data analysis and interpretation of data, and drafting of the manuscript. Daniel Rogowicz contributed to the acquisition of data, analysis, and interpretation of data and helped supervise the project drafting of the manuscript. Joanna Banach contributed to the study conception and design and analysis and interpretation of data. Wojciech Gilewski contributed to the analysis and interpretation of data and drafting of the manuscript. Władysław Sinkiewicz contributed to the study conception and design. Grzegorz Grześk contributed to the analysis and interpretation of data and critical revision. All authors discussed the results and commented on the manuscript.

Acknowledgments

References

[1] A. Mosterd and A. W. Hoes, "Clinical epidemiology of heart failure," *Heart*, vol. 93, no. 9, pp. 1137–1146, 2007.

[2] J. Banach, Ł. Wołowiec, D. Rogowicz et al., "Procalcitonin (PCT) predicts worse outcome in patients with chronic heart failure with reduced ejection fraction (HFrEF)," *Disease Markers*, vol. 2018, 6 pages, 2018.

[3] Ł. Wołowiec, D. Rogowicz, J. Banach et al., "Prognostic significance of red cell distribution width and other red cell parameters in patients with chronic heart failure during two years of follow-up," *Kardiologia Polska*, vol. 74, no. 7, pp. 657–664, 2016.

[4] J. Banach, M. Grochowska, L. Gackowska et al., "Melanoma cell adhesion molecule as an emerging biomarker with prognostic significance in systolic heart failure," *Biomarkers in Medicine*, vol. 10, no. 7, pp. 733–742, 2016.

[5] N. Biswas, E. Curello, D. T. O'Connor, and S. K. Mahata, "Chromogranin/secretogranin proteins in murine heart: myocardial production of chromogranin A fragment catestatin (Chga364–384)," *Cell and Tissue Research*, vol. 342, no. 3, pp. 353–361, 2010.

[6] S. K. Mahata, M. Mahata, G. Wen et al., "The catecholamine release-Inhibitory "Catestatin" fragment of chromogranin a: naturally occurring human variants with different potencies for multiple chromaffin cell nicotinic cholinergic responses," *Molecular Pharmacology*, vol. 66, no. 5, pp. 1180–1191, 2004.

[7] S. K. Mahata, D. T. O'Connor, M. Mahata et al., "Novel autocrine feedback control of catecholamine release. A discrete chromogranin a fragment is a noncompetitive nicotinic cho-

linergic antagonist," *The Journal of Clinical Investigation*, vol. 100, no. 6, pp. 1623–1633, 1997.

[8] S. K. Mahata, M. Mahata, A. R. Wakade, and D. T. O'Connor, "Primary structure and function of the catecholamine release inhibitory peptide catestatin (chromogranin A $_{344-364}$): identification of amino acid residues crucial for activity," *Molecular Endocrinology*, vol. 14, no. 10, pp. 1525–1535, 2000.

[9] S. K. Mahata, N. R. Mahapatra, M. Mahata et al., "Catecholamine secretory vesicle stimulus-transcription coupling in vivo," *The Journal of Biological Chemistry*, vol. 278, no. 34, pp. 32058–32067, 2003.

[10] M. M. Fung, R. M. Salem, P. Mehtani et al., "Direct vasoactive effects of the chromogranin a (CHGA) peptide catestatin in humans in vivo," *Clinical and Experimental Hypertension*, vol. 32, no. 5, pp. 278–287, 2010.

[11] B. P. Kennedy, S. K. Mahata, D. T. O'Connor, and M. G. Ziegler, "Mechanism of cardiovascular actions of the chromogranin A fragment catestatin in vivo," *Peptides*, vol. 19, no. 7, pp. 1241–1248, 1998.

[12] J. R. Gayen, K. Zhang, S. P. RamachandraRao et al., "Role of reactive oxygen species in hyperadrenergic hypertension," *Circulation. Cardiovascular Genetics*, vol. 3, no. 5, pp. 414–425, 2010.

[13] X. Guo, C. Zhou, and N. Sun, "The neuropeptide catestatin promotes vascular smooth muscle cell proliferation through the Ca2+-calcineurin-NFAT signaling pathway," *Biochemical and Biophysical Research Communications*, vol. 407, no. 4, pp. 807–812, 2011.

[14] R. Liu, N. L. Sun, S. N. Yang, and J. Q. Guo, "Catestatin could ameliorate proliferating changes of target organs in spontaneously hypertensive rats," *Chinese Medical Journal*, vol. 126, no. 11, pp. 2157–2162, 2013.

[15] S. Kaddoura, J. D. Firth, K. R. Boheler, P. H. Sugden, and P. A. Poole-Wilson, "Endothelin-1 is involved in norepinephrine-induced ventricular hypertrophy in vivo. Acute effects of bosentan, an orally active, mixed endothelin ETA and ETB receptor antagonist," *Circulation*, vol. 93, no. 11, pp. 2068–2079, 1996.

[16] RayBiotech, *RayBio® human/mouse/rat catestatin enzyme immunoassay kit*, pp. 1–16, 2017, https://www.raybiotech.com/files/manual/EIA/EIA-CAT.pdf.

[17] D. Zhu, F. Wang, H. Yu, L. Mi, and W. Gao, "Catestatin is useful in detecting patients with stage B heart failure," *Biomarkers*, vol. 16, no. 8, pp. 691–697, 2011.

[18] L. Liu, W. Ding, R. Li et al., "Plasma levels and diagnostic value of catestatin in patients with heart failure," *Peptides*, vol. 46, pp. 20–25, 2013.

[19] F. Peng, S. Chu, W. Ding et al., "The predictive value of plasma catestatin for all-cause and cardiac deaths in chronic heart failure patients," *Peptides*, vol. 86, no. 1, pp. 112–117, 2016.

[20] S. J. Simmonds, I. Cuijpers, S. Heymans, and E. A. V. Jones, "Cellular and molecular differences between HFpEF and HFrEF: a step ahead in an improved pathological understanding," *Cell*, vol. 9, no. 1, p. 242, 2020.

[21] D. T. O'Connor, G. Zhu, F. Rao et al., "Heritability and genome-wide linkage in US and Australian twins identify novel genomic regions controlling chromogranin a: implications for secretion and blood pressure," *Circulation*, vol. 118, no. 3, pp. 247–257, 2008.

Research Article

A Novel Gene Signature to Predict Survival Time and Incident Ventricular Arrhythmias in Patients with Dilated Cardiomyopathy

Chenliang Ge[1,2] and Yan He [iD][1]

[1]*The First Affiliated Hospital of Guangxi Medical University, Nanning 530021, China*
[2]*The First Affiliated Hospital of University of South China, Hengyang 421001 ., China*

Correspondence should be addressed to Yan He; hyxjwxy@126.com

The mortality in nonischaemic dilated cardiomyopathy (NIDCM) patients is still at a high level; sudden death in NIDCM can be caused by ventricular tachycardia. It is necessary to explore the pathogenesis of ventricular arrhythmias (VA) in NIDCM. Differentially expressed genes (DEGs) were identified by comparing the gene expression of NIDCM patients with or without VA in the gene expression profile of GSE135055. A total of 228 DEGs were obtained, and 3 genes were screened out to be significantly related to the survival time of NIDCM patients. We established a prediction model on two-gene (*TOMM22*, *PPP2R5A*) signature for the survival time of NIDCM patients. The area under the curve (AUC) was 0.75 calculated by the ROC curve analysis. These risk genes are probably new targets for exploring the pathogenesis of NIDCM with VA; the prediction model for survival time and incident ventricular arrhythmias is useful in clinical decision making for individual treatment.

1. Introduction

Nonischaemic dilated cardiomyopathy (NIDCM) is one of the most common inherited cardiomyopathy and is considered to be one of the main causes of heart failure and sudden cardiac death. Heart transplantation is usually needed [1, 2]. One-third of patients with NIDCM may represent arrhythmogenic phenotypes and have an increased risk of arrhythmias during follow-up; ventricular arrhythmia (VA) is a major cause of clinical deterioration and demise in patients with NIDCM [3–6]. In order to prevent these situations, it is recommended that prophylactic intervention with implantable cardioverter-defibrillators (ICD) in patients with heart failure and left ventricular ejection fraction < 35% in current international guidelines [7, 8]. Although NIDCM is characterized by genetic and clinical heterogeneity, few studies have explored the pathogenesis of VA in patients with NIDCM. In order to reveal the inherent molecular mechanism, NIDCM patients were divided into sinus rhythm (SR) group and VA group and differentially expressed genes (DEGs) were identified via bioinformatic methods.

2. Materials and Methods

2.1. Data Source. We download the microarray expression dataset (GSE135055) from the Gene Expression Omnibus (GEO) database [9]. The multilevel transcriptional data of GSE135055 were generated from the heart tissues of 21 heart failure (HF) patients and 9 healthy donors. Among these HF patients, there are 18 NIDCM patients, during which 6 patients suffered VA, including ventricular premature beats, ventricular tachycardia, and ventricular fibrillation [10]. The characteristics of these patients are listed in Table 1 (supplemental file Table S1). We divided the NIDCM patients into two groups, with 12 patients in the sinus rhythm (SR) group and 6 patients in the VA group. We used the "limma" package [11] to quantile the datasets and screened out DEGs between

TABLE 1: Baseline parameters in NIDCM patients with and without ventricular arrhythmia.

Clinical features	SR (12)	VA (6)	p value
Age (y)	30.33 (16.87)	39.33 (16.17)	0.296
Male sex (n (%))	7 (58.3)	3 (50.0)	0.563
LA (mm)	41.08 (13.53)	35.33 (17.78)	0.454
LVEDD (mm)	68.00 (11.72)	58.33 (28.74)	0.318
LVEF (%)	27.00 (11.50)	24.00 (13.74)	0.631
AF (%)	2 (16.7)	2 (33.3)	0.407
NYHA functional class			
II	2 (16.7)	0 (0.0)	0.806
III	4 (33.3)	2 (33.3)	
IV	6 (50.0)	4 (66.7)	
Diabetes mellitus (%)	1 (8.3)	1 (16.7)	0.569
Smoking history (%)	2 (16.7)	1 (16.7)	0.755
Drug therapy			
Amiodarone (%)	1 (8.3)	2 (33.3)	0.245
β-Blockers (%)	8 (66.7)	4 (66.7)	0.691
Digoxin (%)	10 (83.3)	4 (66.7)	0.407
ACEI/ARB (%)	10 (83.3)	4 (66.7)	0.407
CCB (%)	2 (16.7)	1 (16.7)	0.755
Diuretic (%)	11 (91.7)	5 (83.3)	0.569

Values are mean ± SD, n (%); LA: left atrium; LVEDD: left ventricular diastolic diameter; LVEF: left ventricular ejection fraction; AF: Atrial fibrillation; NYHA: New York Heart Association; ACEI: angiotensin-converting enzyme inhibitors; ARB: angiotensin receptor blocker; CCB: calcium channel blocker.

the SR group and VA group with $p < 0.05$ and |log 2FC| >1 were considered statistically significant. A volcano map and heat map were used to show the DEGs.

2.2. Construction of Survival Time Prediction Model. 17 NIDCM patients (6 patients suffered VA included) with complete survival time (time period of each patient from symptoms to heart transplantation) information were selected for the study. By using univariate Cox regression analysis, we screened out DEG significantly related to survival time ($p < 0.05$) [12]. Then, a gene signature and a prediction model for survival time were constructed via multivariate cox analysis, survival analysis, and random survival forest algorithm.

2.3. Evaluation of Survival Time Prediction Model. Based on the regression coefficient and the expression value of each selected gene obtained by the multivariate Cox regression model, the risk score of each patient was calculated, then we separated 17 patients into high-risk and low-risk groups using the median risk score as the cutoff. A high-risk score indicates poor survival time for the NIDCM patients. The accuracy of the prediction model was evaluated by time-dependent ROC analysis.

2.4. Enrichment Analysis by Metascape. The pathway enrichment of DEGs was analyzed using Metascape. With the species limited to "Homo sapiens," functional enrichment analysis was performed based on Gene Ontology, Kyoto Encyclopedia of Genes and Genomes, Reactive pathways, and Canonical Pathways [13]. All genes in the genome have been used as the enrichment background. Terms with a p value < 0.01, a minimum count of 3, and an enrichment factor > 1.5 are collected and grouped into clusters based on their membership similarities.

3. Results

3.1. Identification of Differentially Expressed Genes (DEGs). A total of 228 DEGs were obtained via the microarray data analysis by Limma, including 86 upregulated and 142 downregulated DEG (supplemental file Table S2). A DEG expression volcano map and heat map were shown in Figure 1.

3.2. Identification of Survival-Related DEGs and Construction of Survival Time Prediction Model. 3 DEGs were screened out to be significantly related to the survival time of NIDCM patients via univariate Cox regression analysis including TOMM22, TMSB4XP8, and PPP2R5A ($p < 0.05$) (Table 2). The 3 genes were used to establish a model for predicting survival time of NIDCM patients. Multivariate Cox proportional hazard regression analysis was performed to confirm the optimal model and a forest map was shown in Figure 2. PPP2R5A and TOMM22 were identified as risk genes in the survival time model. We confirmed PPP2R5A and TOMM22 as high-risk genes in the survival time model which are negatively correlated with patient prognosis (Table 3).

3.3. Testing the Survival Time Prediction Model. The prognostic risk scores for the 17 NIDCM patients were calculated using the gene expression values and the regression coefficients of the risk genes according to the prediction model: risk score for survival time = (0.198883 × expression value of PPP2R5A) + (0.350995 × expression value of TOMM22). Patients were subdivided into high and low-risk groups for survival time based on the median risk scores. Survival analysis revealed that high-risk scores were significantly related to poor survival time (symptoms to heart transplantation). The 2-year and 5-year survival rates for the high-risk patients were 37.5% and 25%, whereas the 8-year and 11-year survival rates for the low-risk patients were 55.6% and 44.4%. We then measured the predictive performance of the prognostic risk models using the time-dependent receiver operating characteristic (ROC) curves. The area under the curve (AUC) was 0.75, which indicated superior predictive accuracy in NIDCM patients for survival time (Figure 3).

3.4. Function Enrichment Analysis by Metascape. The Metascape function enrichment results for DEGs including 204 Gene Ontology terms, 53 Reactome pathways, and 6 Kyoto Encyclopedia of Genes and Genomes pathways. The risk gene PPP2R5A is mainly involved in Influenza Infection, protein localization to membrane, PID IGF1 PATHWAY, CTLA4 inhibitory signaling, Platelet activation, signaling and aggregation, and Hemostasis. TOMM22 is mainly enriched in Influenza Infection, establishment of protein localization to organelle, establishment of protein localization to membrane, protein targeting, protein localization to
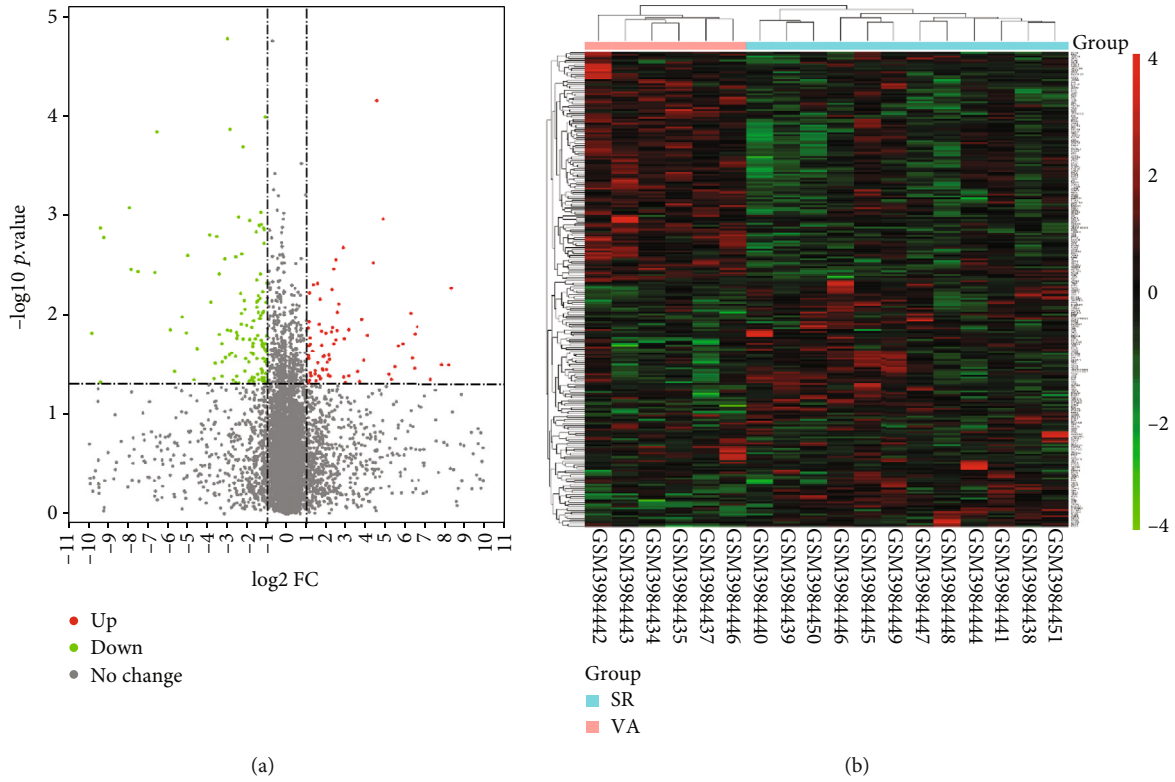
(a)

(b)

Figure 1: DEGs between SR and VA. (a) Volcano map of DEGs between SR and VA. Red represents upregulated differential genes, black represents no significant difference genes, and green represents downregulated differential genes. (b) Heat map of all DEGs between SR and VA. Each column represents a tissue sample, and each row represents a DEG. The gradual color change from green to red indicates the changing process from downregulation to upregulation.

Table 2: DEGs significantly related to survival time of NIDCM patients by univariate Cox regression analysis.

Gene symbol	HR	HR.95L	HR.95H	p value
TOMM22	1.42163	1.063455	1.900439	0.017531
TMSB4XP8	1.119692	1.019037	1.230289	0.018656
PPP2R5A	1.231818	1.009141	1.503629	0.040422

Table 3: Characteristics of risk DEGs in the prognostic risk models.

Gene symbol	Coef	HR	HR.95L	HR.95H	p value
PPP2R5A	0.198883	1.220039	0.999961	1.488553	0.050045
TOMM22	0.350995	1.42048	1.053479	1.915333	0.021358

membrane, mitochondrion organization, autophagy, process utilizing autophagic mechanism, macroautophagy, regulation of mRNA metabolic process, and mitochondrial membrane organization (Figure 4).

4. Discussion

Due to high incidence, poor therapeutic effect, and prognosis, NIDCM is a major health problem that threatens human health, it is necessary to explore its pathogenesis and establish an accurate prediction prognosis model [14–16]. NIDCM is characterized as a genetically determined disease; the genetic basis of NIDCM highlights the importance of screening biomarkers for diagnosis and prognosis [17–19]. Although the survival time of patients with NIDCM is quite different [20, 21], there are few methods to predict the survival time after being diagnosed as NIDCM. We first established a novel two-gene signature to predict survival in patients with NIDCM. To our knowledge, the two-gene signature related prognostic model for NIDCM has not been reported previously.

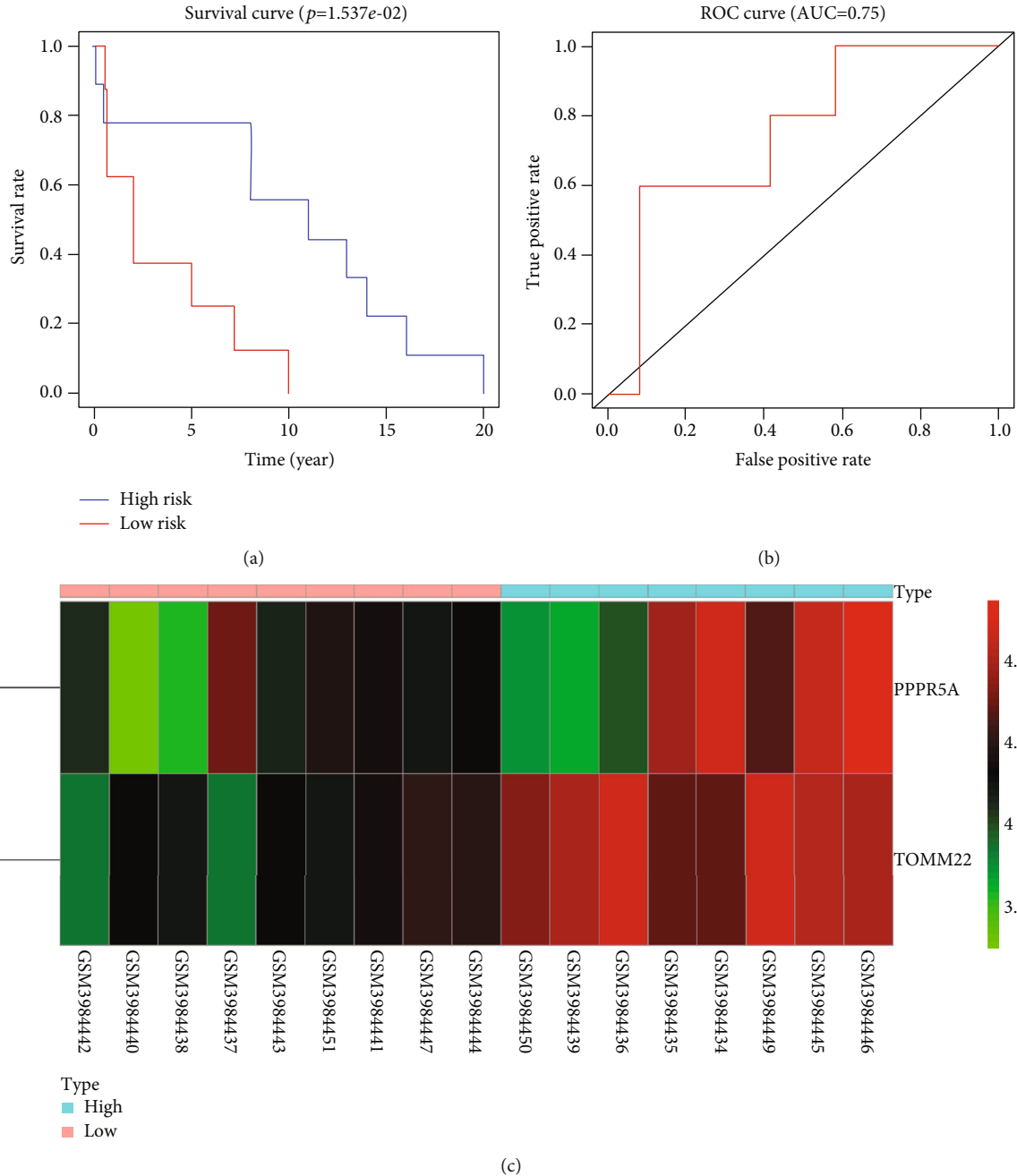Figure 2: Forrest plot of the multivariate Cox regression analysis in NIDCM.

Figure 3: Validation of the survival time prognostic risk models in NIDCM patients. (a) Survival analysis of symptoms to heart transplantation in the high-risk (red line) and low-risk (blue line) NIDCM patients. (b) Time-dependent ROC curve analyses show AUC values for time from symptoms to heart transplantation in NIDCM patients. (c) Expression levels of risk genes in the high-risk and low-risk patients.

The risk score was based on mRNA expression but not somatic mutations or methylation status of only two prognostic genes, which could be more routine and cost-effective in practice.

VA is common in patients with NIDCM. Ventricular fibrillation and cardiac arrest are important reasons for death in patients with NIDCM [22, 23], while there have been few studies focusing solely on VA in NIDCM. Although sudden cardiac death rates have decreased, implantation of ICD for primary prevention in NIDCM patients does not provide overall survival benefits [24].

Establishing a prediction model for incident VA in patients with NIDCM helps make personalized treatment to improve the survival, which can be used as a reference index of whether patients need to be implanted with ICD or not. In this study, we established a novel two-gene signature (including *TOMM22* and *PPP2R5A*) to predict the occurrence of VA in patients. Consistent with our research, some studies support *PPP2R5A* as a novel target for the treatment of arrhythmia. *PPP2R5A*, protein phosphatase 2 regulatory subunit B'alpha, encodes an alpha isoform of
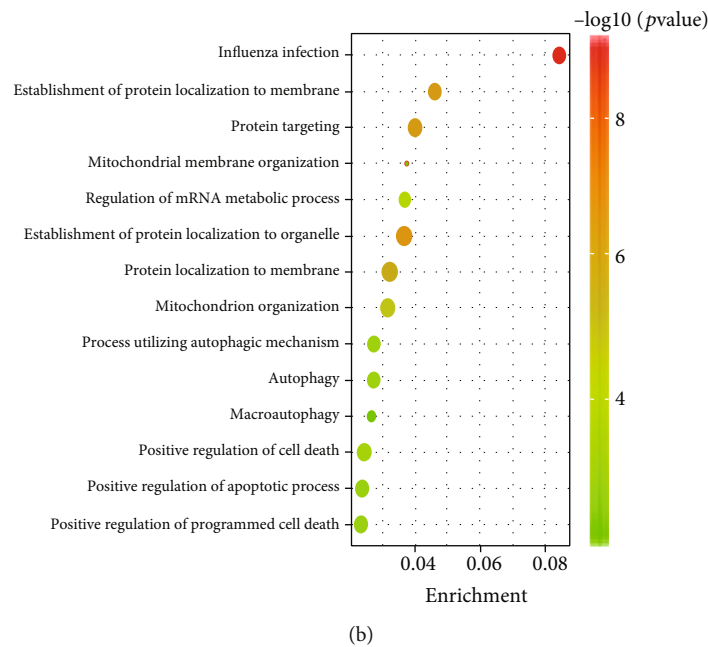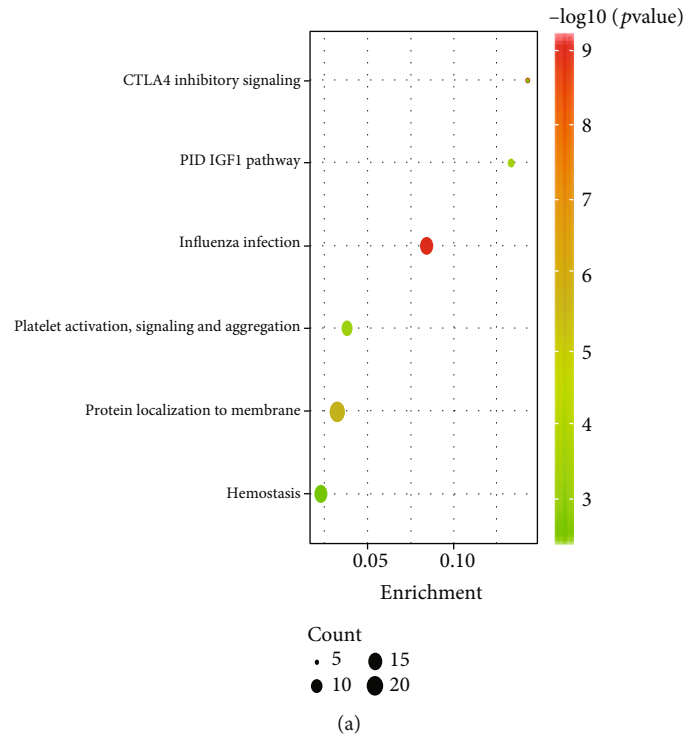
Figure 4: Enrichment analysis by Metascape. (a) Enriched terms of PPP2R5A. (b) Enriched terms of TOMM22.

the regulatory subunit B56 subfamily. Downregulated B56α myocytes are insensitive to isoproterenol-induced induction of arrhythmogenic Na$^+$ channel late component. Voltage-gated Na$^+$ channel 1.5 is critical for normal cardiac excitability, PP2A-B56α complex proved to interact with the primary cardiac voltage-gated Na$^+$ channel 1.5 [25]. *TOMM22*, Translocase of outer mitochondrial membrane 22, is responsible for the recognition and translocation of synthesized mitochondrial precursor proteins; phosphorylation of *TOMM22* is a critical switch for mitophagy [26, 27].

Combined with the functional enrichment analysis results above, *TOMM22* may regulate mitochondrial autophagy in NIDCM, which needs to be confirmed by further research.

Tachycardia-induced cardiomyopathy (TIC) is characterized by diverse tachyarrhythmias, including supraventricular arrhythmias (such as atrial fibrillation) and ventricular arrhythmias [28, 29]. *PPP2R5A* and *TOMM22* show significantly different expression levels between the VA group and SR group in NIDCM patients, which suggests they may be related to the pathogenesis of TIC. More study needs to

be done with *PPP2R5A* and *TOMM22* to determine its exact role in the pathogenesis of TIC.

However, there are some limitations in our research. We studied a small number of patients, although the ROC value (0.75) indicated superior predictive accuracy of the prediction model for survival time in NIDCM patients. In future research, we will carry out a large sample, randomized, and follow-up studies. Besides, the time period of each patient from symptoms to heart transplantation still can represent the prognosis of patients with NIDCM to some extent, overall survival data should be more accurate, and we will carry out patients' long-term follow-up to collect more detail clinical information.

5. Conclusions

Our study identified 3 new genes that were significantly related to the survival time of NIDCM and established a novel two-gene signature to predict survival time and incident VA of NIDCM. Although the sample size of our study is relatively small, these risk genes are probably new targets for exploring the pathogenesis of NIDCM with VA, and the prediction model is useful in clinical decision making for individual treatment.

Abbreviations

NIDCM: Nonischaemic dilated cardiomyopathy
VA: Ventricular arrhythmias
GEO: Gene Expression Omnibus
DEGs: Differentially expressed genes
SR: Sinus rhythm
ROCs: Receiver operating characteristics
AUC: Area under the curve
HF: Heart failure.

Data Availability

The dataset with mRNA expression profiling was taken from GEO: GSE135055. The associated corresponding clinical information of patients in this study was downloaded from BMC Medicine (doi:10.1186/s12916-019-1469-4).

Ethical Approval

The databases are publicly available and open access, and the present study followed the data access policy and publishing guidelines of these databases. Therefore, no local ethics committee is required to approve this study.

Conflicts of Interest

The authors declare that they have no conflicts of interest.

Authors' Contributions

Yan He did the conception and design; Yan He did the administrative support; Chenliang Ge did the provision of study materials or patients; Chenliang Ge did the collection and assembly of data; All authors did the data analysis and interpretation; All authors did the manuscript writing. All authors did the final approval of the manuscript.

Supplementary Materials

Supplementary 1. Supplementary Table 1: summary of the basic information of DCM patients included in the study.

Supplementary 2. Supplementary Table 2: differentially expressed genes.

References

[1] Y. M. Pinto, P. M. Elliott, E. Arbustini et al., "Proposal for a revised definition of dilated cardiomyopathy, hypokinetic non-dilated cardiomyopathy, and its implications for clinical practice: a position statement of the ESC working group on myocardial and pericardial diseases," *European Heart Journal*, vol. 37, no. 23, pp. 1850–1858, 2016.

[2] A. G. Japp, A. Gulati, S. A. Cook, M. R. Cowie, and S. K. Prasad, "The diagnosis and evaluation of dilated cardiomyopathy," *Journal of the American College of Cardiology*, vol. 67, no. 25, pp. 2996–3010, 2016.

[3] A. Spezzacatene, G. Sinagra, M. Merlo et al., "Arrhythmogenic phenotype in dilated cardiomyopathy: natural history and predictors of life-threatening arrhythmias," *Journal of the American Heart Association*, vol. 4, article e002149, 2015.

[4] F. Sedaghat-Hamedani, J. Haas, F. Zhu et al., "Clinical genetics and outcome of left ventricular non-compaction cardiomyopathy," *European Heart Journal*, vol. 38, pp. 3449–3460, 2019.

[5] M. Akhtar and P. M. Elliott, "Risk stratification for sudden cardiac death in non-Ischaemic dilated cardiomyopathy," *Current Cardiology Reports*, vol. 21, no. 12, p. 155, 2019.

[6] M. Ebert, S. Richter, B. Dinov, K. Zeppenfeld, and G. Hindricks, "Evaluation and management of ventricular tachycardia in patients with dilated cardiomyopathy," *Heart Rhythm*, vol. 16, no. 4, pp. 624–631, 2019.

[7] C. W. Yancy, B. Jessup, M. Fau-Bozkurt et al., "2013 ACCF/AHA guideline for the management of heart failure: executive Summary," *Circulation*, vol. 128, no. 16, pp. 1810–1852, 2013.

[8] C. P. S. Fau-Blomström-Lundqvist and C. Blomström-Lundqvist, "European Society of Cardiology Guidelines for the management of patients with ventricular arrhythmias and the prevention of sudden cardiac death summarized by co-chairs," *European Heart Journal*, vol. 36, no. 2015, pp. 2757–2759, 2015.

[9] T. Barrett, P. W. S. Fau-Ledoux, C. L. P. Fau-Evangelista et al., "NCBI GEO: archive for functional genomics data sets–update," *Nucleic Acids Research*, vol. 41, pp. D991–D995, 2013.

[10] X. Hua, Y. Y. Wang, P. Jia et al., "Multi-level transcriptome sequencing identifies COL1A1 as a candidate marker in human heart failure progression," *BMC Medicine*, vol. 18, no. 1, p. 2, 2020.

[11] M. E. Ritchie, B. Phipson, D. Wu et al., "Limma powers differential expression analyses for RNA-sequencing and microarray studies," *Nucleic Acids Research*, vol. 43, article e47, 2015.

[12] B. Wan, B. Liu, G. Yu, Y. Huang, and C. Lv, "Differentially expressed autophagy-related genes are potential prognostic and diagnostic biomarkers in clear-cell renal cell carcinoma," *Aging (Albany NY)*, vol. 11, no. 20, pp. 9025–9042, 2019.

[13] Y. Zhou, B. Zhou, L. Pache et al., "Metascape provides a biologist-oriented resource for the analysis of systems-level datasets," *Nature Communications*, vol. 10, no. 1, p. 1523, 2019.

[14] M. Merlo, B. P. A. Fau-Pinamonti, D. P. B. Fau-Stolfo et al., "Long-term prognostic impact of therapeutic strategies in patients with idiopathic dilated cardiomyopathy: changing mortality over the last 30 years," *European Journal of Heart Failure*, vol. 16, no. 3, pp. 317–324, 2014.

[15] M. Merlo, A. Cannatà, C. Pio Loco et al., "Contemporary survival trends and aetiological characterization in non-ischaemic dilated cardiomyopathy," *European Journal of Heart Failure*, 2020.

[16] A. A.-O. Cannatà, G. De Angelis, A. Boscutti et al., "Arrhythmic risk stratification in non-ischaemic dilated cardiomyopathy beyond ejection fraction," *Heart Failure Clinics*, vol. 106, pp. 656–664, 2020.

[17] B. P. Halliday, J. G. F. Cleland, J. J. Goldberger, and S. K. Prasad, "Personalizing risk stratification for sudden death in dilated cardiomyopathy: the past, present, and future," *Circulation*, vol. 136, no. 2, pp. 215–231, 2017.

[18] P. Charron, E. A. M. Fau-Arbustini, C. A. E. Fau-Basso et al., "Genetic counselling and testing in cardiomyopathies: a position statement of the European Society of Cardiology Working Group on Myocardial and Pericardial Diseases," *European Heart Journal*, vol. 31, pp. 2715–2726., 2010.

[19] R. E. Hershberger, M. M. Givertz, C. Y. Ho et al., "Genetic evaluation of cardiomyopathy-A Heart Failure Society of America practice guideline," *Journal of Cardiac Failure*, vol. 24, no. 5, pp. 281–302, 2018.

[20] D. A.-O. Reichart, C. A.-O. Magnussen, T. Zeller, and S. Blankenberg, "Dilated cardiomyopathy: from epidemiologic to genetic phenotypes: a translational review of current literature," *Journal of Internal Medicine*, vol. 286, no. 4, pp. 362–372, 2019.

[21] R. G. Weintraub, C. Semsarian, and P. Macdonald, "Dilated cardiomyopathy," *The Lancet*, vol. 390, no. 10092, pp. 400–414, 2017.

[22] S. R. Piers, K. Everaerts, R. J. van der Geest et al., "Myocardial scar predicts monomorphic ventricular tachycardia but not polymorphic ventricular tachycardia or ventricular fibrillation in nonischemic dilated cardiomyopathy," *Heart Rhythm*, vol. 12, no. 10, pp. 2106–2114, 2015.

[23] D. Stolfo, N. Ceschia, M. Zecchin et al., "Arrhythmic risk stratification in patients with idiopathic dilated cardiomyopathy," *The American Journal of Cardiology*, vol. 121, no. 12, pp. 1601–1609, 2018.

[24] L. Køber, J. J. Thune, J. C. Nielsen et al., "Defibrillator implantation in patients with nonischemic systolic heart failure," *The New England Journal of Medicine*, vol. 375, no. 13, pp. 1221–1230, 2016.

[25] M. El Refaey, H. Musa, N. P. Murphy et al., "Protein phosphatase 2A regulates cardiac Na(+) channels," *Circulation Research*, vol. 124, no. 5, pp. 737–746, 2019.

[26] B. Kravic, A. B. Harbauer, V. Romanello et al., "In mammalian skeletal muscle, phosphorylation of TOMM22 by protein kinase CSNK2/CK2 controls mitophagy," *Autophagy*, vol. 14, no. 2, pp. 311–335, 2018.

[27] G. Bertolin, M. F.-M. R. Fau-Jacoupy, S. J. M. Fau-Traver et al., "The TOMM machinery is a molecular switch in PINK1 and PARK2/PARKIN-dependent mitochondrial clearance," *Autophagy*, vol. 9, pp. 1801–1817, 2013.

[28] A. Khasnis, G. J. K. Fau-Abela, S. A. G. Fau-Veerareddy, V. V. S. Fau-Reddy, R. R. V. Fau-Thakur, and R. Thakur, "Tachycardia-induced cardiomyopathy: a review of literature," *Pacing and Clinical Electrophysiology*, vol. 28, no. 7, pp. 710–721, 2005.

[29] D. A.-O. Kim, S. A.-O. Kim, and K. A.-O. Ryu, "Tachycardia induced cardiomyopathy," *Vnitřní Lékařství*, vol. 61, pp. 56–59, 2015.